Demand side control for power system frequency regulation

Qingxin Shi
University of Tennessee, qshi1@vols.utk.edu

To the Graduate Council:

I am submitting herewith a dissertation written by Qingxin Shi entitled "Demand side control for power system frequency regulation." I have examined the final electronic copy of this dissertation for form and content and recommend that it be accepted in partial fulfillment of the requirements for the degree of Doctor of Philosophy, with a major in Electrical Engineering.

Fangxing Li, Major Professor

We have read this dissertation and recommend its acceptance:

James Ostrowski, Hector Pulgar, Kai Sun

Accepted for the Council:

Dixie L. Thompson

Vice Provost and Dean of the Graduate School

(Original signatures are on file with official student records.)

Demand Side Control for Power System Frequency Regulation

A Dissertaiton Presented for the

Doctor of Philosopy

Degree

The University of Tennessee, Knoxville

Qingxin Shi

August 2019

Acknowledgement

I would like to express my thanks to those who helped me with various aspects of conducting research and writing this dissertation.

First and foremost, I would like to express my deepest gratitude to my supervisor, Dr. Fangxing (Fran) Li for his continuous guidance and persistent help with this dissertation and all of my other research during my Ph.D. study at the University of Tennessee at Knoxville (UTK). Throughout the hundreds of hours he devoted to my study, he guided me to think as a researcher and showed me how to present my work in logical and elegant ways. He also created a free and vigorous atmosphere in our research group that made the research work enjoyable for my peers and me. I am honored to have been his Ph.D. student.

I would also like to thank my committee members Dr. James Ostrowski, Dr. Hector Pulgar, and Dr. Kai Sun for devoting time to my proposal defense and offering insightful suggestions for improving my dissertation.

In additoin, I would like to express my special thanks to graduate students Qinran Hu, Xue Li, Haoyu Yuan, Xin Fang, Can Huang, Riyasat Azim, Linquan Bai, Hantao Cui, Xiao Kou, Wei Feng, Yan Du, Mariana Kamel, Cody Rooks, Qiwei Zhang, and Evan McKee, for being supportive of my research as well as for offering their kind advice throughout my course study and research. I would also like to thank all of my friends and professors in the Center for Ultra-Wide-Area Resilient Electric Energy Transmission (CURENT). Specifically, I'd like to thank the associate professor Dr. Chien-fei Chen, the

visiting scholars Dr. Yonghui Sun, Dr. Tao Jiang, and former Ph.D. candidates Yichen Zhang and Bin Wang for helping me with my research.

Additionally, it is necessary to mention my four-people "cooperation group" consisting of Yajun Wang, Siqi Wang, Wenyun Ju and me. We formed this group via Wechat app in the summer of 2016 to share our happiness and our sorrows. We had dinners to celebrate our new paper publications or achievements in job hunting. Although we were of stressed about our Ph.D. studies and future careers, every group member has found satisfaction in research achievements and job opportunities. The support of these friends will always be a valuable memory in my life.

Finally, I would like to thank my parents Yunxing Shi and Yuzhi Liang for their continuous support through the many years that I have studied abroad.

Abstract

The increasing penetration of renewable energy resources brings a number of uncertainties to modern power system operation. In particular, the frequent variation of wind or solar power output causes a short-term mismatch between generation and demand and system frequency fluctuation. The traditional approach to dealing with this problem is to increase the amount of system spinning reserve, which increases costs. In recent years, researchers have been actively exploring the utilization of residential and commercial loads in frequency regulation without affecting customers' comfort level. This is called dynamic demand control (DDC). This dissertation describes an in-depth study of DDC for bulk power system frequency regulation, from both a technical and economic perspective.

Fist, an analytical method was proposed for aggregating a multi-machine system frequency response (SFR) model. The SFR model can accurately represent the bus frequency response of small-scale systems and the center-of-inertia frequency of large systems. The method is a fast tool for simulating the system frequency response after a disturbance. Therefore, it has wide applications in power system dynamic studies and acts as a solid theoretical foundation for DDC studies.

Second, DDC strategies for both primary and secondary frequency regulation were studied. The control strategy has the following features. 1) The target load reduction amount can be achieved in a decentralized manner, while the control parameters are updated by the control center. Therefore, the control strategy is easy to implement in the hardware. 2) The daily demand profiles of thermostatic loads are modeled. 3) The load recovery process is considered in the control strategy. Consequently, the aggregate loads

can provide flexible frequency control capability without causing significant power rebound. Therefore, demand side control is an essential compensation for traditional frequency regulation approaches and can improve the frequency response of the bulk power system.

Furthermore, this dissertation also conducts an economic analysis on demand response (DR). Based on a large-scale customer survey, we estimate the expense of frequency regulation and peak load reduction via incentive-based demand response (IBDR). The results provide useful suggestions for utility companies when implementing IBDR programs.

Key words: demand response, frequency regulation, system frequency response, thermostatic load, electric water heater, HVAC, incentive-based demand response, demand profile.

Table of Contents

List of Tables

List of Figures

List of Abbreviations

AGC   Automatic Generation Control

ASFR   Aggregated System Frequency Response

COI   Ceter of Inertia

DDC   Dynamic Demand Control

DR   Demand Response

EV   Electric Vehicle

EWH   Electric Water Heater

FDR   Frequency Disturbance Recorder

HVAC   Heating, Ventilation and Air Conditioner

HWCA   Hot water consumption activity

IBDR   Incentive-based Demand Reponse

LFC   Load Frequency Control

LQR   Linear Quadratic Regulator

PBDR   Price-based Demand Reponse

PRFR   Primary Frequency Regulation

PV   Photovoltaic

RES   Renewable Energy Source

RoCoF   Rate of Change of Frequency

RS-CR   Random Switching and Cycle Recovery

SCFR   Secondary Frequency Regulation

SDM   Stochastic Decision Method

SFR   System Frequency Response

TLC   Thermostatic Load Control

TRFR   Tertiary Frequency Regulation

VSHP   Variable Speed Heat Pump

WECC   Western Electricity Coordinating Council

Chapter 1

Introduction

This chapter discusses the general techniques of demand side control for power system frequency regulation.

1.1 Overview

One essential requirement for power system operation is to ensure the balance between power generation and demand in real time. As a result of the considerable unbalance between generation and demand, frequency instability is usually associated with poor coordination of control and protection equipment, insufficient generation reserves, and inadequacies in equipment responses [1]. In recent years, however, the increasing penetration of renewable energy resources and the development of the power market bring three challenges to frequency stability, which amplify the need for frequency regulation for both long-term (hourly) and short-term (minute to second timescale). Those challenges are as follows:

- The intermittent nature of renewable energy causes a mismatch between power generation and demand [2]-[4], therefore, frequency fluctuation is more likely to happen than ever before;

- Some synchronous generators are replaced by converter-based energy sources, which may decrease the mechanical inertia of the present system [4]-[6]; and

- Hourly-based electricity market or system operations (like Union for the Coordination of Transmission of Electricity and Western Electricity Coordinating Council (WECC)) are likely to cause a mismatch between generation and load in the first few minutes of an hour [7].

In regard to the aforementioned problems, conventional thinking suggests that the generation side should always be prepared to satisfy all required generation-demand

mismatches, while new theories state that the system will be most efficient if the large mismatches, mainly due to wind power fluctuation in recent years, are minimized by suitable demand control [8]-[9]. Demand Response (DR) has been introduced to adjust demand-side power consumption whenever necessary. From the power system operation perspective, the essential purpose of DR is to reduce the amount of spinning reserve while maintaining frequency stability to improve the system. A wide variety of DR programs have been designed for peak load shaving and valley load filling, which can be regarded as mitigating long-term (usually 24 hours) frequency fluctuation. Based on the objective, DR programs can be divided into three categories: incentive-based programs that focus on a utility's welfare [10]-[11], price-based programs that focus on customer' welfare [12], and the hybrid programs that focus on both [13]. In all, study on DR applications for economic-related issues began in the 1980s with many established research works.

To mitigate short-term frequency fluctuation, turbine governor control and automatic generation control (AGC) are designed to automatically adjust the output power of generation units in order to compensate for power shortfalls or to avoid power surplus. On the demand side, under-frequency load shedding (UFLS), is activated as a protection approach when system frequency falls under a particular threshold (e.g., 59.30 Hz) [14]-[15]. In 2007, J. A. Short proposed a new frequency regulation approach, named as *dynamic demand control* (DDC) [16]. Compared with conventional frequency regulations, DDC is superior for the following reasons:

- *Fast response*: Compared with generator-side control, DDC can capture sudden frequency drops and restore the frequency faster than AGC, which typically takes several minutes [17].

- *Flexibility*: Compared with UFLS which is activated at a large frequency drop, DDC is more flexible because it is activated at a relatively small frequency drop with multiple frequency thresholds (e.g., 59.85 ~ 59.95Hz) [7], [18].

- *Economic efficiency*: A large number of controlled loads can emulate the frequency droop characteristic of a generation unit in order to mitigate frequency fluctuation, which is caused by short-period wind power shortage or generator outage [18]-[21]. Therefore, we can expect that the wide application of DDC helps reduce the

2

requirement for spinning reserve capacity and further reduce the system operation costs [22]-[23].

In summary, DDC can be a useful compensation for conventional power system frequency regulation approaches.

1.2 Brief Description of Frequency Regulation

The mission of frequency regulation is to quickly respond to system frequency deviation by increasing or decreasing power generation or load demand to bring frequency back to a nominal value (50 or 60 Hz). This section first introduces the so-called load-frequency control (LFC) model to illustrate the relationship between frequency and power unbalance, and then discusses the concept of frequency regulation in the industry. The model and concept are the theoretical basis of various DDC strategies that will be discussed in later chapters.

1.2.1 Power system frequency response

Consider a single-machine system in which the exciter is neglected. The rotating speed of the generator follows the 2nd Newton Law. Applying small deviations around the nominal frequency, we have [24],

$$2H\frac{d\Delta f(t)}{dt} + D\Delta f(t) = P_m(t) - P_d(t) = \Delta P_m(t) - \Delta P_d(t) \tag{1.1}$$

where $P_m(t)$ is the generator mechanical power, $P_d(t)$ is the load demand, and $\Delta f(t)$ is the system frequency deviation $(=f(t) - 60)$, all at time t. Note: Power and frequency variables are in per-unit values here. H is the inertia constant, denoting the kinetic energy at the rated speed divided by the rated power base. D is the system load damping coefficient which is expressed as a percent change in load for a 1% change in frequency. If we assume the pre-disturbance state as the steady state, then the accelerating power $(P_m - P_d)$ equals to the difference between the generation and demand power deviations from the steady state $(\Delta P_m - \Delta P_d)$.

The complete LFC system is presented in Figure 1.1 [24]. When a step disturbance ΔP_L happens, representing a generation outage or a sudden load increase, the turbine governor

3

modifies the power output of the prime mover $P_m(t)$ to regulate system frequency. The prime mover model consists of the boiler, governor, and reheater. The governor and turbine transfer function are expressed by (1.2). The LFC system may include two types of generators: one does not participate in AGC, and its generation reference is determined by the economic dispatch (Load ref. 1 in Figure 1.1); the other one participates in AGC, and its generation reference is controlled by AGC center (Load ref. 2 in Figure 1.1). Both generators reserve a specified amount of capability such that they can perform frequency droop control. The system also includes the DDC, which acts as a "fast power compensator" in response to the frequency change. The formulation of $D(s)$ is determined by the specific load control strategy. Because of the effect of the generator turbine inertia, droop value and load damping factor, the system frequency can experience a dynamic process and enter another equilibrium point. The system parameters are listed in Table 1.1 [24]-[25].

$$G(s) = \frac{1}{1+T_G s} \text{ and } T(s) = \frac{1+F_H T_R s}{(1+T_C s)(1+T_R s)} \tag{1.2}$$

When the system consists of multiple generators, the parameters are aggregated from each generator with its capacity as a weighting factor, according to the definition of H [24].

$$H = \frac{\sum_i S_i H_i}{\sum_i S_i} \tag{1.3}$$
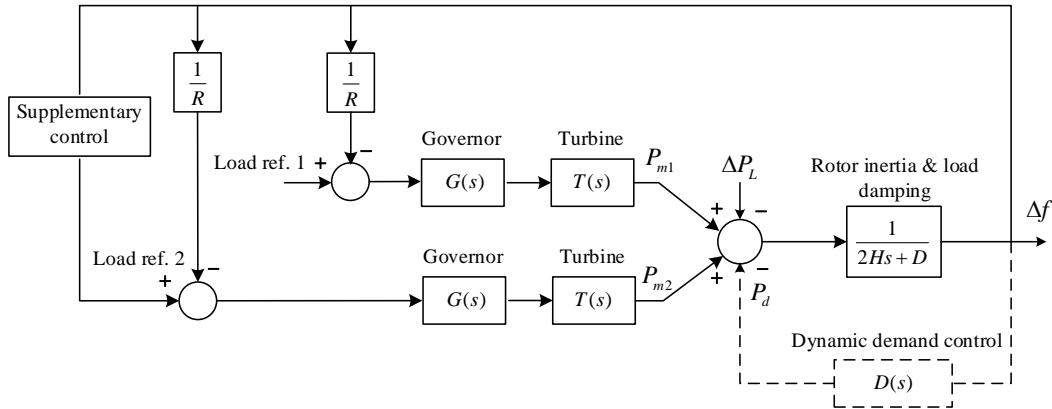
Figure 1.1. LFC system with DDC participation.

Table 1.1. Typical parameters of LFC system.

Parameter	Typical value
Governor time constant T_G	0.2s
Steam chest time constant T_C	0.3s
Reheat time constant T_R	6~14s
High-pressure turbine fraction F_H	0.15~0.4
Inertia constant H	3~6s
Governor speed regulation droop R	0.04~0.1
Load damping coefficient D	1

where S_i is the rated apparent power of the i-th generator.

In the ideal steady state, the system frequency is very close to the nominal value. In dynamic state, however, the real-time frequency differs with the electrical distance to the disturbance point. It is proven and observed that the frequency disturbance (or the so-called electromechanical dynamics) is propagated in the form of traveling waves through long transmission lines [26]-[28]. Different locations would have different frequency responses after a generator trip. The wave propagation speed is affected by the transmission line impedance, system inertia and line voltage ratings. The wave propagation speed varies from 500 to 700 miles/sec in transmission systems [29]. Therefore, within a system of 60 miles (or 100 km) geographical size, the frequency is almost identical everywhere such that we can consider the global system frequency the same as a local frequency that is measured at the low-voltage side or the demand side.

1.2.2 Description of power system frequency regulation

Frequency regulation is an important ancillary service and can be generally classified into three categories [22], [30]:

- *Primary Frequency Regulation (PRFR)*: PRFR refers to governor control that adjusts the active power of generation units and the consumption of loads to arrest frequency variations within a few seconds.

- *Secondary Frequency Regulation (SCFR):* SCFR refers to automatic generation control (AGC) that adjusts the active power output of generation units to bring system frequency back to the nominal value. The reacting time of SCFR is about 30 seconds,

5

and it will sustain for 5~20 minutes.

- *Tertiary Frequency Regulation (TRFR)*: TRFR means manual changes in the dispatching and commitment of generation units (reacting in more than 15 minutes). TRFR is used to restore PRFR and SCFR reserves and to manage congestions in the transmission networks.

In the practical ancillary market of different countries, different terminologies are used for frequency regulation. For example, PRFR are named as frequency response in North America, operating reserve in Britain and contingency service in Australia. The terminology details are summarized in [31]. The general scope of frequency regulation approaches is summarized in Figure 1.2, which includes both traditional approaches and emerging approaches. In particular, DDC has the advantage of faster responsive speed over traditional approaches and has received considerable attention [16]. Other emerging approaches include the control of renewable energy source [32]-[35], EV smart charging [36] and energy storage [37]-[39].

Figure 1.3 illustrates the frequency response of an actual generation outage in the UK system with the participation of frequency regulation services [40].
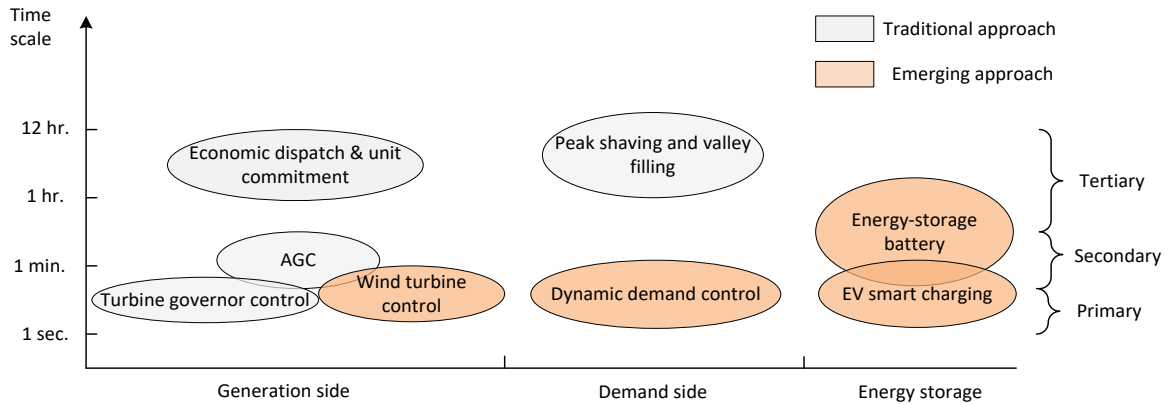
Figure 1.2. Approaches for balancing power generation and consumption.
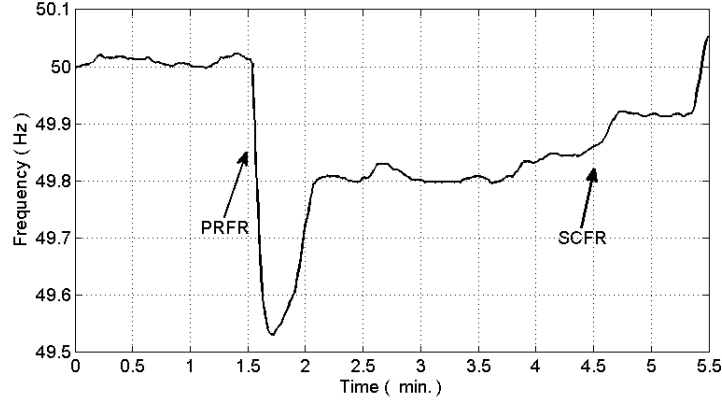
Figure 1.3. Example of frequency response following a major generation outage.

1.3 Responsive Load

So-called "responsive loads" may adjust their operation status to provide reserves for frequency regulation based on locally measured system frequencies [7]. Since a power system with high renewable energy penetration has many short-term frequency variations with large mismatches (due to the high penetration of wind), responsive loads are expected to be large in order to provide reserves for frequency regulation. Conventionally, some large-scale industrial loads (i.e., aluminum smelting plants [41]) and agricultural loads such as water pumps [42] may participate in frequency regulation. However, this dissertation is focused on residential loads for DDC, including only some commercial loads. Generally, the ideal candidates among residential loads for frequency regulation should satisfy the following requirements: First, they must be in operation continuously or regularly, since frequency regulation is needed at all times; Second, a high power rating is needed in order to obtain a considerable total power compensation with a relatively low number of loads, which require a small number of controllers; Third, participating in frequency regulation should have little impact on customers' comfort levels [43]. Therefore, electro-thermal and space-cooling loads, including electric water heaters (EWHs) and heating, ventilation and air-conditioners (HVAC), are considered perfect candidates due to their thermal inertias and high power ratings [44].

In contrast to generation spinning reserve, responsive loads are not always in operation. In particular, the operation cycles of EWHs and HVACs are determined by various unpredictable factors including random hot water consumption and outdoor air temperature,

respectively. Consequently, the available capacity of responsive loads in real time ($P_{RL,avai}(t)$) is a stochastic variable, and it is smaller than the registered capacity of the loads ($P_{RL,reg}$). Therefore, load behavior uncertainty should be assessed before designing a DDC strategy. This section will briefly discuss several important practical considerations for implementing DDC strategies.

1.3.1 Classification of responsive loads

Based on existing studies [7], [36], [45]-[46], responsive loads can be divided into four categories according to their control characteristics.

Type I: This type is referred to as pure resistive loads for electric heating. A *Type I* load can immediately disconnect and reconnect to the grid when system frequency drops and recovers, respectively. Space heaters and EWHs are examples of Type I load. EWH has one or two resistive heating elements controlled by thermostats. The heating elements are switched on when the water temperature reaches a low setpoint, and switched off when the temperature reaches a high setpoint [47]. Although one EWH can provide at least 1.5 kW frequency reserve when staying on, its operation cycle is determined by customers' random hot water consumption. Based on the heat transfer model of EWHs [48] (presented in Appendix A), a typical profile of the water temperature and on/off operating cycle is simulated, as shown in Figure 1.4. The figure indicates that a hot water consumption event makes the water temperature drop below the temperature lower limit. Then the EWH is switched on for some time in order to bring the water temperature to the normal value. Since taking a shower consumes more hot water than dishwashing, the EWH will be switched on for a longer time to recover the water temperature. Also, the water cools down 0.3˚C per hour if hot water consumption does not happen and the heating element is off. Therefore, the customers' comfort level will not be affected if EWHs are utilized for frequency regulation at the time scale of second to minutes.

Type II: This type refers to compressor-based loads, which can be controlled by modifying the temperature setpoints [7], [16], [49]. Type II loads include HVACs, refrigerators/freezers, etc. Taking HVAC (in cooling mode) as an example, the on and off states are determined by the high and low temperature setpoint limits, θ_{high} and θ_{low}.
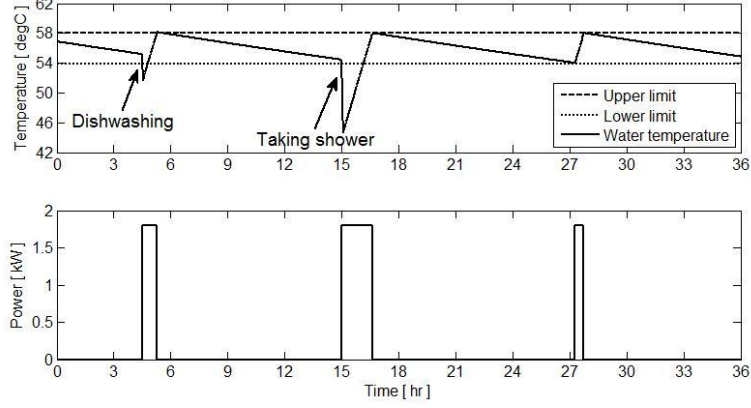
Figure 1.4. Water temperature and power demand profile of EWH.

$$State = \begin{cases} Off & \theta < \theta_{low} \\ On & \theta > \theta_{high} \\ Keeping & \theta_{low} \leq \theta \leq \theta_{high} \end{cases} \qquad (1.4)$$

where θ is the indoor air temperature. Based on the heat transfer model of HVACs [50] (presented in Appendix A), a typical profile of the indoor temperature and on/off operating cycle is simulated and presented in Figure 1.5. According to the figures, the operating cycle of HVACs (usually 1~2 hours) is much shorter than that of EWHs (around 10 hours).

If the system frequency drops, we can modify the temperature setting by [7]

$$\begin{cases} \theta'_{low} = \theta_{low} + k_f \Delta f \\ \theta'_{high} = \theta_{high} + k_f \Delta f \end{cases} \qquad (1.5)$$

where k_f is the coefficient of frequency change (°C/Hz). We have $k_f < 0$ when the HVAC is on cooling mode, meaning that the temperature setpoint is increased when the system frequency drops below the rated value. Similarly, we have $k_f > 0$ when the HVAC is on heating mode. Hence, the power consumption of a large number of HVACs decreases and the frequency can be promoted accordingly.

Type III: The variable speed heat pump (VSHP) is another type of compressor-based load. As mentioned in Appendix A, the Type II load has a constant heat transfer rate and compressor power (both in Watt) once it is switched on. By contrast, the heat transfer rate of a Type III load can be adjusted by the compressor variable-speed controller. Therefore, the Type III load is not periodically switched between on and off states when in operation

9
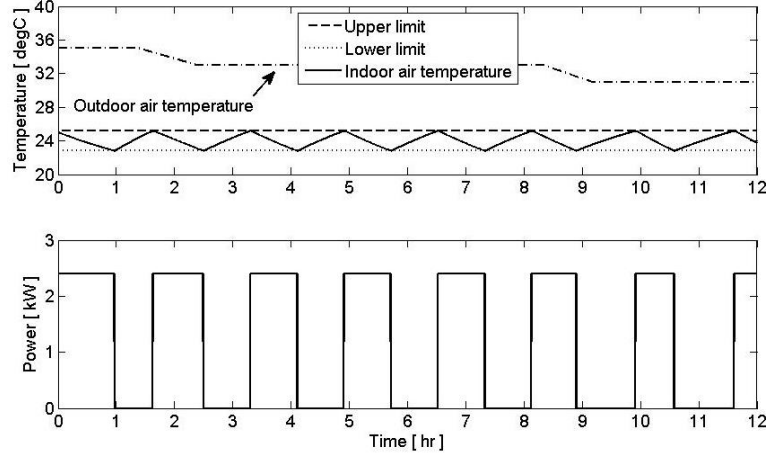
Figure 1.5. Temperature and power demand profile HVAC (cooling mood).

[45]. A data-driven dynamic model of VSHP is derived for demand control study [46]. In this model, the compressor rotor frequency (f_c), the evaporator return water temperature (θ_{wr}), and the condenser ambient temperature (θ_{amb}) together determine the steady-state compressor power (P_{HP}). It is given by

$$P_{HP} = k_f f_c + k_{amb}\theta_{amb} + k_{wr}\theta_{wr} + k_{offset} \tag{1.6}$$

where the coefficients k_f, k_{amb}, k_{wr}, and k_{offset} are determined by a linear regression method.

The reference power of VSHP (P_{HP_ref}) can be modified according to the measured frequency deviation. The VSHP dynamic power with respect to the reference power signal is approximated by a first-order transfer function:

$$\Delta P_{HP}(s) = \frac{n_{HP}}{sT_{HP}+1} \cdot \Delta P_{HP\_ref}(s) \tag{1.7}$$

where the coefficients n_{HP} and T_{HP} are typically determined by simulation. This model is able to approximate the aggregated dynamic response of a large number of VSHPs, regardless of their parameter difference.

Type IV: Electric vehicles (EVs) can be regarded as Type IV loads, although some literature considers EVs as an energy storage unit for frequency regulation [36]. EVs can both charge and discharge, therefore they are able to provide both under- and over-frequency regulation. The charging/discharging power can be dynamically controlled by

10

considering both the system frequency deviation and the state of charge (SOC) of the battery [36].

1.3.2 Assessment of responsive load uncertainty as frequency reserve

In order to assess the effect of a DDC strategy on system frequency response, it is necessary to propose a probabilistic model to estimate $P_{RL,avai}(t)$. The operation cycles of two major responsive loads, EWHs and HVACs, are affected by hot water usage and ambient temperature, respectively. Based on the statistic hot water demand profile, a simulation of 10,000 EWHs is conducted [51]. The $P_{RL,avai}(t)$ profile with 5-minute resolution is shown in Figure 1.6. The figure indicates that $P_{RL,avai}(t)$ fluctuates over a day. In the morning and evening hours, hot water consumption is higher than other hours, consequently a larger portion of EWHs are switched on and the total power demand becomes high. In contrast, little hot water is consumed at midnight, consequently the total power demand is low. In this case, the 10,000 EWHs with $P_{RL,reg}(t) = 18$MW can provide $P_{RL,avai}(t) = 0.95 \sim 5.2$ MW throughout the day, or $2.0 \sim 5.2$MW during the daytime (6:00 – 24:00). Since the ratio between $P_{RL,avai}(t)$ and $P_{RL,reg}$ depends on the resident's hot water consumption behavior, it can be diverse in different regions. Therefore, for the same frequency deviation occuring at different times of day in different regions, the system frequency response can be different even if we apply the same DDC strategy, due to the uncertainty of load availability. Similarly, given the outdoor temperature profile, the $P_{RL,avai}(t)$ parameter of aggregated HVACs can also be estimated.
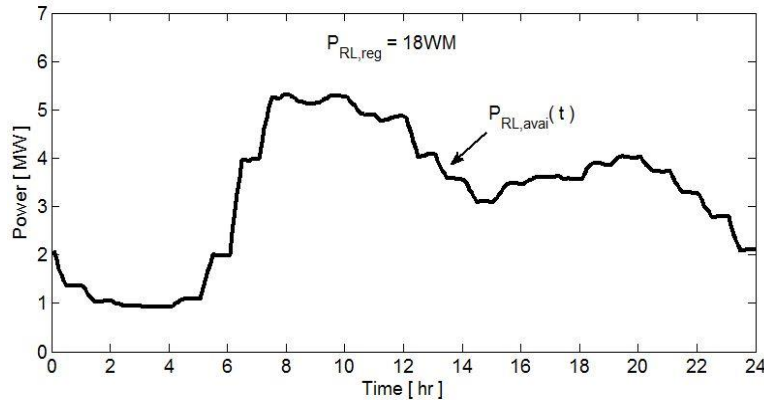
Figure 1.6. Total power demand of 10,000 EWHs.

1.4 Dissertation Outline

Chapter 2 summarizes the technical features and advantage/disadvantages of three types of DDC algorithms, namely centralized control, decentralized control and hybrid control. The technical and economic concerns of this research field are also discussed, which indicates the necessity of this research.

Chapter 3 proposes an analytical method for aggregating the multi-machine system frequency response (SFR) model into a single-machine model. The verification study indicates that the proposed aggregated SFR (ASFR) model can accurately represent the multi-machine SFR model. The SFR model can support many research areas related to power system dynamics, such as frequency control, renewable energy integration and power system dynamic model reduction. In particular, the ASFR model is an important theoretical basis for the DDC study in latter chapters.

Chapter 4 proposes a hybrid DDC strategy for the primary and secondary frequency regulation. The study is based on some idealized assumption that the responsive load is always available.

Chapter 5 presents an in-depth study on DDC. In this chapter, the thermostatic load control strategy (TLC) is proposed, with the consideration of daily load profile and the progressive load recovery after disturbance. In particular, the control strategy is simulated for both step disturbance and ramp disturbance. Therefore, the result is closer to the industry application.

In comparison with former chapers that are focused on technical aspect of DR, Chapter 6 conducts an economic study of DR. A DR survey is designed considering the social-behavioral factors. Then, the modeling of load profile is proposed for major home appliances, such as HVAC and EWH. Based on the survey result and the load profile model, we evaluate the potential of DR and the cost of reducing a particular amount of peak load through incentive-based demand response (IBDR) programs.

Chapter 2

Literature Review

This section reviews different categories of DDC strategies and compares their advantages and disadvantages. Then, the technical and economic concerns of this research field are also discussed.

2.1   Review and Comparison of Dynamic Demand Control Strategies

Generally, a good control strategy should satisfy the following two "conflicting" requirements:

- *From the utility's side*: Maximizing the response speed of responsive loads and reducing the frequency regulation reserves at the generation side.

- *From the customer's side*: Minimizing the impact on the customer's comfort level without reducing the appliance's life span (e.g., repetitive off/on switches should be avoided).

The control strategies are divided into three categories according to their means of communication: centralized control, decentralized control, and hybrid control, as illustrated in Figure 2.1. Hybrid control combines the features of centralized and decentralized control. In particular, hierarchical hybrid control is an effective approach to implementing large-scale DDC for frequency regulation. In a hierarchical hybrid system, a number of responsive loads (1st level) that are controlled by a load aggregator can emulate a generator with spinning reserve. Different load aggregators (2nd level) can work either in communication with each other or in a decentralized way, as shown in Figure 2.1 (c).

The previous literatures define DDC in different focus. Some literatures are focused on optimizing the frequency response curve, while ignoring methods for implementing a control strategy to achieve this "optimal" response [52]. In contrast, other literature focuses on the responsive load characteristics for implementing frequency regulation [7], [45].

(a) Centralized control   (b) Decentralized control

(c) Hierarchical hybrid control
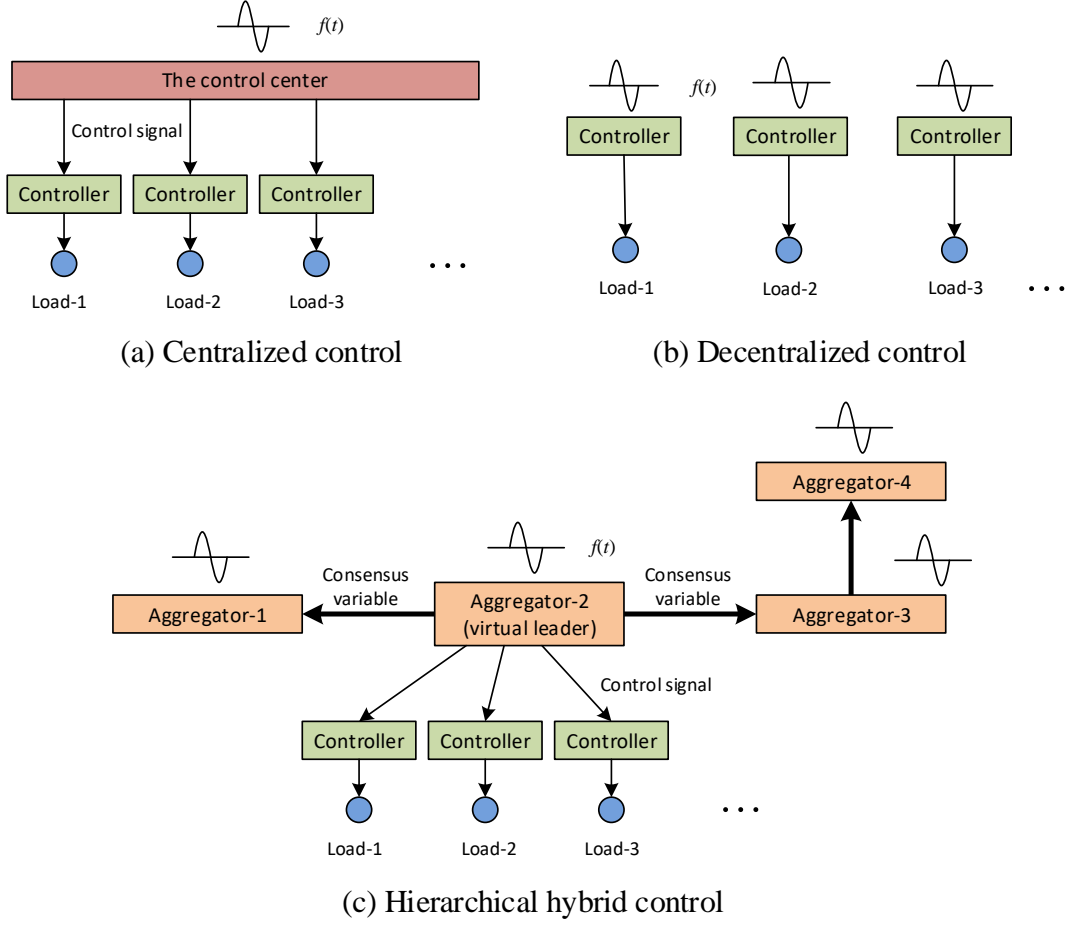
Figure 2.1. Communication structure of three control strategies.

However, all these studies share a similar target: to make a large number of responsive loads to emulate the generator spinning reserve for PRFR and SCFR. Consequently, we can reduce the amount of spinning reserve in a system with high penetration of renewable energy.

2.1.1 Centralized control

In a centralized control scheme, the control center measures the system frequency deviation, determines the load regulation amount, and sends the control signal to a large number of responsive loads. This control requires a significant number of communication channels and has high cost but achieves accurate frequency response. For now, it is mostly applied to microgrids [45]-[46], [53]-[56]. The existing centralized control strategies can

be classified into two subcategories: the adaptive approach and the ΔP_L-estimation approach.

In the adaptive approach, at each time step, the controller measures the frequency and computes the load reduction accordingly until the frequency is restored. The specific method includes proportional-integral control [45]-[46], droop control [53]-[57], and a linear quadratic regulator (LQR) [52]. This approach does not estimate the disturbance magnitude ΔP_L. S. A. Pourmousavi made a representative study [53]-[55]. The system frequency deviation is divided into three states: 0 (normal, $|\Delta f| \leq 0.05\text{Hz}$), 1 ($|\Delta f| > 0.05\text{Hz}$), and 2 ($|\Delta f|$ recovers from beyond 0.05Hz to within 0.05Hz). When there is a loss of generation bringing the frequency to state 1, the control center will gradually switch off the aggregated loads [53], [55]:

$$\% P_{load}(k) = \% P_{load}(k-1) + \Delta f \times M \tag{2.1}$$

where $\% P_{load}(k)$ is the percentage of remaining load at time step k with regard to the pre-disturbance load, $\% P_{load}(0)$ (let $\% P_{load}(0) = 100$), and M is the power-frequency droop factor. Once the frequency deviation is smaller than a specified threshold (entering state 2), the control center will minimize the amount of activated responsive loads [54], [55]:

$$\% P_{load}(k) = 0.95 \times \% P_{load}(k-1) \tag{2.2}$$

In the ΔP_L-estimation approach, ΔP_L is estimated at the instant ($t=0^+$) when the disturbance happens. Then, the control center directly manages the load reduction. Since the turbine governor control has not been activated at $t=0^+$, ΔP_L can be calculated if the system inertia H is known. In a single-area system, ΔP_L is computed by the 1st derivative of the frequency [58].

$$\Delta P_L = 2H \cdot \left. \frac{df(t)}{dt} \right|_{t=0^+} \tag{2.3}$$

In a multi-area system, ΔP_{Li}, which represents the magnitude of the disturbance applied to area i, can be computed by the 2nd derivative of tie-line power [59].

$$\Delta P_{Li} = -\frac{H_i}{\pi \sum_{j=1, j\neq i}^{N} T_{ij}} \cdot \frac{d^2}{dt^2} \left(\Delta P_{tie,i}(t) \right) \Bigg|_{t=0^+} \tag{2.4}$$

where $\Delta P_{tie,i}$ is the total tie-line power change between area i and the other areas, and T_{ij} is the tie-line synchronizing torque coefficient. After ΔP_{Li} is estimated, some control algorithms are applied to improve the dynamic performance of the controller (e.g., fuzzy-PI-based method [59]).

Overall, centralized control strategies presented in the literature are quite diverse. This control requires two-way real-time communication, and the communication delay can degrade the dynamic performance of the control strategy to some degree [52], [55], [59]. Table 2.1 summarizes general information about the centralized control strategies, including the type of frequency regulation (FR), the type of responsive loads, and highlights of control strategies.

2.1.2   Decentralized control

In a typical decentralized control scheme, each load controller measures the local frequency on its own and then makes the switch-on/off decision. It can be proven both analytically and numerically that the system frequency at all buses will converge to a unique equilibrium after a disturbance. This conclusion provides decentralized control with a rigorous theoretical basis [60]-[61]. The previous study demonstrated that existing decentralized control strategies achieve smooth, fast frequency response under some idealized assumptions [7], [16]-[18], [42], [44]. The main advantage of the decentralized control is that it does not require communication devices. The disadvantage is that without a central organization or controller, the aggregated load response may result in an excessive or insufficient power response than what is needed. The reason for excessive or insufficient power response is that without knowing H, the measured frequency deviation cannot evaluate exactly how much of a power response is needed to regulate this disturbance. Below is a brief summary of several representative references.

In Reference [7], Type I and Type II loads are controlled differently. After a frequency drop, the load controller will turn off the Type I loads and also reduce the total power

Table 2.1. Comparison of centralized DDC algorithms.

Ref. No.	Type of FR	Type of loads	Highlights of control strategies
[45], [46]	PRFR and SCFR	Type III	(1) A simplified dynamic VSHP model is developed. (2) A proportional-integral controller is applied to adjust the power consumption of VSHPs, emulating the PRFR and SCFR of generators.
[53]-[55]	PRFR	N/A*	(1) When f drops, the aggregated loads are reduced at each time step to arrest the frequency drop. (2) When f recovers, the loads are gradually switched back on.
[52]	PRFR	N/A	(1) The system frequency response is modeled by state-space equations. (2) LQR algorithm is applied to optimize the dynamic response. (3) An analytical study is made on how DDC enhances system frequency stability.
[58]	PRFR and SCFR	N/A	(1) Two groups of responsive loads participate in PRFR and SFR respectively. (2) The disturbance magnitude ΔP_L (in MW) is estimated by (2.3). (3) Then, the load reductions of two groups are determined by both ΔP_L and Δf.
[59]	PRFR and SCFR	Types I&II	(1) The control strategy is focused on a multi-area system. (2) When frequency drops, ΔP_L is estimated by (2.4). (3) The load reduction is implemented by the proposed fuzzy-PI-based method.

* "N/A" means this paper did not specify which loads are applied to implement DDC.

consumption of Type II loads by modifying their temperature setpoints. Another control algorithm defines an "*f*-time" control region in the Δf-time plane [18], which can be regarded as a "two-dimension threshold". If the coordinate point (Δf, the time duration of Δf) exceeds the rectangular boundary that indicates a sustained under-frequency or over-frequency event, the frequency regulation will be activated and both Type I and Type IIloads will be switched off (or back on). As an extension of [18], the coordination of wind generator and DDC for PRFR is studied in [19]. Other studies [17], [42], [44] also proposed control strategies based on fixed or random frequency setpoint and time delay. Through these demand controls, the maximal frequency deviation is reduced, and the frequency recovery is accelerated after a disturbance event. In [62], however, a frequency-dependent price signal is applied when there is a mismatch between load and generation. Then, the loads can autonomously adjust their behavior as defined by their bid functions. The loading levels are dependent on frequency, while the system welfare remains maximal. At time steps when loads are not used for frequency reserves, the price will be independent of the frequency.

Based on the first-order heat transfer model (as presented in Appendix A), the authors in [63]-[64] proposed decentralized control strategies to make a large number of Type II loads to track the predetermined power profile, $\Pi(t)$, without violating the temperature constraint of [θ_{low}, θ_{high}]. Built upon [64], the authors of [65] proposed two controllers for implementing $\Pi(t)$ for frequency regulation. Furthermore, the controllers were compared by a simulation study of a practical U.K. power system. The result concluded that when generator outages happen, the participation of aggregated loads can significantly promote the frequency nadir, especially in low-inertia regions.

It can be concluded that most of the existing decentralized control strategies share three factors: state (usually 3 or 4 operation states), frequency (frequency thresholds) and time (time delay). Based on these three factors, a general template of the decentralized DDC is summarized in Figure 2.2. The related control parameters are listed in Table 2.2 [7], [18]. Note that in the literatures, some parameters such as f_{OFF} and $T_{delayOFF}$ are required while some parameters such as T_{minOFF} are optional. In addition, either frequency setpoint or time delay can be defined as a uniformly-distributed random variable to achieve a smooth

State 0 (normal operation): load is on

Disturbance occurs

Next time step

f < f$_{OFF}$? — No

Yes

State 1 (contingency): switch off loads with random T$_{delayOFF}$ (Type I) or modify the temperature setpoint (Type II)

T$_{maxOFF}$ expires or f > f$_{ON}$? — No

Yes

State 2 (Load recovery): switch back on loads with random T$_{delayON}$

State 0 (normal operation)
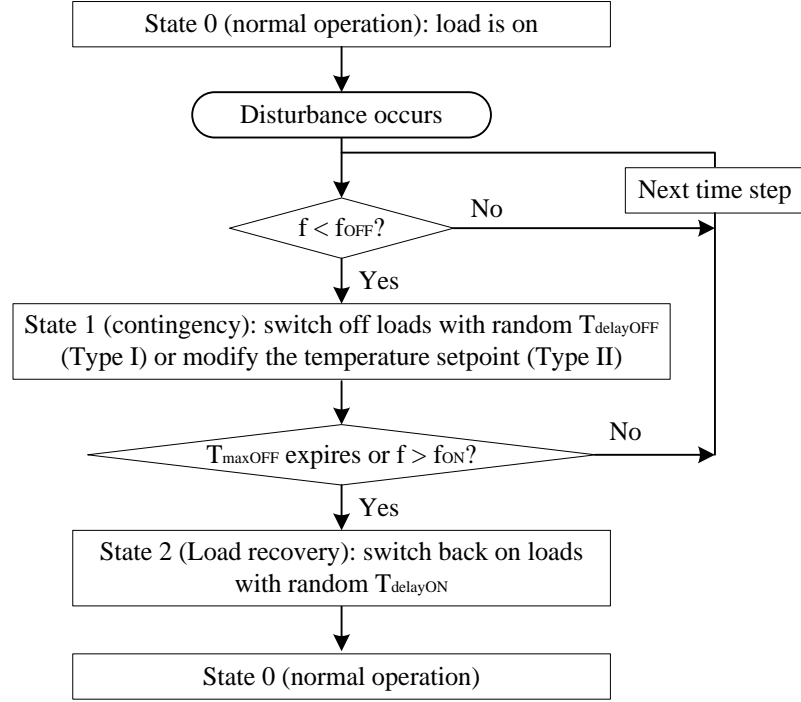
Figure 2.2. A general template of decentralized DDC for primary frequency regulation.

Table 2.2. Load controller parameters.

Parameter	Typical value (F=Fixed; R=Random)	Function description
Frequency setpoint for disconnection, f_{OFF}	F or R	Threshold for switching off (or on) the load or modifying its power rating.
Frequency setpoint for reconnection, f_{ON}	F or R	
Time delay for disconnection, $T_{delayOFF}$	F or R	To avoid the simultaneous response of large amount of loads.
Time delay for reconnection, $T_{delayON}$	F or R	
Minimal disconnection time, T_{minOFF}	F	To avoid the repetitive switch-on/off of loads.
Maximal disconnection time, T_{maxOFF}	F	To avoid loads from staying off for a long time.
Coefficient of frequency change, k_f	F (i.e., 20 ℃/Hz)	To modify the temperature setpoints of Type II loads according to the frequency deviation.

frequency response. Consequently, the aggregated loads can emulate the droop characteristic of turbine governor controls.

Based on the above discussion, we can compare the critical parameters (frequency threshold and time delay) of typical decentralized DDC strategies, as shown in Table 2.3. Note: in some papers Type I and Type II loads are controlled in different ways [7]; while in other papers both type of loads are controlled in an ON/OFF manner instead of modifying the temperature setpoints [18], [44].

In general, most studies in literature adopt residential loads for DDC, in which a load is turned on/off without modifying its supply voltage. According to [67], however, a group of non-critical commercial or industry loads can be exploited to provide frequency regulation if the supply voltage/frequency is controlled by power converters. The combination of a load and its power converter forms a so-called smart load, which can tolerate wide voltage/frequency variations for a short period of time. As shown in Figure 2.3, the system voltage and frequency are V_s and f_s, respectively. The converter can control the supply voltage (V) of static loads and supply frequency (f) of motor loads, respectively, in order to modify their power consumption for frequency regulation. The static loads are mainly lighting loads, while motor loads include Type III load and large water pumps. The commercial and industry loads have considerable frequency reserve due to their regular and predicable power profiles. Since there is no communication among different smart loads, this control is also classified as decentralized control.
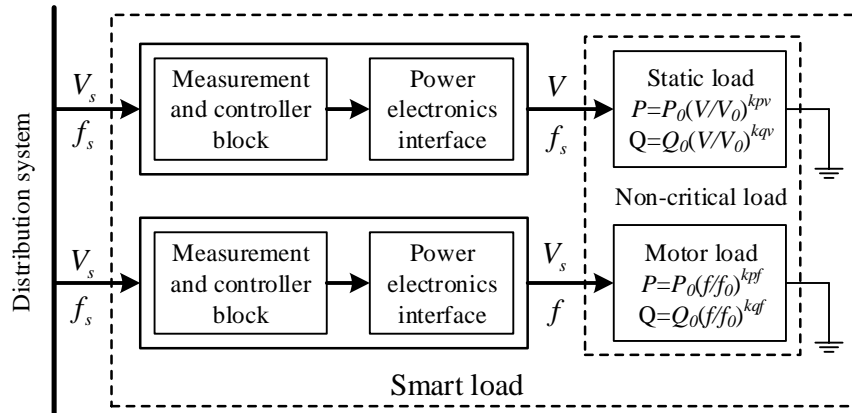
Figure 2.3. Smart load with series-parallel converter.

Table 2.3. Comparison of decentralized DDC algorithms.

Ref. No.	Type of FR	Type of loads	Highlights of control strategies and control parameters
[7]	PRFR	Types I and II	(1) Type I: Random f threshold, $f_{OFF} \leq f_{ON}$, and the controller acts with fixed $T_{delayOFF}$ (2) Type II: Modify θ_{low} and θ_{high} according to (1.5).
[16]	PRFR, SCFR, and TRFR	Type II	Modify θ_{low} and θ_{high} according to (1.5).
[17]	PRFR	Type I	Fixed f threshold, $f_{OFF} = f_{ON}$; and the controller acts with random $T_{delayOFF}$
[18]	PRFR	Types I and II	For both types of loads: (1) Fixed f threshold for one type of load, and $f_{OFF} = f_{ON}$; different f thresholds for different types of loads. (2) T_{minOFF} is introduced to avoid repetitive activation of loads
[44]	PRFR and SCFR	Types I and II	For both types of loads: (1) Fixed f threshold, $f_{OFF} < f_{ON}$, and the controller acts with random $T_{delayOFF}$ (2) f thresholds are different for Type I&II. Type I loads deal with severe f disturbances while Type II loads deal with small disturbances.
[66]	PRFR and SCFR	Type II	(1) Fixed frequency derivative (f') threshold for determining whether to activate the controller. (2) The amount of load reduction is determined by random switching with the computed probability.

2.1.3 *Hybrid control*

Hybrid control was proposed in [68]-[71], combining the advantages of centralized and decentralized controls to some degree. The first hybrid control scheme is the "centralized parameter-setting, decentralized decision-making" control. In [68]-[69], a hybrid DDC was designed for PRFR and SCFR. The individual load controller measures the system frequency and makes the switch ON/OFF decision, which is similar to the decentralized control. The control parameters (e.g., f_{OFF} and $T_{delayOFF}$) can be updated by the control center instead of being permanently programmed in the individual controller. The control center monitors the ON/OFF states of responsive loads and computes the control parameters. The main advantage of the hybrid control method is that the communication bit-rate requirement is much lower than in the centralized control method.

The second hybrid control scheme is hierarchical control, also called distributed control [70]-[71]. A load aggregator controls hundreds of or thousands of loads in a centralized way, while the multiple load aggregators are controlled in a distributed way. The aim of this control is to ensure the equal participation of different load aggregators, which means that each load aggregator shares the same load increase/reduction ratio (μ) with respect to its $P_{RL,avai}(t)$ [71]. The parameter μ is initialized by the leader load aggregator (also called "virtual leader") and communicated from one aggregator to another, as shown in Figure 2.1 (c). For example, three load aggregators have a responsive load capacity of 1.0, 1.5 and 2.0 MW respectively. When an under-frequency disturbance occurs, the control center determines that 1.8 MW of load reduction is needed. Then, each aggregator shares the same ratio 1.8/(1.0+1.5+2.0)=40% and reduces its load at the amount of 0.4, 0.6 and 0.8 MW, respectively.

The hybrid DDC strategy for coordinating the operation of multiple load aggregators was discussed in [71]. Taking the single-area case as an example, a general transfer function model is shown in Figure 2.4. A state-space equation can be derived, given by (2.5):
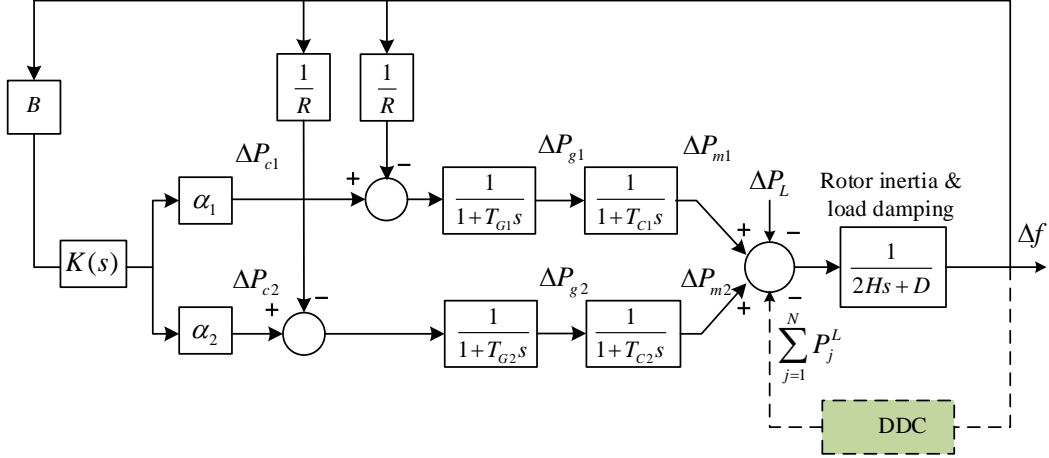
Figure 2.4. Single-area LFC system model.

$$\begin{cases} \Delta \dot{f} = -\dfrac{D}{2H}\Delta f + \dfrac{1}{2H}\left(\displaystyle\sum_{i=1}^{2}\Delta P_{mi} + \sum_{j=1}^{N}\Delta P_{j}^{L} - \Delta P_{L}\right) \\[4mm] \Delta \dot{P}_{mi} = -\dfrac{1}{T_{Ci}}\Delta P_{mi} + \dfrac{1}{T_{Ci}}\Delta P_{gi} \\[4mm] \Delta \dot{P}_{gi} = -\dfrac{1}{T_{Gi}}\Delta P_{gi} + \dfrac{1}{T_{Gi}}\left(\Delta P_{ci} - \dfrac{1}{R_{i}}\Delta f\right) \end{cases} \qquad (2.5)$$

where ΔP_{j}^{L} is the load reduction of the *j*-th aggregator, and other parameters are defined in Section 2.1. Note: (2.5) can also be expressed in a matrix form [71], which is omitted here for simplicity. For a multiple-area control model, the tie-line power should also be considered as a control variable [1]. Then, a series of optimal control algorithms (e.g. pinning control) can be applied to adjust the control gain parameters in every time step [71]. The advantage of distributed control is higher frequency nadir, smaller frequency recovery time, and less activated loads. However, the reliability is a concern because the failure of one communication channel may cause many load aggregators to fail following the ratio μ.

2.2 Techno-Economic Concerns

As reviewed in Section 2.1, the existing research on DDC strategies demonstrated good performance under idealized assumptions. However, if the control strategies were implemented in the real world, several practical concerns would have to be considered because they might degrade the performance of the DDC strategies that work well in the idealized cases. In addition to technical concerns, how DDC participates in ancillary market is also an important research topic. These techno-economic problems are a subject for future works related to DDC.

2.2.1 Technical concerns of DDC application

1) *Communication delay*: The length of time from when a request is made by a control center to when the responsive load receives the request and takes action based on it. With existing Internet infrastructure, a delay of around 500 milliseconds is achievable [53]. It has been proven by both simulation and analytical study that under the same DDC, the system frequency takes a longer time to recover if a communication delay exists [52], [55].

2) *Temperature setpoint adjustment resolution*: For Type II loads, it has been proposed that the thermostat setpoint adjustment ($\Delta\theta_s$) be computed from the frequency deviation (given by (1.5)). However, this assumes that $\Delta\theta_s$ is a continuous variable, which is infeasible for traditional thermostats [50]. One conservative assumption is that the thermostat has a temperature setpoint adjustment resolution, e.g., 0.3ºC or 0.5 ºF. If that is the case, the $\Delta\theta_s$ computed by a DDC algorithm will need to be rounded to integers of its resolution. This may cause considerable errors since the temperature band of controllable HVACs is in a small range, e.g. 3ºC or 5ºF. However, the resolution can be smaller in the future when the commercial thermostats are technically upgraded.

3) *Post-disturbance load recovery and oscillation prevention*: Although much research has focused on switching off responsive loads when a disturbance occurs, the load recovery after a disturbance is cleared or compensated has not been fully explored, especially for Type II loads. Furthermore, although a sudden change to a large number

of HVACs' temperature setpoints can achieve the desired load reduction in a short time [7], [16], long term simulation indicates that the ON/OFF cycles of HVACs tends to synchronize operation cycles, which causes serious power rebound and consequently, frequency oscillation [63]-[64]. Therefore, it is essential to study how to modify the temperature setting of Type II loads to achieve a continuous smooth response.

To summarize, future DDC strategies should be more comprehensive and practical in consideration of the aforementioned technical concerns.

2.2.2   Economic concerns

Similar to generators, DDC is technically able to participate in frequency ancillary service markets [72]-[74]. The implementation of DDC for frequency regulation also involves several marketing and economic issues. Therefore, future works can be extended in the following aspects:

1) *Participation in ancillary service markets*: Due to the small power rating of residential loads, most end users do not directly participate in the ancillary market. Generally, a load serving entity (LSE) aggregates end users and then participates in the market [75], while end users receive a reward by adjusting their loads for frequency regulation whenever needed. Therefore, it is important to design an effective reward mechanism to stimulate end user participation while maintaining an appropriate expense paid by LSEs [76].

2) *Economic evaluation*: In addition to the technical study of DDC, it is also necessary to thoroughly evaluate its economic advantages over conventional frequency control. For an LSE, the long-term expense of implementing DDC consists of two parts: reward payments to customers for their frequency regulation service; and the expense of building control center (for centralized and hybrid control) and installing controllers for end users [75].

3) *Comparison with alternative approach* (*energy storage*): Dynamic control of energy storage units is an alternative way to mitigate the fluctuation of renewable generation as well as regulate system frequency [37]. Some studies suggest that EVs can be

controlled (charge/discharge) in a decentralized way to facilitate system operation [36]. Control methods for energy storage are similar to DDC, but energy storage is more expensive and powerful. It can not only supply electricity to the grid but also absorb the redundant portions of renewables which would otherwise be curtailed. Hence, as it is for frequency regulation, it is recommended to perform a techno-economic comparison of using DDC versus using energy storage for certain application scenarios.

2.2.3 Summary of DDC research scheme

Based on the theoretical analysis discussed in Sections 1.2 and 1.3, and control strategies in 2.1, respectively, we can conclude a general scheme for designing and implementing a DDC strategy, as shown in Figure 2.5. The entire scheme consists of three parts:

- *Input information*: both the power system electric model and the responsive load behavior model should be established;

- *Control strategy*: the traditional generation side control should be considered when verifying DDC strategy; and
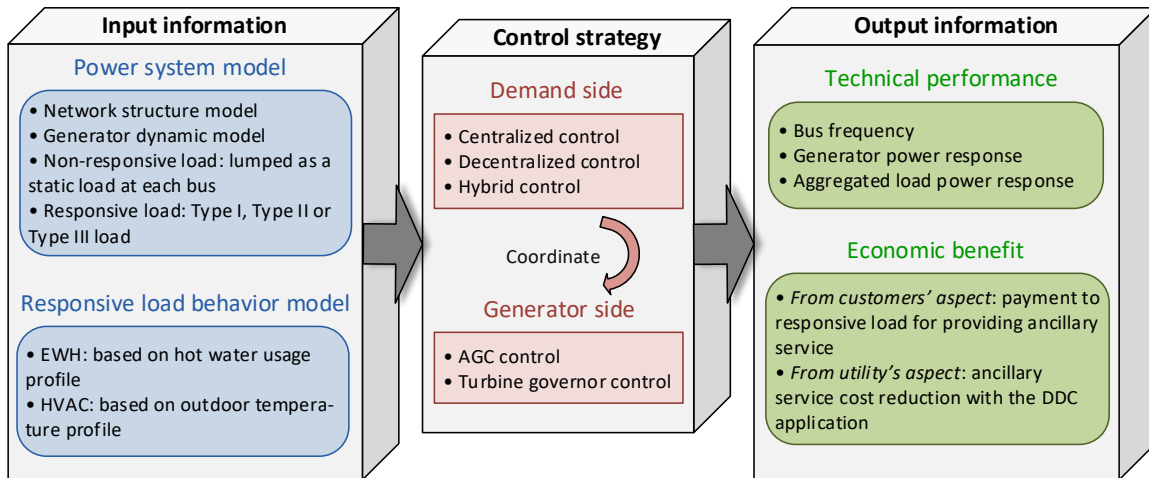
Figure 2.5. Overall scheme of conducting DDC research.

- *Output information*: both technical performance and economic benefit are worth being evaluated.

Overall, the nature of the DDC problem can be summarized as this: to identify the system frequency deviation and to "organize" a large population of responsive loads such that they can emulate a single large generator for frequency regulation. Although the behavior of an individual load is stochastic, thousands of loads can display statistically predictable patterns due to the large population of potential controllable loads. The "control" concept in DDC is different from generator droop control, wind turbine control, etc., in that the control subject is a number of small-scale devices instead of a single, or a limited number of, large devices. The available capacity of response loads should not be a constant value. This feature was not particularly addressed in previous works and should be closely studied in the future for better practical applications.

Chapter 3

Analytical Method to Aggregate Multi-Machine SFR Model with Applications in Power System Dynamic Studies

The SFR model describes the average network frequency response after a disturbance and has been applied to a wide variety of dynamic studies. However, the traditional literature does not provide a generic, analytical method for obtaining the SFR model parameters when the system contains multiple generators. In this chapter, an analytical method is proposed for aggregating the multi-machine SFR model into a single-machine model. The verification study indicates that the proposed aggregated SFR model can accurately represent the multi-machine SFR model. Furthermore, the detailed system simulation illustrates that the SFR model can also accurately represent the average frequency response of large systems for power system dynamic studies. Finally, three applications of the proposed method are explored: system frequency control, frequency stability, and dynamic model reduction.

3.1   Introduction

Power system frequency stability can be challenged by such significant disturbances as a generator unit trip, a sudden heavy load change, or a system islanding event that is caused by a tie-line trip [24]. Following such disturbances, the system frequency experiences a drop, reaches the nadir and then enters a new equilibrium point (f_{nep}) below the nominal value (i.e., 60Hz). During this process, there are several indices for describing the dynamic performance of a system, including the frequency nadir (f_{nadir}), time to reach frequency nadir (t_{nadir}), and rate of change of frequency (RoCoF).

A low-order SFR model is proposed in [25]. The model represents the average response of all generators following a load-generation unbalance. However, the process of computing the equivalent model parameters if the system consists of multiple machines with heterogeneous parameters is not made clear. It is true that system identification is a useful approach if the high-resolution frequency response data is available. Numerical simulation studies and operators' experience can also be applied to obtain the parameters [77]-[78]. However, since the number of integrated generators is always changing due to unit-commitment, the computation workload will be extremely high if we use the system identification method many times. In short, there is a lack of analytical method for aggregating multi-machines to a single-machine SFR model with high accuracy, which is the initial motivation for this research work.

The SFR model can be applied to a wide variety of studies related to power system dynamics, as follows:

1) *Demand response for frequency regulation:* References [79]-[81] evaluate the impact of under-frequency load shedding (UFLS) on the frequency response based on a multi-machine SFR (MM-SFR) model. Compared with a severe disturbance that triggers the UFLS, frequency control strategies deal with smaller frequency disturbances. It has been proposed that DDC participate in frequency regulation [45], [52], [71], [82], [83]. Based on the MM-SFR model, a state-space equation has been established and a robust control algorithm adopted to optimize the frequency response [71]. In a system with many generators, however, the state-space equation is of high order due to the presence of a large number of machines. This situation challenges the implementation of the frequency regulation algorithms because online computation is required.

2) *Frequency stability analysis:* In recent years, some conventional generators have been replaced by renewable energy sources, which lower system mechanical inertia and capability of frequency regulation [84]-[88]. In particular, with the same amount of generation outage, f_{nadir} will be lower and closer to the UFLS threshold [89]. The maximum renewable energy source penetration should be determined based on the system frequency security criterion [90]. The SFR model can provide a fast and straightforward tool for conducting this study.

3) *Coherency-based dynamic model reduction*: In industry applications, power utilities usually employ the reduced model instead of the full model for dynamic security assessment. For instance, the widely-used 179-bus Western Electricity Coordinating Council (WECC) system is reduced from the original 10,000+ bus transmission system based on the concept of coherency and generator aggregation. The dynamic model reduction involves the aggregation of turbine governors. The proposed method is an effective tool for this task.

To summarize, we desire to aggregate the MM-SFR model into a single-machine model, which is called an aggregated SFR (ASFR) model, this will make it more convenient to implement the above studies.

In addition, SFR is a simplification of the detailed power system model, which consists of exciters, synchronous generators, network topology, and ZIP loads. Therefore, it is reasonable that the frequency output of the SFR model contains some errors. First, inter-machine frequency oscillation exists in the multi-machine system [91]. Second, the exciter's voltage control and voltage-dependent loads can also affect frequency response [92]. Following from these factors, the frequency response of the SFR model has some error if compared with that of the detailed system model. This issue has not been thoroughly discussed in the previous works such as [25] or [93]. It is necessary to conduct a comprehensive analysis on the accuracy of the SFR model for representing the detailed system. This also provides the theoretical foundation for the aforementioned research topics.

Based on the above discussions and motivations, this chapter proposes an ASFR model and verifies it by large-scale system simulation. The model is an extension of P. M. Anderson's work in [25] and is helpful in power system dynamic studies.

3.2 Description of Inter-Machine Oscillation

This section provides an overview of inter-machine oscillation, which describes the dynamic behaviors of multiple generators that are caused by a system's sudden power unbalance. The theory is described in [91]. An understanding of this theory is helpful to evaluate the accuracy of the ASFR model that is proposed in later sections.

At any instant, the electric power produced by the generators should be equal to the power consumed by the load. When a disturbance (e.g., a large generator outage) occurs, a power unbalance is formed between generation and network consumption. However, the RoCoF of each generator is not identical because each one covers different portions of the power unbalance.

3.2.1 Swing equation of a single machine

The swing equation (1.1) was introduced in Section 1.2.1. It is recalled here.

$$2H \frac{d\Delta f(t)}{dt} + D\Delta f(t) = \Delta P_m(t) - \Delta P_d(t) \tag{3.1}$$

3.2.2 Equivalent parameter of multi-machine system

In the multi-machine system, the frequency response of each generator is not necessarily identical. Therefore, to derive a swing equation for the system, we should define an equivalent generator that reflects the average behavior of all the generators. This generator is called the center of inertia (COI) [94]-[95]. According to the definition of the inertia constant, the individual inertia constant with respect to the system rated power is

$$H_{i,sys} = H_i \cdot \frac{S_i}{\sum_{j=1}^{N} S_j} = H_i \cdot \frac{S_i}{S_{sys}} \tag{3.2}$$

where S_i is the rated apparent power of the generator #i, and S_{sys} is the sum of the system installed generation capacity:

$$S_{sys} = \sum_{j=1}^{N} S_j \tag{3.3}$$

By applying the procedure that is given in [91], the COI frequency (f_{COI}) is given as follows [95]-[96]:

$$f_{COI} = \frac{\sum_{i=1}^{N} f_i H_{i,sys}}{\sum_{i=1}^{N} H_{i,sys}} \tag{3.4}$$

3.2.3   *Power unbalance at t = 0$^+$*

Immediately after the moment of the disturbance (at $t=0^+$), the turbine governor control has not yet taken effect. The power unbalance is distributed among the generators according to their synchronizing power coefficients (P_{sij}) [91]. As is shown in Figure 3.1, at $t = 0$, the disturbance ΔP_L at Bus k causes a change of the voltage phasor at Bus i. Then,

$$\Delta P_{di}(0^+) = \frac{P_{sik}}{\displaystyle\sum_{j=1}^{N} P_{sjk}} \cdot \Delta P_L \tag{3.5}$$

where $\Delta P_{di}(0^+)$ is the power unbalance share of generator i. The coefficient P_{sik} is defined as

$$P_{sik} = V_i V_k (B_{ik} \cos \delta_{ik0} - G_{ik} \sin \delta_{ik0}) \tag{3.6}$$

where V_i and V_k are the voltage magnitude of bus i and k, respectively. B_{ik} and G_{ik} are the real and imaginary parts of the admittance between bus i and k. δ_{ik0} is the pre-disturbance angle difference between bus i and k. For each generator, substituting (3.5) into (3.1), we can find the initial RoCoF [91]:

$$2H_i \frac{d\Delta f_i(0^+)}{dt} = -\Delta P_{di}(0^+) \tag{3.7}$$
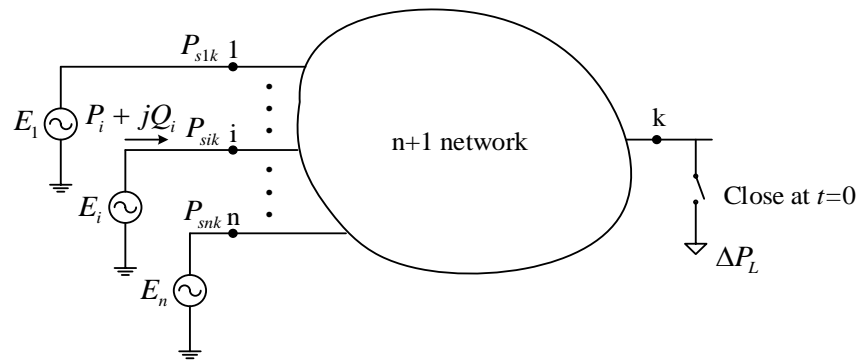
Figure 3.1. Network with power unbalance at bus k [91].

According to (3.6), the machines that have a smaller electrical distance from the point of disturbance will pick up the greater share of the power unbalance ΔP_L due to its larger admittance. Consequently, the closer generators will have larger RoCoF at the instant the disturbance occurs.

3.2.4 *Oscillation and power unbalance after t = 0$^+$*

During a very short period after $t=0^+$, the impact of the turbine governor control is negligible. Each generator shares ΔP_{sys} according to its inertia. Then, the share of power unbalance is determined by (3.8) [91]:

$$\Delta P_{di}(t) = \frac{H_i}{\sum_{i=1}^{N} H_i} \cdot \Delta P_L \tag{3.8}$$

For a generator, $\Delta P_{di}(t)$ is not necessarily equal to $\Delta P_{di}(0^+)$ because its P_{sik} and H_i may take different portions of the entire system parameter. Thus, right after 0^+, the power unbalance share of generator i gradually changes from $\Delta P_{di}(0^+)$ to $\Delta P_{di}(t)$. In this process, the generators may exchange real power with each other, which is called inter-machine oscillation [97]. After several seconds, the oscillation decays and the frequency at all buses gradually becomes identical [91].

3.3 Single-machine SFR Model

The complete SFR model is presented in Figure 3.2 (a). The parameters are listed in Table 3.1 [24], [25], [98]. Since T_G and T_C are much smaller than T_R, we can simplify the SFR model by neglecting these two parts [25]. Then, the low-order SFR model is shown in Figure 3.2 (b). The frequency deviation in s-domain is given by (3.9) [25]:

$$\Delta f(s) = \frac{R\omega_n^2}{DR + K_m} \cdot \frac{\left(1 + F_H T_R s\right)\Delta P}{s\left(s^2 + 2\zeta\omega_n s + \omega_n^2\right)} \tag{3.9}$$

where the natural oscillation frequency ω_n and the damping ratio ζ are calculated from the SFR model parameters:

(a) Full-order model

(b) Low-order model
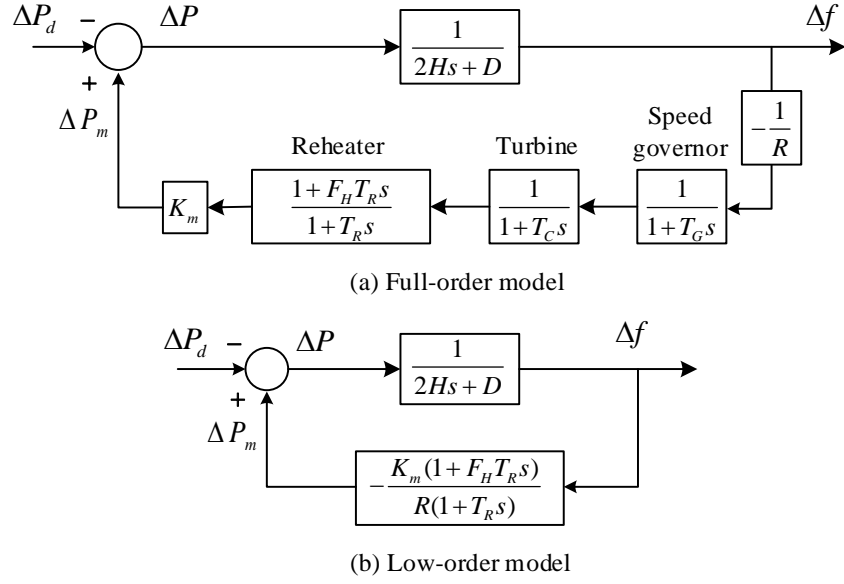
Figure 3.2. Single-machine SFR transfer function model.

Table 3.1. Typical ranges of SFR model parameters.

Parameter	Typical value
Governor time constant T_G	0.15~0.3 s
Steam chest time constant T_C	0.2~0.5 s
Reheat time constant T_R	6~14 s
High-pressure turbine fraction F_H	0.15~0.4
Inertia constant H	3~9 s
Governor speed regulation R	0.04~0.1
Load damping factor D	0~2%

$$\omega_n^2 = \frac{DR+1}{2HRT_R}$$

$$\varsigma = \frac{2HR+\left(DR+F_H\right)T_R}{2\left(DR+1\right)}\omega_n$$

(3.10)

The time-domain frequency deviation, Δf (= $f - f_{rated}$), is obtained by inverse Laplace transform:

$$\Delta f(t) = \frac{R\Delta P}{DR+1}\cdot\left[1+ae^{-\varsigma\omega_n t}\sin\left(\omega_r t+\varphi\right)\right]$$

(3.11)

where the damped frequency ω_r, and coefficients a, φ are given by (3.12):

$$a = \sqrt{\frac{1 - 2T_R \varsigma \omega_n + T_R^2 \omega_n^2}{1 - \varsigma^2}}$$

$$\omega_r = \omega_n \sqrt{1 - \varsigma^2} \quad (\varsigma < 1) \tag{3.12}$$

$$\varphi = \varphi_1 + \varphi_2 = \tan^{-1}\left(\frac{\omega_r T_R}{1 - \varsigma \omega_n T_R}\right) + \tan^{-1}\left(\frac{\sqrt{1 - \varsigma^2}}{\varsigma}\right)$$

Then, the frequency derivative is obtained:

$$f'(t) = \frac{d\Delta f(t)}{dt} = -\frac{R\Delta P}{DR + 1} \cdot a\omega_n e^{-\varsigma \omega_n t} \sin(\omega_r t + \varphi_1) \tag{3.13}$$

At the frequency nadir, the derivative of the frequency curve should be 0, as shown in Figure 3.3. In other words, at f_{nadir}, we should have the very first instance of $f'(t) = 0$. Therefore, t_{nadir} can be solved by

$$t_{nadir} = \frac{1}{\omega_r} \tan^{-1}\left(\frac{\omega_r T_R}{\varsigma \omega_n T_R - 1}\right) \tag{3.14}$$

Thus, substituting (3.14) to (3.11) gives the frequency deviation. Since $\Delta f_{nadir} = f_{nadir} - f_{rated}$, we have

$$\Delta f_{nadir} = \frac{R\Delta P}{DR + 1} \cdot \left[1 + \sqrt{1 - \varsigma^2} \, a e^{-\varsigma \omega_n t_{nadir}}\right] \tag{3.15}$$

Also, the steady-state frequency deviation of the new equilibrium is

$$\Delta f_{nep} = \frac{R\Delta P}{DR + K_m} \approx \frac{R\Delta P}{DR + 1} \tag{3.16}$$
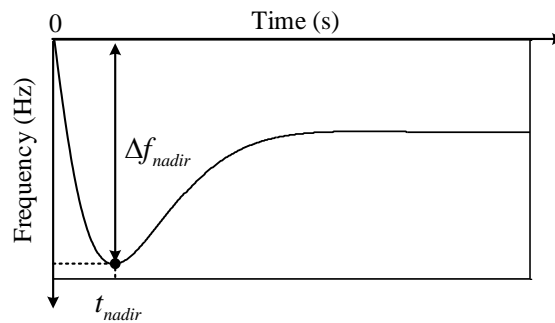
Figure 3.3. Frequency response after step disturbance.

Therefore, the frequency nadir can be calculated by (3.15) instead of performing the time-domain simulation. It clearly indicates that Δf_{nadir} and Δf_{nep} are proportional to ΔP. In a practical system, however, the premise of making use of (3.13)-(3.16) is that the multiple machines with various parameters can be aggregated to a single machine.

3.4 Analytical Method to Aggregate SFR Model

Based on the works in [25], this section demonstrates how to aggregate the MM-SFR model to the ASFR model. The method is validated by the mathematical proof.

3.4.1 Formulation of the ASFR model

In Figure 3.4 (a), the droop value R_i is correlated to S_i (after reaching the steady state, $\Delta P_{mi}=S_i \cdot \Delta f/R_i$). The multiple turbine governors are also summed up with a constant gain $K_{mi}=S_i/S_{sys}$, which represents the portion of rated power of machine i with respect to the whole system. The equivalent droop value R is given by (3.17) [24]:

(a) Multi-machine model

(b) Aggregated single-machine model
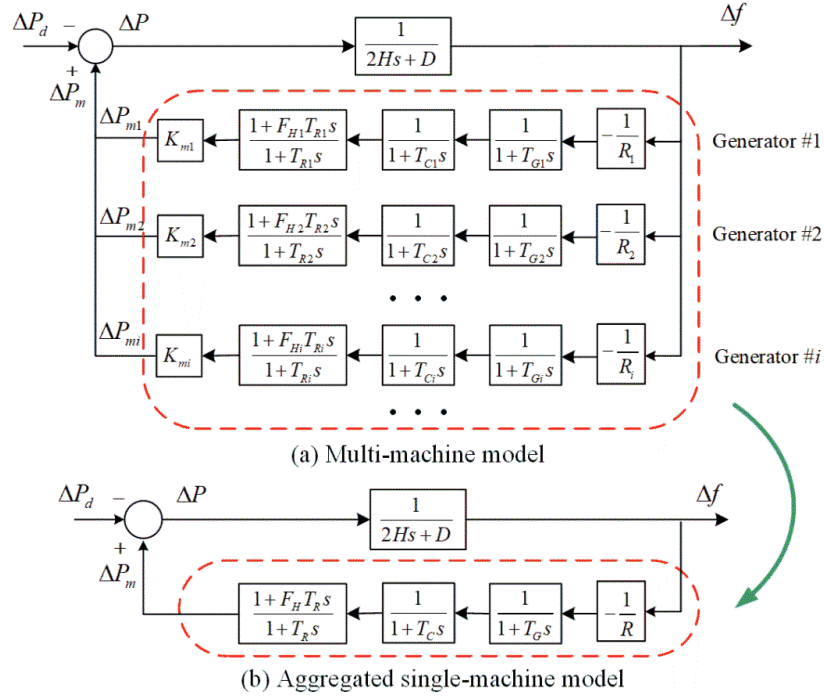
Figure 3.4. Aggregation of SFR model.

$$\frac{1}{R} = \sum_{i=1}^{N} \frac{K_{mi}}{R_i} = \sum_{i=1}^{N} \kappa_i \tag{3.17}$$

where the equivalent gain is defined as $\kappa_i = K_{mi}/R_i$. In the ASFR model (shown in Figure 3.4 (b)), the four equivalent parameters (T_G, T_C, T_R and F_H) represent the combined effect of N turbine governors. To simplify the description, we define the normalized gain λ_i of each branch in Figure 3.4 (a).

$$\lambda_i = \kappa_i \Big/ \sum_{i=1}^{N} \kappa_i \tag{3.18}$$

$$\sum_{i=1}^{N} \lambda_i = 1 \tag{3.19}$$

According to the red dashed blanket in Figure 3.4, the transfer function of a single machine can represent that of multiple machines. Then, (3.20) can be deducted (the detail is presented in Appendix A).

$$\sum_{i=1}^{N} \lambda_i \frac{1 + F_{Hi}T_{Ri}s}{(1 + T_{Gi}s)(1 + T_{Ci}s)(1 + T_{Ri}s)} = \frac{1 + F_H T_R s}{(1 + T_G s)(1 + T_C s)(1 + T_R s)} \tag{3.20}$$

Traditionally, the parameters $X = \{T_G,\ T_C,\ F_H,\ T_R\}$ can be obtained by system identification [77]. The principle of system identification is to find the optimal X, with the objective that the equivalent machine output approximates the output of all machines as closely as possible, if the same Δf is input [77]. This paper, however, proposes an analytical method for calculating X. Since a larger λ_i value means that generator #i has a larger rated power and more sensitive frequency droop, it has a larger impact on the equivalent X. Therefore, it is reasonable to guess that the ASFR model parameters are equal to the weighted average of those of each machine:

$$X = \sum_{i=1}^{N} \lambda_i X_i \tag{3.21}$$

The following sections will prove that the ASFR model parameters can be calculated by (3.21) with high accuracy.

To simplify the proof work, the transfer function is split into two parts with proper coefficients A_R and A_G. It can be verified in Appendix A that the error of this representation is not significant:

$$\frac{1+F_{Hi}T_{Ri}s}{(1+T_{Gi}s)(1+T_{Ci}s)(1+T_{Ri}s)} \approx \frac{A_R(1+F_{Hi}T_{Ri}s)}{1+T_{Ri}s} + \frac{A_G}{(1+T_{Gi}s)(1+T_{Ci}s)} \tag{3.22}$$

Therefore, (3.20) is also split into equations, given by (3.23) and (3.24). We only need to prove that both of the two equations are valid.

$$\sum_{i=1}^{N} \lambda_i \frac{1+F_{Hi}T_{Ri}s}{1+T_{Ri}s} = \frac{1+F_H T_R s}{1+T_R s} \tag{3.23}$$

$$\sum_{i=1}^{N} \lambda_i \frac{1}{(1+T_{Gi}s)(1+T_{Ci}s)} = \frac{1}{(1+T_G s)(1+T_C s)} \tag{3.24}$$

3.4.2   *Mathematical validation*

In this paper, (3.23) and (3.24) are proven by the *mathematical induction method*, which consists of two steps.

1) Two-machine case: The first step is to consider the simplest case, $N=2$. The problem is formulated as: proving the magnitudes of the error functions $e_R(s)$ and $e_G(s)$ are negligible, where $e_R(s)$ is defined as

$$e_R(s) = \lambda_1 \frac{1+F_{H1}T_{R1}s}{1+T_{R1}s} + \lambda_2 \frac{1+F_{H2}T_{R2}s}{1+T_{R2}s} - \frac{1+F_H T_R s}{1+T_R s} = \frac{P_R(s)}{Q_R(s)} \tag{3.25}$$

where

$$\frac{P_R(s)}{Q_R(s)} = \frac{a_3 s^3 + a_2 s^2 + a_1 s + a_0}{b_3 s^3 + b_2 s^2 + b_1 s + b_0}$$

Similarly, $e_G(s)$ is defined as

$$e_G(s) = \lambda_1 \frac{1}{1+T_{G1}s} + \lambda_2 \frac{1}{1+T_{G2}s} - \frac{1}{1+T_G s} = \frac{P_G(s)}{Q_G(s)} \tag{3.26}$$

where

$$\frac{P_G(s)}{Q_G(s)} = \frac{c_2 s^2 + c_1 s + c_0}{d_3 s^3 + d_2 s^2 + d_1 s + d_0} \tag{3.27}$$

First, we analyze the frequency characteristic of $e_R(s)$. Expanding $P_R(s)$ gives the expression of polynomial coefficients a_i ($i = 0, 1, 2, 3$). Based on (3.19) and (3.21) in $N = 2$ case, we can simplify the expression of a_i (the detailed deduction is presented in Appendix A). Then, we have

$$a_0 = a_3 = 0 \tag{3.28}$$

Two non-zero terms are a_1 and a_2. Although they depend on the turbine governor parameters, we can determine their upper bound and compare them with b_1 and b_2.

$$a_1 = \lambda_1 \lambda_2 (F_{H1} - F_{H2})(T_{R1} - T_{R2}) \tag{3.29}$$

Obviously, $|a_1|$ is proportional to two terms $|F_{H1} - F_{H2}|$ and $|T_{R1} - T_{R2}|$. Since

$$\lambda_1 \lambda_2 \leq \left(\frac{\lambda_1 + \lambda_2}{2}\right)^2 = 0.25 \tag{3.30}$$

The upper bound of $|a_1|$ is determined:

$$\begin{aligned}
|a_1| &= |\lambda_1 \lambda_2 (F_{H1} - F_{H2})(T_{R1} - T_{R2})| \\
&\leq 0.25 \cdot |0.4 - 0.15| \cdot |14 - 6| \\
&= 0.5
\end{aligned} \tag{3.31}$$

The expression of a_2 is the most complex one. We can determine its upper-bound by amplifying the expression:

$$a_2 \leq 0.25 \cdot (T_{R1} - T_{R2})^2 = 0.25 \cdot (14 - 6)^2 = 16 \tag{3.32}$$

Expanding $Q_R(s)$ gives the expression of polynomial coefficients b_i ($i = 0, 1, 2, 3$).

$$\begin{aligned}
b_3 &= T_{R1} T_{R2} T_R \\
b_2 &= T_{R1} T_R + T_{R2} T_R + T_{R1} T_{R2} \\
b_1 &= T_{R1} + T_{R2} + T_R \\
b_0 &= 1
\end{aligned} \tag{3.33}$$

Equations (3.31)-(3.33) indicate that a_1, a_2 are more sensitive to $|F_{H1}-F_{H2}|$ and $|T_{R1}-T_{R2}|$ than b_1, b_2. Therefore, the "worst case" that maximizes the ratios $|a_1/b_1|$ and $|a_2/b_2|$ is: $\lambda_1=\lambda_2=0.5$, meanwhile $|F_{H1}-F_{H2}|$ and $|T_{R1}-T_{R2}|$ reaches the maximum. For example, $T_{R1}=14$, $T_{R2}=6$, and $F_{H1}=0.4$, $F_{H2}=0.15$. Then, we have $T_R = 10$ and $F_H = 0.28$. The ratios can be estimated by

$$\left|\frac{a_1}{b_1}\right| \leq \frac{0.5}{6+14+10} = 0.025 \tag{3.34}$$

$$\left|\frac{a_2}{b_2}\right| \leq \frac{16}{6\cdot14+6\cdot10+14\cdot10} = 0.056 \tag{3.35}$$

Equations (3.34) and (3.35) indicate that the magnitude of the error function is much smaller than 1. Then, we define the per-unit error function $e_{R,pu}(s)$, which means the error of ΔP_m that is caused by the ASFR model.

$$e_{R,pu}(s) = \frac{e_R(s)}{\Delta P_m(s)} = \frac{e_R(s)}{\lambda_1 \dfrac{1+F_{H1}T_{R1}s}{1+T_{R1}s} + \lambda_2 \dfrac{1+F_{H2}T_{R2}s}{1+T_{R2}s}} \tag{3.36}$$

Let $s = j\omega$, where ω is the oscillation frequency in rad/s. The frequency characteristic of $e_{R,pu}(s)$ is calculated for discrete values of frequency from 0.01-1Hz, as presented in Figure 3.5. The damped frequency ω_r of the SFR model is usually less than 0.5rad/s ($\approx$0.08Hz) [25]. Therefore, the magnitude of $e_{R,pu}(s)$ is less than 5.5% according to Figure 3.5. However, the magnitude of $e_{R,pu}(s)$ will significantly decrease if $|F_{H1} - F_{H2}|$ and $|T_{R1} - T_{R2}|$ become smaller. Therefore, the "$N=2$" case of (3.23) is proven.

Second, we analyze the frequency characteristic of $e_G(s)$ in a similar way. In $P_G(s)$, the only non-zeros term is c_2. The upper bound is

$$\begin{aligned} \left|\frac{c_2}{d_2}\right| &\leq \frac{0.25(T_{G1}-T_{G2})^2}{T_{G1}T_{G2} + T_{G1}T_G + T_{G2}T_G} \\ &< \frac{0.25\cdot(0.15-0.3)^2}{0.15\cdot0.3+0.15\cdot0.225+0.3\cdot0.225} \\ &= 0.038 \end{aligned} \tag{3.37}$$
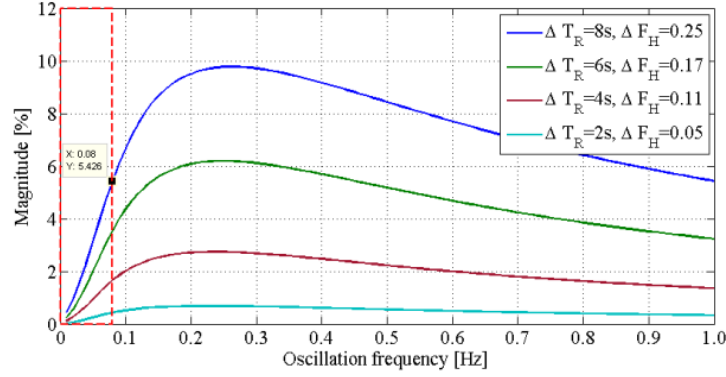
Figure 3.5. Frequency characteristic of $e_{R,pu}(s)$.

Therefore, we can approximately consider that the upper bound of the error function $|e_G(s)|$ is determined by $|T_{G1} - T_{G2}|$. Then, the following equation is proven:

$$\lambda_1 \frac{1}{1+T_{G1}s} + \lambda_2 \frac{1}{1+T_{G2}s} = \frac{1}{1+T_G s} \tag{3.38}$$

Similarly, we have

$$\lambda_1 \frac{1}{1+T_{C1}s} + \lambda_2 \frac{1}{1+T_{C2}s} = \frac{1}{1+T_C s} \tag{3.39}$$

Since the transfer function of two series-connected inertia elements is a linear combination of them, given by (3.40), equation (3.24) is also proven.

$$\frac{1}{(1+T_G s)(1+T_C s)} = \frac{1}{T_G - T_C}\left(\frac{T_G}{1+T_G s} - \frac{T_C}{1+T_C s}\right) \tag{3.40}$$

Based on the above analysis, (3.21) is proven for the "$N=2$" case.

2) Multi-machine case: The second step is to prove the multiple-machine case. The main idea is to "merge" the machines one by one. Here we take the parameter T_R as an example for illustrating the method. As is shown in Figure 3.6, assume the former k machines can be aggregated into an equivalent machine:

$$T_{R,\Sigma k} = \sum_{i=1}^{k} \lambda_i T_{Ri} = \sum_{i=1}^{k} \frac{\kappa_i}{\kappa_{\Sigma k}} T_{Ri} \tag{3.41}$$
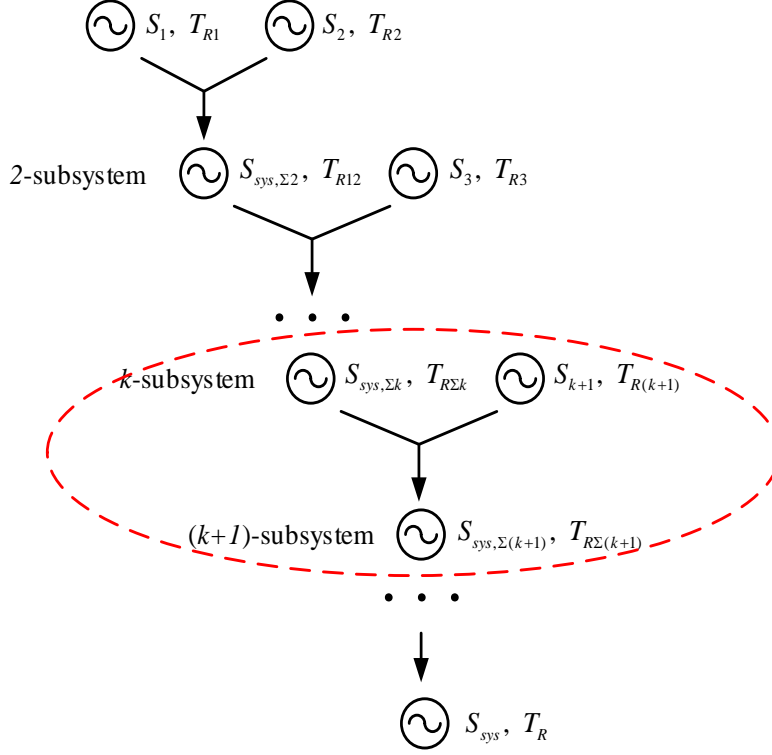
Figure 3.6. Flowchart of aggregating the time constant.

Then, we target to prove that the $(k+1)$-th machine can also be merged into this equivalent machine:

$$T_{R,\Sigma(k+1)} = \sum_{i=1}^{k+1} \lambda_i T_{Ri} = \sum_{i=1}^{k} \frac{\kappa_i}{\kappa_{\Sigma(k+1)}} T_{Ri} \tag{3.42}$$

If a system consists of N machines, we assume that the former k $(k<N)$ machines have been merged as a k-th equivalent machine. If we consider this as the "k-subsystem" of the entire system, then the subsystem base power is defined as

$$\kappa_{\Sigma k} = \sum_{i=1}^{k} \kappa_i \tag{3.43}$$

If the $(k+1)$-th machine is merged, the resulting "$(k+1)$-subsystem" consists of two parts: the previous k-subsystem and the $(k+1)$-th machine, shown in the red dashed circle of Figure 3.6. Then, the base power of the $(k+1)$-subsystem is updated. The equivalent gain κ_i with respect to the $(k+1)$-subsystem is determined as

$$\lambda_{\Sigma k} = \frac{\kappa_{\Sigma k}}{\kappa_{\Sigma(k+1)}} = \frac{\kappa_{\Sigma k}}{\kappa_{\Sigma k} + \kappa_{k+1}}$$

$$\lambda_{k+1} = \frac{\kappa_{k+1}}{\kappa_{\Sigma(k+1)}} = \frac{\kappa_{k+1}}{\kappa_{\Sigma k} + \kappa_{k+1}} \tag{3.44}$$

Based on (3.44), the equivalent reheat time constant of the $(k+1)$-subsystem can be deducted:

$$
\begin{aligned}
T_{R,\Sigma(k+1)} &= \lambda_{\Sigma k} T_{R,\Sigma k} + \lambda_{k+1} T_{R(k+1)} \\
&= \frac{\kappa_{\Sigma k}}{\kappa_{\Sigma k} + \kappa_{k+1}} \sum_{i=1}^{k} \lambda_i T_{Ri} + \frac{\kappa_{k+1}}{\kappa_{\Sigma k} + \kappa_{k+1}} T_{R(k+1)} \\
&= \frac{\kappa_{\Sigma k}}{\kappa_{\Sigma k} + \kappa_{k+1}} \sum_{i=1}^{k} \left(\frac{\kappa_i}{\kappa_{\Sigma k}} T_{Ri} \right) + \frac{\kappa_{k+1}}{\kappa_{\Sigma k} + \kappa_{k+1}} T_{R(k+1)} \\
&= \sum_{i=1}^{k} \left(\frac{\kappa_i}{\kappa_{\Sigma k} + \kappa_{k+1}} T_{Ri} \right) + \frac{\kappa_{k+1}}{\kappa_{\Sigma k} + \kappa_{k+1}} T_{R(k+1)} \\
&= \sum_{i=1}^{k+1} \left(\frac{\kappa_i}{\kappa_{\Sigma(k+1)}} T_{Ri} \right) \\
&= \sum_{i=1}^{k+1} \lambda_i T_{Ri}
\end{aligned}
\tag{3.45}
$$

By following similar steps until $k+1 = N$, all the machines are then merged into one equivalent machine. Therefore, (3.21) is proven for any N value because it can satisfy (3.20) with considerable accuracy. In the same way, other parameters F_H, T_G and T_C of the ASFR model can be proven.

Admittedly, each merging step can cause errors. After many steps of merging, we have $\lambda_{\Sigma k} \gg \lambda_{k+1}$. According to (3.31) and (3.32), a_1 and a_2 will be very small and $X_{R(k+1)}$ will not fluctuate much in each merging step. Then, the accumulative error will finally converge. Although it is impossible to accurately estimate the upper-bound of the error, this section provides a method to illustrate which is the "worst case" that results in the maximal ΔP_m error. In the next section, the maximal error can be simulated to verify the accuracy of the proposed model.

3.4.3 Discussions on the SFR model

The SFR model is mainly based on turbine governor control, which modifies the mechanical power output of the prime mover according to the rotor-angle speed deviation. Overall, the SFR model extracts the turbine governor and frequency-dependent load from the detailed power system. It neglects those elements that do not directly affect the generator mechanical power output, including the exciter, synchronous generator, and voltage-dependent loads. The SFR model can be used to analyze the dynamic behavior of multi-machine systems. However, it should be noticed that there are some intrinsic limitations in the SFR model because the following factors are neglected:

- *Turbine governor nonlinearity*: The traditional SFR model is an idealized model which ignores the frequency deadband and maximal turbine governor response. In North America, the frequency deadband is ± 0.03 or ± 0.04 Hz and the maximal response is usually 6% of the generator rated power [99]. For some generators, the percentage of maximal response can be higher due to the operators' setting [100]. Thus, we can add a limiter to the SFR model at the ΔP_m output terminal if a more accurate simulation result is needed.

- *Inter-machine oscillation*: In the MM-SFR model, all the turbine governors are preserved while the inertia constants are aggregated [25]. Also, the network model is ignored. Therefore, the SFR can only represent the average system frequency because the frequency oscillation depends on both the network topology and each generator's inertia constant.

- *The impact of a voltage-dependent load*: The power unbalance causes not only a frequency deviation but also a voltage deviation. These two deviations in turn affect the power consumption of frequency- and voltage-dependent loads. Therefore, neglecting the voltage-dependent load brings a little error to the frequency [92].

- *The impact of network loss variation*: The network loss may also change after a disturbance. Then, ΔP_L slightly differs from the generator outage or load increase amount. Consequently, f_{nep} estimated by the SFR model is slightly different from f_{nep} estimated by the detailed system model.

Based on the above limitations, it can be expected that the dynamic frequency generated by the SFR model may have a little error from the detailed system model, both in a dynamic state and in a steady state. The next section will evaluate through simulation studies whether the errors are significant.

3.5 Simulation Study

The performance of the proposed model is verified in this section. The simulation study will compare three dynamic models, which are named Level 1, 2 and 3, according to the degree of simplification:

- *ASFR model* (*Level 1*): includes an aggregated turbine governor element and the total inertia;

- *MM-SFR model* (*Level 2*): includes turbine governor element and the total inertia;

- *Detailed system model* (*Level 3*): includes network topology, turbine governor, exciter, and a synchronous generator.

The SFR model is simulated by the Matlab-Simulink with a time step of 0.01s, while the detailed system is simulated by the Matlab-based PSAT software package [101].

3.5.1   The ASFR model v.s. MM-SFR model

The MM-SFR and ASFR model are shown in Figure 3.4 (a) and Figure 3.4 (b), respectively. In this section, we verify the proposed aggregation method by simulating a 6-machine system. Since the model parameters X can be any values within the normal range (listed in Table 3.1), we should simulate the worst case that maximizes the frequency nadir error. If a system contains a large number of generators, the distribution pattern of X can be classified into three cases:

Case 1 (Parameter evenly distributed): The parameters are listed in Table 3.2.

Case 2 (Parameter saddleback-shaped distributed): The X value of most machines is close to its upper bound or lower bound. The parameters of a 6-machine system are listed in Table 3.3. For example, the T_R value is close to either 6s or to 14s.

Table 3.2. Parameters of 6-machine SFR model-Case 1*.

Gen. No.	K_m	T_G (s)	T_C (s)	T_R (s)	F_H (pu)	$1/R$	λ
1	0.14	0.20	0.37	10.5	0.28	13.33	0.113
2	0.18	0.12	0.24	9	0.17	10	0.109
3	0.19	0.27	0.41	6	0.23	20	0.230
4	0.22	0.30	0.48	14	0.32	16.67	0.222
5	0.14	0.22	0.36	12	0.39	20	0.169
6	0.13	0.19	0.21	8.5	0.24	20	0.157
Equivalent	1.00	0.231	0.363	10.0	0.278	16.5	1.00

* H=4.96s, D=1.2.

Table 3.3. Parameters of 6-machine SFR model-Case 2*.

Gen. No.	K_m	T_G (s)	T_C (s)	T_R (s)	F_H (pu)	$1/R$	λ
1	0.14	0.16	0.27	6	0.19	13.33	0.113
2	0.18	0.19	0.23	7.5	0.17	10	0.109
3	0.19	0.17	0.22	6.5	0.22	20	0.230
4	0.22	0.24	0.42	12	0.39	16.67	0.222
5	0.14	0.26	0.49	14	0.36	20	0.169
6	0.13	0.29	0.46	13.5	0.35	20	0.157
Equivalent	1.00	0.221	0.355	10.1	0.293	16.5	1.00

* H=4.96s, D=1.2.

Case 3 (Parameter olive-shaped distributed): The *X* value of most machines is close to the average value. According to the analysis in Section 3.4.2, Case 3 is not the worst case because *X* falls within a more narrow range than the other two cases. Thus, the simulation of Case 3 is neglected.

In the bottom row of Table 3.2 and Table 3.3, the equivalent parameters are calculated by equations (3.17), (3.18) and (3.21). In addition, the practical prime movers are classified as "with reheater" and "no reheater" types, which are adopted by different literatures [69], [71]. In this section, we set all T_R and F_H to 0 when simulating the "no reheater" type.

In simulation Case 1, we apply a step disturbance of $\Delta P = 0.05 S_{sys}$ to the 6-machine system and obtain the frequency deviation and mechanical power deviation. Note: the ΔP_m curve of the MM-SFR model is the sum of 6 generators. Figure 3.7 is the comparison of "with reheater" SFR models. Figure 3.8 is the comparison of "no reheater" SFR models.

The same simulation is done for Case 2. The relative errors of Δf_{nadir} and t_{nadir} are defined as
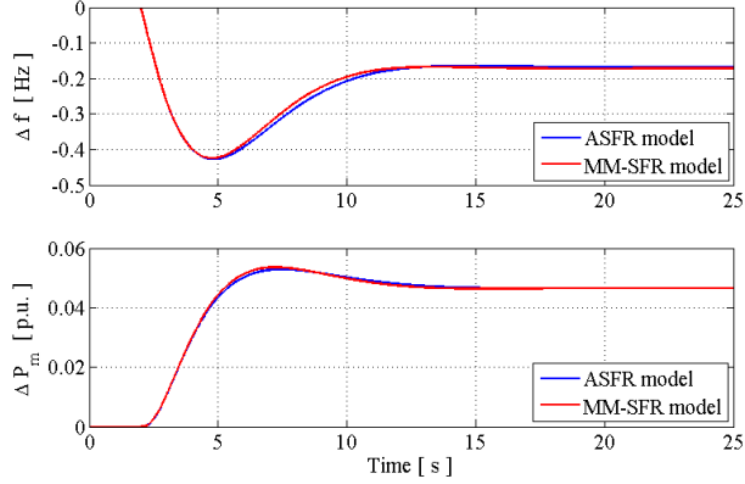
Figure 3.7. Frequency & generation response of the ASFR model of Case 1 (with reheater model).
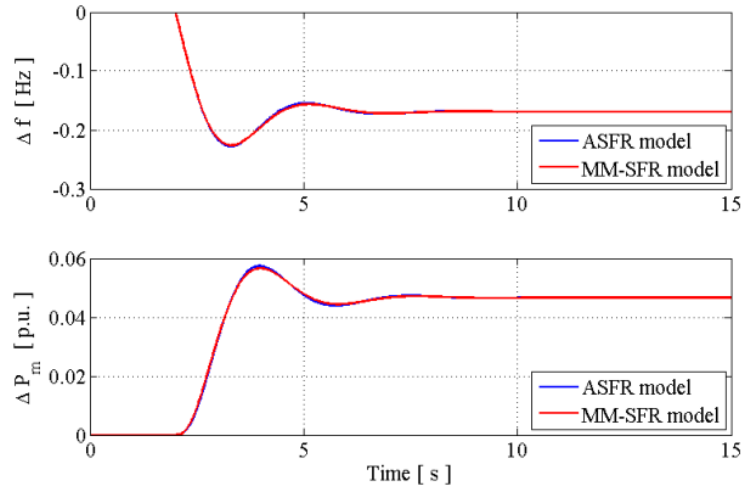
Figure 3.8. Frequency & generation responses of the ASFR model of Case 1 (non-reheater model).

$$err_f = \frac{\Delta \hat{f}_{nadir} - \Delta f_{nadir}}{\left| \Delta f_{nadir} \right|} \times 100 \tag{3.46}$$

$$err_t = \frac{\hat{t}_{nadir} - t_{nadir}}{t_{nadir}} \times 100 \tag{3.47}$$

where the head sign means the value is estimated by the ASFR model. It should be noticed that the above relative error remains constant when ΔP changes because of the linearity of

the inverse Laplace Transformation [102]. The frequency nadir errors are summarized in Table 3.4, which indicates that the error in Case 2 is slightly higher than in Case 1. However, the frequency nadir errors are generally very small even for the two worst cases ($|err_f|$<1% and $|err_t|$<2%). Then, we can conclude that the errors of all other cases are almost within this threshold. Based on the mathematical proof in Section 3.4 and the simulation study of a "bad" case, we can conclude that the ASFR model can replace the MM-SFR model with high accuracy.

Furthermore, a worse-than-normal case is also simulated in order to verify the robustness of the ASFR model. As shown in Table 3.5, the two main parameters T_R and F_H range from 4~19 and 0.09~0.55, respectively. Note that these ranges exceed the normal parameter range.

With the same disturbance ΔP = 0.05p.u., Figure 3.9 shows the frequency and generator power response. The relative errors are: err_f = -1.05%, err_t = 1.72%. Therefore, the simulation result is accurate even if the value range is wide, and it is reliable to use the analytical method to aggregate the MM-SFR model to an ASFR model.

In addition, some references [25], [93] claim that T_G and T_C can be neglected in the SFR model ("with reheater" type) due to their small values. A simulation study between low-

Table 3.4. Error summary of simulation cases.

Types	With reheater		Non-reheater	
	err_f	err_t	err_f	err_t
Case 1	-0.77%	1.26%	-0.75%	-0.33%
Case 2	-0.89%	1.71%	-0.95%	-0.36%

Table 3.5. Parameters of 5-machine SFR model.

Gen. No.	K_m	T_G (s)	T_C (s)	T_R (s)	F_H (pu)	$1/R$	λ
1	0.11	0.20	0.37	8	0.28	13.33	0.091
2	0.18	0.12	0.24	14	0.09	10	0.111
3	0.21	0.26	0.21	4	0.55	20	0.258
4	0.36	0.21	0.35	19	0.27	16.67	0.369
5	0.14	0.16	0.31	11	0.41	20	0.172
Equivalent	1.00	0.2034	0.2966	12.42	0.3501	16.27	1.00

H=4.96, D=1.2
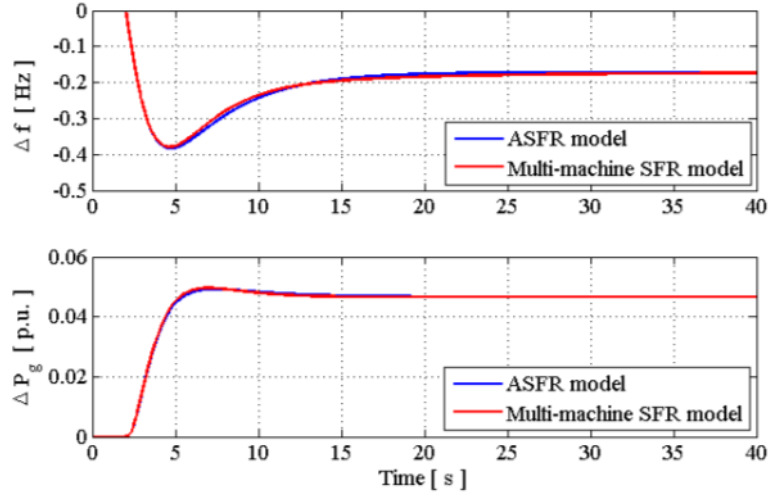
Figure 3.9. Frequency & generation response of an ASFR model.

order and full-order SFR model is done with the parameters in Table 3.2. As is shown in Figure 3.10, the low-order model results in an err_f of more than 10%. Therefore, the low-order SFR model is more suitable for analytical and qualitative studies.

3.5.2 The ASFR Model vs. small-scale detailed system model

The SFR model is compared with an IEEE 14-bus, 5 machine system, as shown in Figure 3.11. The turbine governor parameters are listed in Table 3.6. We still apply a sudden load increase of $\Delta P = 0.05S_{sys}$ to both models. The computation time of the ASFR model is less than 0.5s, while that of the detailed model is 33s.
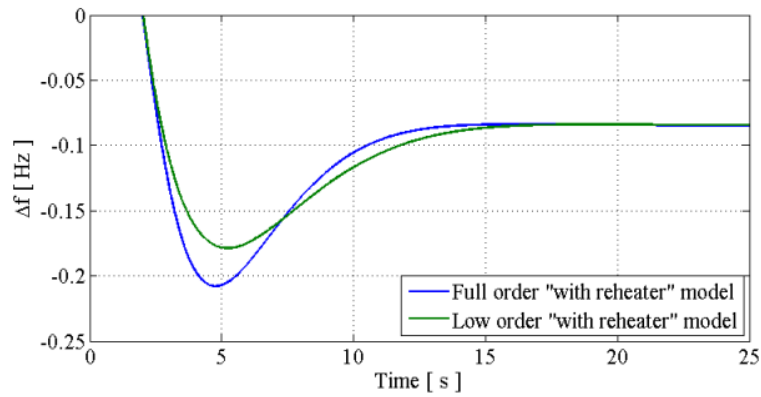
Figure 3.10. Frequency response of full-order and low-order SFR model.
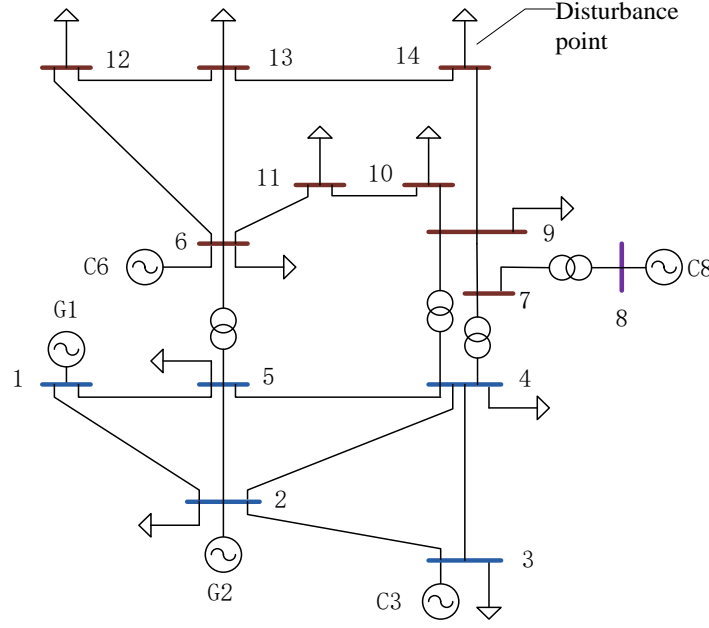
Figure 3.11. IEEE 14-bus testing system.

Table 3.6. Parameters of 5 turbine governors.

Gen. No.	K_m	T_G (s)	T_C (s)	T_R (s)	F_H (pu)	$1/R$	λ
1	0.469	0.2	0.33	10	0.23	25	0.564
2	0.25	0.13	0.25	12	0.21	20	0.240
3	0.188	0.22	0.26	14	0.35	12.5	0.113
4	0.047	0.24	0.37	8	0.29	16.7	0.038
5	0.047	0.18	0.25	9	0.2	20	0.045
Equivalent	1.00	0.186	0.301	10.8	0.240	20.8	1.00

Scenario 1: As is presented in Figure 3.12 (a), the frequency response curves obtained by the two models are quite close. The relative errors are $err_f = -4.41\%$ and $err_t = 5.27\%$, respectively. Right after the disturbance, the frequency responses of the separate buses are slightly different (shown in the dashed green blanket), which is caused by the inter-machine oscillation. There is also a 3.35% (0.0028Hz) error with Δf_{nep}. According to the discussion in Section 3.4.3, system power loss can increase slightly after a sudden load increase of $0.05S_{sys}$, and the equivalent ΔP in the ASFR model should be slightly larger than "0.05p.u.". Since we still take $\Delta P = 0.05$p.u. in the ASFR model, the resulting f_{nep} is slightly higher than f_{nep} in the detailed system model.
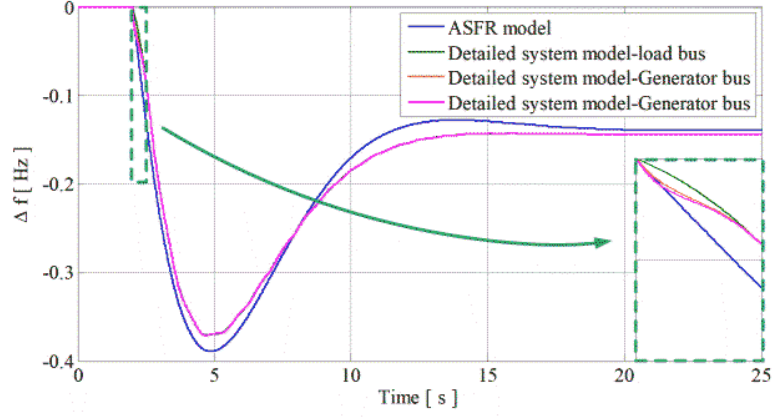
(a) Without DR
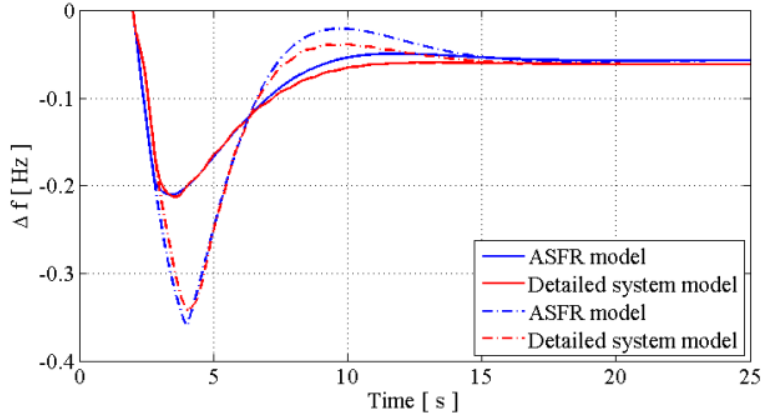
(b) With DR

Figure 3.12. Frequency response of ASFR model and IEEE 14-bus detailed system.

Scenario 2: We further verify the accuracy of the ASFR model by including demand side control. The first case shows that a load reduction of $0.03S_{sys}$ is activated at 2.8s, while the second case shows that the same load reduction is activated at 4.0s. The results of both cases are presented in Figure 3.12 (b). Based on the two scenarios, the factors (discussed in Section 3.4.3) do not have significant impact on the accuracy of the ASFR model.

3.5.3 *ASFR model v.s. large-scale detailed system model*

In this section, a 179-bus, 29-machine U.S. simplified WECC system is simulated. The geographic diagram of the testing system is shown in Figure 3.13. In this system, the system base power S_{sys} is 130.5GVA, and the total loading level is 60.9GW. The distribution of two parameters (T_R, F_H) of 29 machines is plotted in Figure 3.14. In this

51

Figure 3.13. WECC 179-bus testing system.
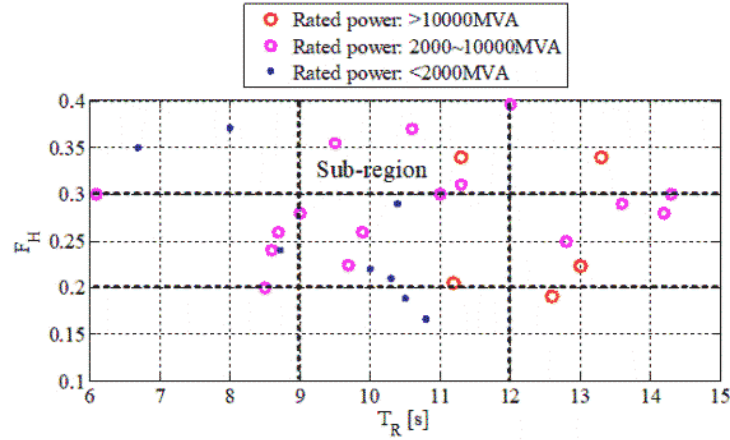
Figure 3.14. Distribution of turbine governor parameters.

large system, we can divide the T_R-F_H plane into nine sub-regions. In each sub-region, since T_R and F_H are within a narrow range of 3s and 0.1 (as the dashed line shows), respectively, the merging error is negligible according to (3.31) and (3.32). Then, we can

expect that no matter how many machines are aggregated, the indices err_f and err_t will not be obviously larger than the 6-machine system.

We apply a sudden load increase of $0.2\%S_{sys}$ at a bus near Los Angeles and observe the frequency response of three representative load buses according to their distance from Los Angeles: Los Angeles (nearby), Phoenix (medium), and Portland (far). Meanwhile, the equivalent parameters are fed into the ASFR model. The frequency responses of two models are presented in Figure 3.15. We have the following observations.

- As shown in Figure 3.15 (a), the frequency responses at different buses have significant differences. At more distant buses, the frequency drops more slowly after the disturbance, because the remote generators have a smaller share of power unbalance at
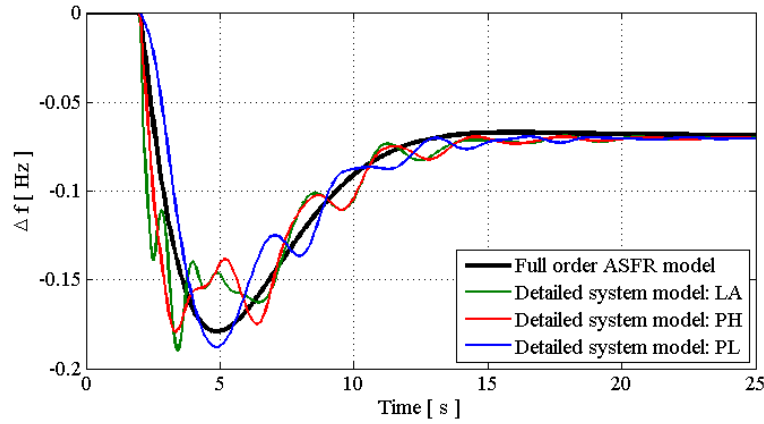
(a) Three typical bus frequency
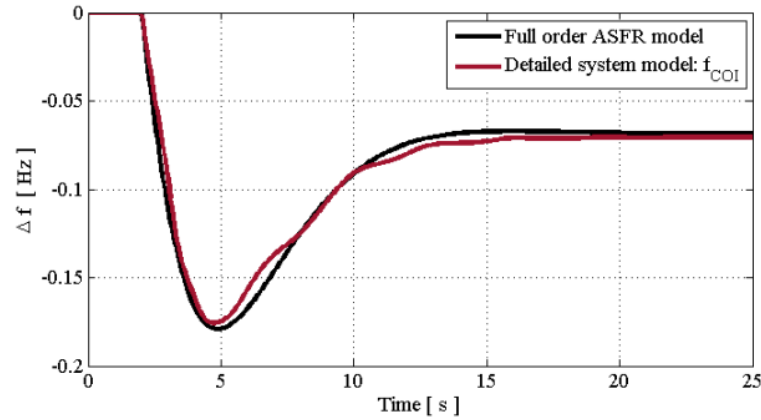
(b) COI frequency

Figure 3.15. Frequency response of ASFR model and 179-bus detailed system.

the time instant $t = 0^+$, according to the discussion in Section 3.2.3. Therefore, the large system has more significant inter-machine oscillations.

- In a large-scale system, f_{COI} (calculated by (3.4)) is an essential index for evaluating the overall frequency response [89]. Figure 3.15 (b) indicates that the ASFR model can also simulate f_{COI} of a large-scale system with high accuracy. The relative errors are err_f = -4.69% and err_t = 1.75%, respectively. Furthermore, the authors in [103] proposed a frequency-propagation-based method to estimate the local bus frequency based on f_{COI} and network parameters.

3.5.4   A summary of the ASFR model

The SFR model extracts the turbine governor from the detailed power system and simulates its average frequency response. Based on the above analytical and simulation studies, different frequency response models and their relations are summarized in Figure 3.16. The green arrow means this model simplification brings negligible error in frequency response, while the orange arrow means this model simplification perhaps brings considerable error. Among the six models, only the low-order ASFR model can give an analytical expression of the frequency nadir. This model is mainly applicable to two aspects of current studies: one is a qualitative analysis on frequency response features; the other is security-based unit commitment [93]. The full-order ASFR model can replace small-scale systems for quantitative study with an acceptable error, although it ignores the inter-machine oscillation. Also, it can represent the average frequency response of large-scale systems, which is critical in industry applications [89].

As is discussed in Section 3.1, the ASFR model has applications in several research areas. When the size of the target system is not large, we can replace the detailed system with an ASFR model to obtain the parameters f_{nadir} and t_{nadir} with very low computation workload and satisfactory accuracy. For a large-scale system, however, the ASFR model is a fast tool for the researchers to find a rough estimate of f_{nadir} with respect to a specified ΔP. Then, the detailed system simulation is conducted to figure out the accurate value. Therefore, the ASFR model and detailed system model are complementary.
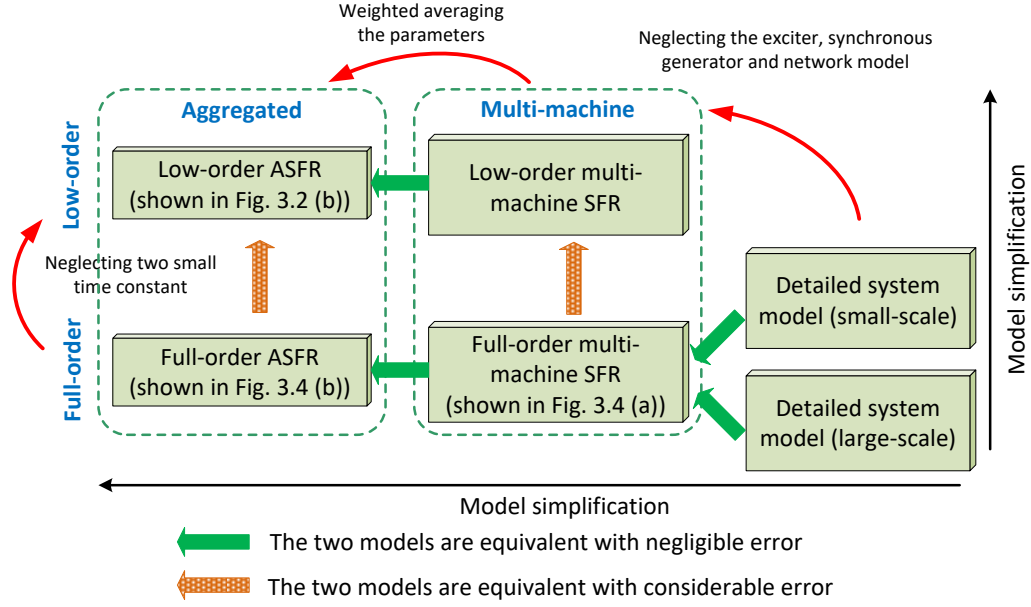
Figure 3.16. Summary of different models for studying the frequency dynamic.

3.6 Applications of ASFR Model

3.6.1 Demand response for frequency regulation

Section 3.5.1 concludes that the ASFR model (both "with reheater" and "no reheater" type) can replace the MM-SFR model with high accuracy. An enhanced version of the SFR model is called the "load frequency control" (LFC) model, which includes an AGC element $K(s)$. Many studies have been done on DR for frequency regulation [45], [52], [69], [71], [82]. Figure 3.17 shows a single-area, 5-machine system, where α_i is the regulation amount share of each generator. The state-space model for frequency control is given by (3.48) [52]:

$$\dot{x} = Ax + Bu + \Gamma w$$
$$y = Cx \tag{3.48}$$

In a conventional approach, the state vector x is 11-order: $x = [\Delta f, \Delta P_{m1}, \dots \Delta P_{m5}, \Delta P_{g1}, \dots \Delta P_{g5}]^T$. The expressions of A, B, C and Γ are also 11-order and omitted here due to space limitations. Based on the ASFR model, we can merge the five machines into one machine and x is reduced to 3-order:
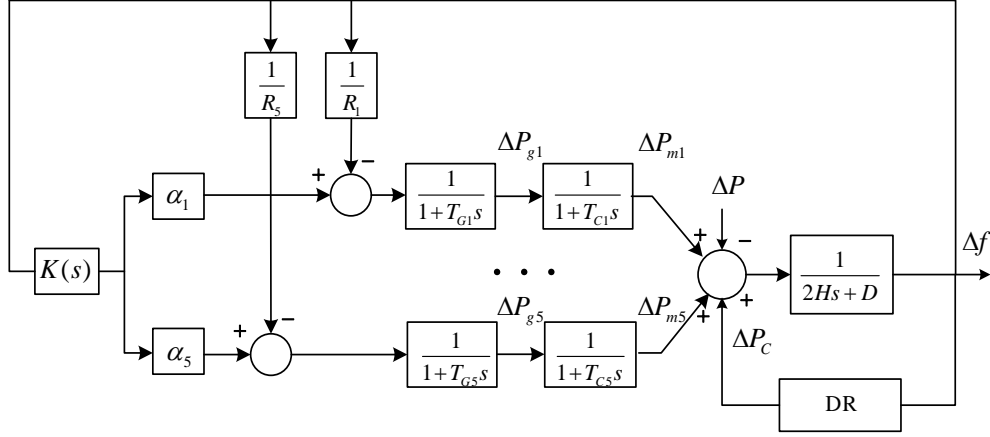
(a) Original model
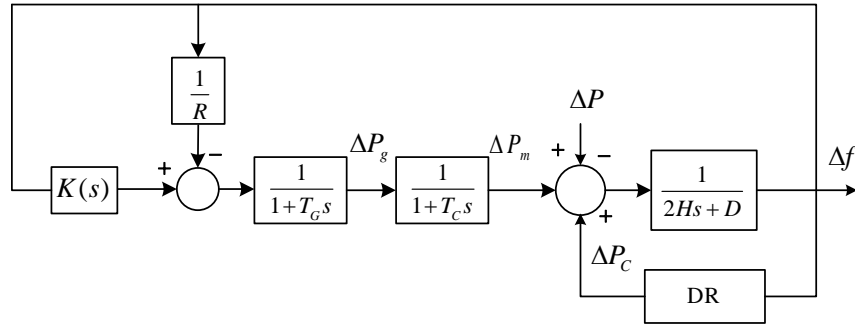
(b) Aggregated model

Figure 3.17. Multi-machine LFC model with secondary frequency regulation.

$$x = \begin{bmatrix} \Delta f \\ \Delta P_m \\ \Delta P_g \end{bmatrix}, \ A = \begin{bmatrix} -\dfrac{D}{2H} & \dfrac{1}{2H} & 0 \\ 0 & -\dfrac{1}{T_C} & \dfrac{1}{T_C} \\ -\dfrac{1}{T_G R} & 0 & -\dfrac{1}{T_G} \end{bmatrix}, \ B = \begin{bmatrix} \dfrac{\mu-1}{2H\mu} \\ 0 \\ \dfrac{1}{T_G} \end{bmatrix}, \ \Gamma = \begin{bmatrix} -\dfrac{1}{2H} \\ 0 \\ 0 \end{bmatrix}, \ u = \Delta P_S, \ w = \Delta P$$

$$y = \Delta f, \ C = [1, 0, 0], \ \Delta P_{DR} = \frac{1-v}{v} \Delta P_S$$

where v ($0 < v < 1$) is the share of DR in the total frequency regulation effort, and $v = 0.1$ in this case. The turbine governor parameters are shown in Table 3.2. The linear quadratic regulator (LQR) algorithm is applied to optimize the frequency response. After a disturbance of $\Delta P = 0.025$p.u., the control strategies based on the ASFR and MM-SFR models achieve very close frequency responses, as shown in Figure 3.18. Furthermore, the ASFR model is also applicable to multi-area frequency regulation problems [71], in which
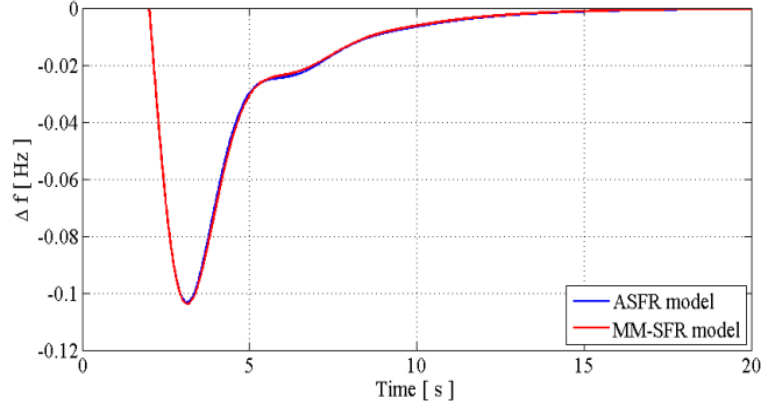
Figure 3.18. Comparison between MM-SFR model and ASFR model.

each area can be aggregated to a single machine.

3.6.2 Estimation of maximal renewable energy penetration

The maximal RES penetration is generally determined based on several frequency security criteria, such as f_{nadir}, f_{nep} and a 15-second rolling window [90]. The ASFR model provides a fast technique for this study, which is useful in power planning and generation dispatch [88]-[89].

The RES penetration mainly affects the system total inertia and frequency regulation reserve. Traditional wind generators contribute much less to the system inertia and frequency droop than the same capacity of synchronous generators [85], [104]. In recent years, however, it has been proposed that wind turbines can utilize DC-link capacitor energy and rotor kinetic energy to provide system inertia support [105]-[106]. With this control scheme, wind generators can contribute more to the system inertia. Assuming that the fraction of inertia that wind power contributes to the system is k_w, the fraction of synchronous generator inertia that is reduced in the presence of wind is k_s (normally $k_w < k_s$). The new inertia constant and speed droop is calculated by (3.49) and (3.50) [85]:

$$H_{sys,new} = H_{sys,old}(1 + k_w - k_s)$$ (3.49)

$$R_{sys,new} = \frac{R_{sys,old}}{1 + k_w - k_s}$$ (3.50)

The equivalent turbine governor parameters should also be recalculated by (3.17), (3.18), and (3.21) because some part of the synchronous generators are replaced by wind generators. This model can also be extended to multi-area system. The system frequency response can be simulated after substituting the new parameters to the SFR or LFC model. For instance, the authors in [85] concluded that the frequency deviation, the tie-line power flow and the area control error tend to increase.

3.6.3   Coherency-based power system model reduction

The system dynamic model reduction technique is based on coherency. Coherency means that some synchronous generators, which are usually close to each other, exhibit similar frequency responses and rotor angle swings after a disturbance. The overall procedure for forming coherency-based dynamic equivalents can be divided into two main steps. The first step is to identify groups of coherent generators in the study area. The second is to aggregate each coherent group of machines into a single equivalent machine, followed by eliminating unnecessary generator/load buses. Machine aggregation includes turbine governors, exciters and synchronous generators. The details of the model reduction technique are discussed in [77].

Based on the accuracy of the ASFR model that is verified in Section 3.5, the proposed weighted-average method can be used to aggregate multiple turbine governors that are identified as coherent. Therefore, this method is an essential addition to the existing technique of power system model reduction. For instance, the full WECC system consists of about 18,000 buses. The aforementioned WECC 179-bus system is an example of the reduced-order model, which is normally used in online dynamic security assessment [77].

3.7   Conclusion

This chapter proposes an analytical method for obtaining the ASFR model parameters based on individual generator parameters.

The first contribution is to propose an analytical method by which we can aggregate the MM-SFR model with high accuracy. The model is proven by a mathematical induction method and further verified by simulation studies.

The second contribution is the investigation of the accuracy of the ASFR model for replacing the detailed system model. It can be concluded from dynamic simulation studies that the ASFR model can accurately represent the bus frequency response of a small-scale system. In a large-scale system, the ASFR model is less accurate for the bus frequency but can still represent the COI frequency accurately. Therefore, as a fast calculation tool, the ASFR model can support studies related to power system dynamics.

Last but not least, the applications of the proposed method are demonstrated with three studies: frequency regulation via DR, maximal wind power penetration, and dynamic model reduction. This shows the promising potential of applying the proposed method to other related research.

Chapter 4

A Hybrid Dynamic Demand Control Strategy for Frequency Regulation

This chapter proposes a hybrid DDC strategy for the primary and secondary frequency regulation. Specifically, the loads not only arrest the sudden frequency drop, but also bring the frequency closer to the nominal value. With the proposed control strategy, the demand side can provide a fast and smooth frequency regulation service, thereby replacing some generation reserve to achieve a lower expense.

4.1 Introduction

Frequency stability is a critical concern regarding power system operation. Frequency fluctuation or deviation is a result of unbalance between generation and load demand. The power unbalance might be caused by the large generator unit trip, tie-line trip, sudden change of loads, etc. [1]. In the power industry, frequency regulation is divided into three levels. Primary frequency regulation (PRFR), secondary frequency regulation (SCFR) and tertiary frequency regulation (TRFR). In recent years, the developments of renewable energy source integration and the power market have brought several challenges to frequency stability, as discussed in Section 1.1.

DDC has been proposed to mitigate short-term frequency fluctuation [16]. Some residential loads with a thermal storage feature can be switched off for a short period when the frequency drops below a threshold and is switched back on again when the frequency recovers, such as EWHs and HVACs [7], [16], [18]. Switching off EWHs or HVACs for a few minutes hardly affects customers' living comfort because the water temperature or air temperature remains almost constant. If the control scheme is properly designed, the aggregated responsive loads can provide frequency reserve and thus help reduce the capacity of generator spinning reserve for frequency regulation.

The DDC strategy can be classified into decentralized control [7], [16]-[18], centralized control [52], [53], [55], and hybrid/distributed control [57], [71]. Decentralized control has received a great deal of attention because it does not require any communication infrastructure. A controller device is installed between the load and the household power outlet [16]. If a frequency drop is detected, the controller compares it with the pre-defined frequency set-point and decides whether to switch off the load or to adjust its power consumption. These control algorithms usually set random frequency set-points or random time delays for each load controller [7], [16]-[18], [44]. Consequently, we can avoid the synchronous disconnection of a large number of loads and the resultant frequency overshoot. Some technical concerns, however, still exist in the literature. First, such studies fail to verify how the aggregated responsive loads provide accurate power compensation in reaction to different levels of frequency deviations [7], [17]. Second, some simulation studies ignore the frequency droop characteristics of the generators [16]-[17]. Furthermore, other simulation studies do not consider the detailed dynamic system model [16]-[18], [44]. As a result, the conclusions are not adequate to reflect practical industry cases.

This chapter proposes a DDC strategy for frequency regulation. When an under-frequency disturbance happens, the load controller first forecasts the frequency nadir in order to decide whether to perform PRFR (1st level). After the frequency enters the steady-state, the controller then decides whether to participate in SCFR (2nd level) to bring the frequency closer to the nominal value. In this DDC strategy, the control parameters are sent from the control center, while the load controller acts in a decentralized manner. Therefore, it is a hybrid control strategy. The simulation study considers a detailed power system model, which includes a turbine governor, exciter, synchronous generator, and network topology. Consequently, the simulation result fully represents the practical power system frequency response.

The rest of the chapter is organized as follows. Section 4.2 reviews the characteristics of the system frequency response, which is the theoretical basis of frequency regulation. Section 4.3 proposes the DDC strategy, including PRFR and SCFR. In particular, the least square (LS)-based frequency nadir forecast method is introduced. Section 4.4 verifies the control strategy through time-domain simulation and analyzes how to determine appropriate control parameters. Section 4.5 concludes the chapter.

4.2   Principle of System Frequency Response

The multi-machine aggregation method of SFR model and is presented in Chapter 3. It is briefly recalled here. According to the single-machine, low-order SFR model, the time-domain frequency deviation Δf after ΔP disturbance is given by

$$\Delta f(t) = \frac{R\Delta P}{DR+1} \cdot \left[1 + ae^{-\varsigma\omega_n t}\sin(\omega_r t + \varphi)\right] \tag{4.1}$$

At the frequency nadir, the derivative of the frequency curve should be 0. The time to reach frequency nadir is

$$t_{nadir} = \frac{1}{\omega_r}\tan^{-1}\left(\frac{\omega_r T_R}{\varsigma\omega_n T_R - 1}\right) \tag{4.2}$$

Thus, the frequency nadir Δf_{nadir} is

$$\Delta f_{nadir} = \frac{R\Delta P}{DR+1} \cdot \left[1 + \sqrt{1-\varsigma^2}\,ae^{-\varsigma\omega_n t_{nadir}}\right] \tag{4.3}$$

After the disturbance, the steady-state frequency deviation of the new equilibrium is

$$\Delta f_{ss} = \frac{R\Delta P}{DR+K_m} = \frac{R\Delta P}{DR+1} \tag{4.4}$$

Based on (4.3) and (4.4), we can make the following observations of the system frequency response:

- t_{nadir} depends on turbine governor parameters, generator inertia, and system damping. t_{nadir} is unrelated to ΔP.

- If ΔP is multiplied by coefficient k, the frequency response $\Delta f(t)$ is also multiplied by k in real time.

- According to the above two points, Δf_{nadir} is proportional to ΔP if the dynamic system parameters remain constant.

4.3 Dynamic Demand Control Strategy

The decentralized DDC is able to participate in both the PRFR [7], [18] and SCFR [16]. An intrinsic concern with decentralized DDC is that an individual load controller does not "know" the action of other controllers. Consequently, the aggregated responsive loads may provide excessive or insufficient power compensation and fail to bring the frequency back to the nominal value. Therefore, the DDC algorithm should have adaptive characteristics and coordinate with the turbine governor control.

In this section, a hybrid DDC method is proposed. When the system frequency falls below the frequency dead-band, we can forecast the frequency nadir (f_{nadir}) through a number of frequency measurement data. If the forecast f_{nadir} is not low enough, then the DDC only needs to participate in the SCFR; it will wait until the new frequency steady-state is reached and then bring the frequency back to the frequency dead-band. If f_{nadir} is low enough, then the DDC needs to participate in the PRFR and some responsive load will be switched off immediately. The next two subsections will explain the algorithms of the frequency nadir forecast and demand control, respectively.

4.3.1 Frequency nadir forecast

Based on the three observations made in Section 4.2, the LS-based method is proposed for forecasting f_{nadir}. As is shown in Figure 4.1, the t_0–t_{nadir} segment of nonlinear curve $f(t)$ can be fitted by a quadratic curve. For the next frequency disturbance, it is possible to roughly forecast f_{nadir} before it actually happens. By assuming the system total inertia to be constant, we can forecast f_{nadir} in three steps:

1) Base Frequency Curve ($f_b(t)$) Fitting: Small frequency disturbances often happen because of small load step changes. As is shown in Figure 4.1, N frequency samples $\{f_b(t_1), f_b(t_2), \dots f_b(t_N)\}$ ($N > 3$) are selected from the data segment between t_0 and t_{nadir}. The curve $f_b(t)$ is fitted by a quadratic function:

$$f_b(t) = a_{b2}t^2 + a_{b1}t + a_{b0} \tag{4.5}$$

The coefficient vector A is determined by,
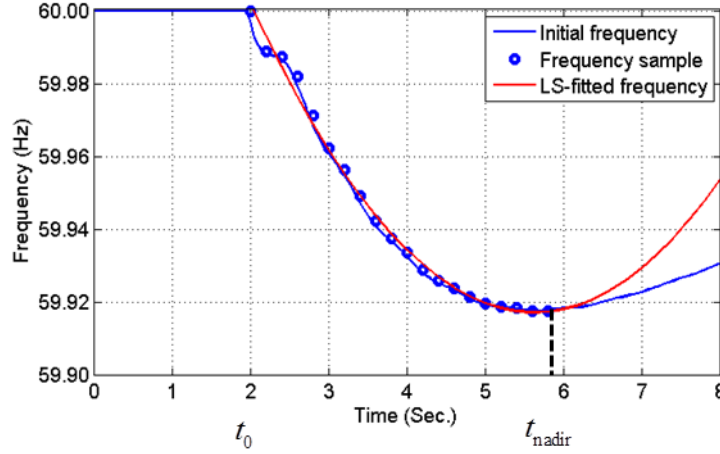
Figure 4.1. LS-fitted base frequency curve.

$$F = TA \tag{4.6}$$

where

$$F = \begin{bmatrix} f(t_1) \\ \vdots \\ f(t_N) \end{bmatrix}, \quad T = \begin{bmatrix} t_1^2 & t_1 & 1 \\ \vdots & \vdots & \vdots \\ t_N^2 & t_N & 1 \end{bmatrix} \text{ and } A = \begin{bmatrix} a_{b2} \\ a_{b1} \\ a_{b0} \end{bmatrix}.$$

2) Coefficient Solution: A is solved by least square method:

$$\hat{A} = \left(T^T T\right)^{-1} T^T F \tag{4.7}$$

where $\hat{A} = \begin{bmatrix} \hat{a}_{b2} & \hat{a}_{b1} & \hat{a}_{b0} \end{bmatrix}^T$. Then, the fitted base frequency curve is,

$$\hat{f}_b(t) = \hat{a}_{b2} t^2 + \hat{a}_{b1} t + \hat{a}_{b0} \tag{4.8}$$

Since $t_N = t_{nadir}$, the minimal value of the quadratic function $\hat{f}_b(t)$ is equal to the nadir of $f_b(t)$.

$$\hat{f}_{nadir} = \hat{f}_{b,\min} = \hat{a}_{b0} - \frac{\hat{a}_{b1}^2}{4\hat{a}_{b2}} \tag{4.9}$$

3) Frequency Nadir Forecast: As is shown in Figure 4.2, when a larger disturbance ΔP happens (called "current disturbance curve"), the frequency response curve is proportional to the base frequency curve. The new frequency curve $f(t)$ is
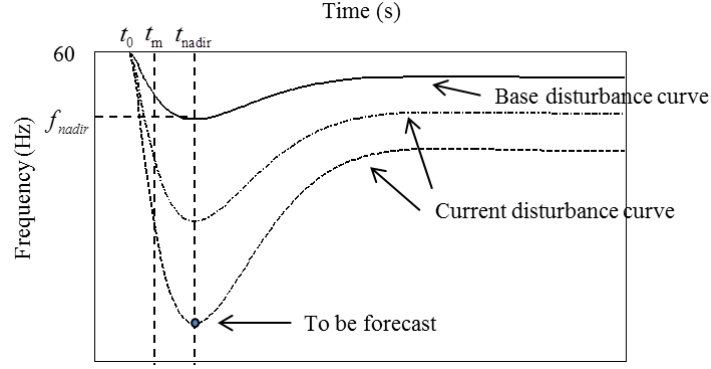
Figure 4.2. Frequency response for different power disturbances.

$$f(t) = a_2 t^2 + a_1 t + a_0 = \lambda \cdot f_b(t) \tag{4.10}$$

where $\lambda = a_2 / \hat{a}_{b2}$. Before the frequency nadir is reached, we select M frequency samples from $t_0 - t_M$ segment ($t_M < t_{nadir}$) with the same sampling rate as 1). The coefficient λ is estimated by a linear regression:

$$\hat{\lambda} = \sum_{n=1}^{M} f(t_n) \cdot f_b(t_n) \bigg/ \sum_{n=1}^{M} f_b^2(t_n) \tag{4.11}$$

Finally, the forecast frequency nadir is given by (4.12):

$$\hat{f}_{nadir} = \hat{\lambda} \cdot \left(\hat{a}_{b0} - \frac{\hat{a}_{b1}^2}{4\hat{a}_{b2}} \right) \tag{4.12}$$

The accuracy of the frequency measurement device is essential for frequency nadir forecast. Nowadays, the accuracy of a frequency disturbance recorder (FDR) is ± 0.0005 Hz or better [107]-[108], which is sufficient for frequency regulation. Furthermore, since the load controller only needs a part of the functions of the FDR (i.e., a GPS receiver is unnecessary), we can expect that the expense of a load controller is acceptable.

4.3.2   Dynamic demand control

The frequency nadir indicates how serious this frequency disturbance is. First, if at the time step t_0 the measured frequency falls below the dead-band (59.95 Hz), this indicates a "suspicious" under-frequency disturbance. Then, the controller starts to sample the frequency with a time interval of 0.1s for a 1.5s duration (T_{samp}). When T_{samp} is expired, the

controller immediately forecasts the frequency nadir using the latest frequency data between t_0 and $t_0 + T_{samp}$ to decide whether to perform PRFR. Furthermore, when the frequency reaches the steady state f_{ss}, the controller will also decide whether to perform SCFR.

4.3.2.1 Primary Frequency Regulation (PRFR)

Case 1: If $\hat{f}_{nadir} \geq 59.75\,\text{Hz}$, the frequency deviation is not serious enough. The turbine governors themselves are adequate to arrest the frequency deviation.

Case 2: If $\hat{f}_{nadir} < 59.75\,\text{Hz}$, the frequency deviation requires an immediate load control. The amount of load to be switched off is determined by (4.13),

$$\Delta P_{PRFR} = k_P \cdot \frac{\Delta \hat{f}_{nadir}}{60} \tag{4.13}$$

where k_P is the load-frequency sensitivity factor of PRFR (MW/Hz or p.u./p.u.). k_P depends on the available power of the responsive load, and is sent from the control center. Furthermore, in this hybrid control scheme, since a responsive load neither communicates with the control center nor with other loads, the difficulty is in making the aggregated responsive loads provide the accurate power compensation given by (4.13). A stochastic decision method (SDM) is proposed. That is, each load should be switched off at a specified probability (p_{off}). The mathematical implementation is that the load makes an "on/off decision" according to a uniformly distributed random value,

$$\begin{aligned} p_{off} &= \min\left(\frac{\Delta P_{PRFR}}{P_{resp\_total}},\ 1 \right) \\ &\begin{cases} if\ U(0,1) \leq p_{off},\ \text{switch\ off} \\ if\ U(0,1) > p_{off},\ \text{remain\ on} \end{cases} \end{aligned} \tag{4.14}$$

For example, there are 1000 responsive loads for PRFR and each has a power rating of 2×10^{-5} p.u.. Thus, the total frequency reserve power is 0.2 p.u.. At a frequency disturbance event, suppose 0.14 p.u. (70%) of the loads should be switched off according to (4.13). Thus, each load is switched off at a probability of 70% according to (4.14). We can expect that there are around 700 loads being switched off. In order to demonstrate the accuracy of

66

the SDM, a Monte Carlo simulation is performed for 1,000 times and the discrete probability distribution of "off" loads is counted each time, as shown in Figure 4.3. We can observe that the probability of providing the expected power reduction with ±5% error (665–735 loads) is 98.1%. Therefore, the aggregated loads are able to provide real power compensation that is roughly proportional to the frequency deviation, acting as a very large-scale energy-storage battery with frequency droop control.

4.3.2.2 Secondary Frequency Regulation (SCFR)

The turbine governor control can arrest a sudden frequency drop. However, according to (4.4), it will result in a steady-state frequency deviation Δf_{ss}. If $f_{ss} < 59.95$ Hz, it is necessary for the DDC to participate in SFR and replace some capacity of spinning reserve for a short while. Generally, DDC should satisfy two main technical requirements:

- Steady-state requirement: bringing the frequency to within the frequency dead-band (i.e., 59.95 Hz);

- Dynamic requirement: providing a smooth frequency response and avoiding a big frequency overshoot.

For the steady-state requirement, the responsive load reduction is determined by (4.15).

$$\Delta P_{SCFR} = k_S \cdot \frac{\Delta f_{ss}}{60} \tag{4.15}$$
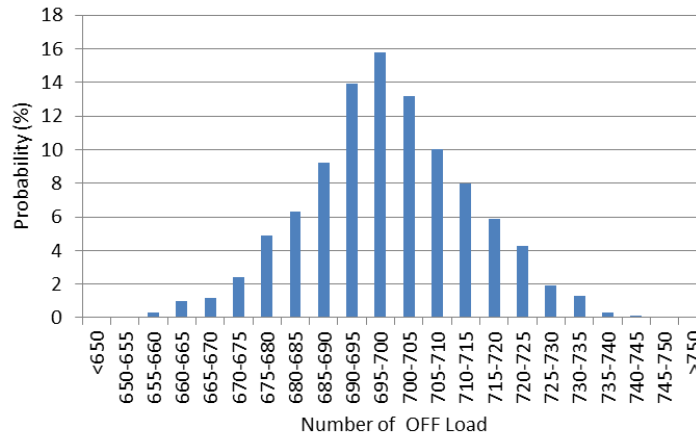
Figure 4.3. Probability of off-loads among 1000 loads.

67

where k_S is the load-frequency sensitivity factor of SCFR (MW/Hz or p.u./p.u.). k_S is also sent from the control center. Similar to PRFR loads, each SCFR load should be switched off according to (4.14) (by replacing ΔP_{PRFR} with ΔP_{SCFR}). Consequently, the total load power reduction is close to ΔP_{SCFR}. One problem is to determine a sufficient k_S that can bring the frequency to within the dead-band f_{db}. Since the frequency increment $\Delta f = \Delta f_{db,low} - \Delta f_{ss}$ is caused by ΔP_{SCFR} ($f_{db,low}$ is the lower bound of f_{db}), (4.15) can be modified as:

$$\Delta f = 60 \cdot \frac{R \Delta P_{SCFR}}{DR+1} \text{ or } \Delta P_{SCFR} = \frac{\Delta f (DR+1)}{60R} \tag{4.16}$$

Therefore, k_S should ensure that ΔP_{SCFR} offsets the generator power reduction. Substituting (4.15) into (4.16) gives

$$k_S \frac{\Delta f}{60} \geq \frac{\Delta f (DR+1)}{60R} \tag{4.17}$$

That is,

$$k_S \geq \frac{DR+1}{R} \tag{4.18}$$

It should be noticed that (4.18) is derived from an ASFR model shown in Figure 3.2. In practice, since the system contains multiple generators, R represents the system equivalent frequency droop, which is the weighted average of each generator droop value [25].

As for the dynamic requirement, a uniformly-distributed time delay T^i_{delay2} is introduced to ensure a ramp increment of the power reduction. For the responsive load i, the random time delay is generated by (4.19).

$$T^i_{delay2} \sim U(0, T_{delay2,\max}) \tag{4.19}$$

When T^i_{delay2} is expired, the load i is switched off immediately. If the total number of loads is large enough, this method can achieve a smooth power response. The principle is illustrated in Figure 4.4.
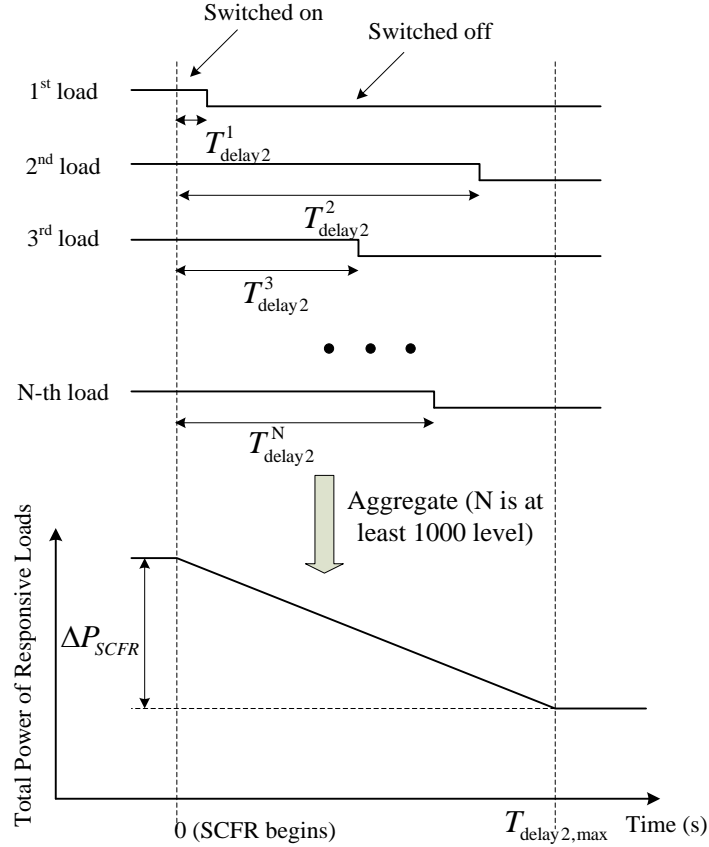
Figure 4.4. Load action time delay and aggregated response.

4.3.3   Summary

The hybrid DDC algorithm is summarized in Figure 4.5. In the steady-state, the time step for frequency measurement is 1 second. First, a low-frequency snapshot (<59.95 Hz) is detected, which indicates a suspicious under-frequency event. The time step for frequency measurement is switched to 0.1 second. After a sampling time of 1.5s, the controller forecasts f_{nadir}. Second, if $\hat{f}_{nadir} < 59.75\text{Hz}$, the controller performs PRFR immediately. Third, when the steady-state frequency is reached, the controller determines whether to perform SCFR according to the measured frequency $f(t)$. Note: The "steady-state" is identified by the formula $|f_{mav}(t) - f_{mav}(t - \Delta t)| < \varepsilon$, where f_{mav} is the moving average frequency of the latest few samples and $\Delta t = 1$s. In a large-scale system, the possibility of large frequency deviation is quite low. In some cases, the DDC perhaps only needs to perform the SCFR. By defining an appropriate load-frequency sensitivity factor
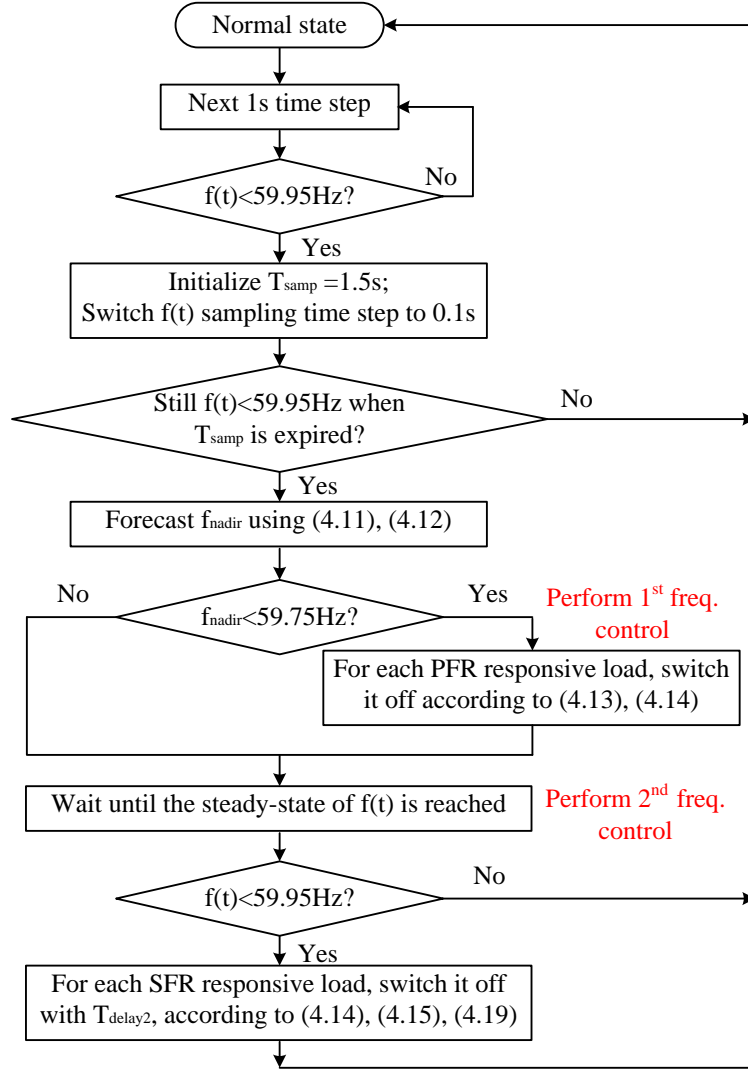
Figure 4.5. Overall flowchart of bi-level DDC algorithm.

and time delay, the aggregated responsive loads can achieve similar results to generators with AGC.

Two practical issues are critical for the control scheme. First, an individual load can either participate in PRFR or SCFR during one under-frequency event. A possible implementation is that customers sign contracts with the load aggregator company to choose whether to participate in PRFR or SCFR. The second issue is the responsive load availability because the responsive loads are not always in operation.

4.4 Simulation Study

This section verifies the proposed method through a detailed system simulation using the Matlab PSAT toolbox (V. 2.1.9) [101].

The IEEE 14-bus dynamic testing system is shown in Figure 4.6. Buses 1~5 are 69 kV level, buses 7 and 9~14 are 13.8 kV level, and bus 8 is 18 kV. G_1 is a slack generator, G_2 is a constant-PV generator, and C_3, C_6, and C_8 are three synchronous phasor compensators. Several PQ constant loads are connected to the buses. The parameters are shown in Table 4.1. The system base power is $S_{base} = 100$MVA. The testing system includes the turbine governor model and exciter model along with the synchronous generator. The turbine governor parameters are listed in Table 4.2 [101].

In Subsections 4.4.1-4.4.4, the simulation result is presented to demonstrate the performance of the proposed method. Furthermore, the sensitivity study shows how to tune the control parameters.
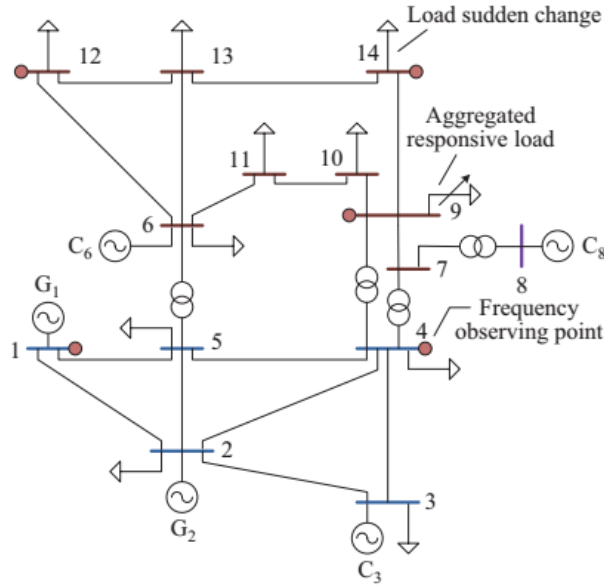
Figure 4.6. IEEE 14-bus testing system.

Table 4.1. PQ load parameters.

Node order	P (p.u.)	Q (p.u.)
2	0.217	0.127
3	0.942	0.19
4	0.478	0.04
5	0.076	0.016
6	0.112	0.075
9	0.295	0.166
10	0.09	0.058
11	0.035	0.018
12	0.061	0.016
13	0.135	0.058
14	0.149	0.05
Total power loss	**0.122**	**0.093**
Total loading level	**2.71**	**0.907**

Table 4.2. Turbine governor parameters.

Bus order connected	R	T_G (s)	T_C (s)	F_H	T_R (s)	$2H$ (s)
1	0.05	0.1	0.45	0.2	15	13.1
3	0.05	0.1	0.45	0.2	15	10.3

4.4.1   No demand control

Sudden load increase $\Delta P = 0.135$ p.u. (5% of the system total loading level) happens at bus 14 at $t = 2$ s. This ΔP can also emulate the sudden trip of wind generators because they traditionally contribute little to the system total inertia and frequency regulation. Without applying DDC, the frequency and generator power responses and their partial amplitudes are presented in Figure 4.7. It can be observed that the frequency curves of five different locations are almost identical except for some noises. However, during 2~2.4 seconds, the frequencies of buses 1 and 3 drop slower than that of bus 14, where the disturbance occurs. The reason is that bus 1 and bus 3 have longer electric distances from the disturbance source. As for the generator power response, generators #1 and #3 experience a real power oscillation and the corresponding damped sinusoidal curves are in the opposite phase. Therefore, the two generators exchange power in the dynamic process due to inter-machine oscillation. As a result, the frequency response curves at different buses are not identical [1], [91].
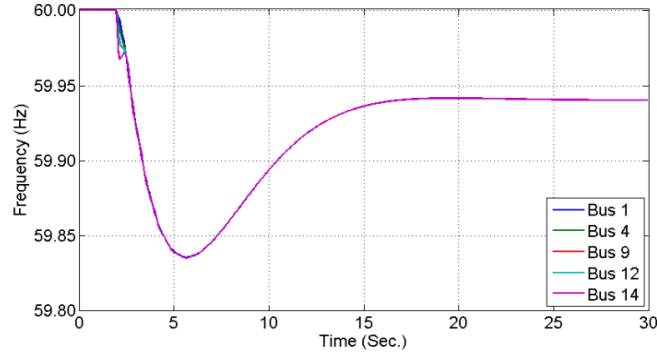
(a) Frequency response of 5 buses
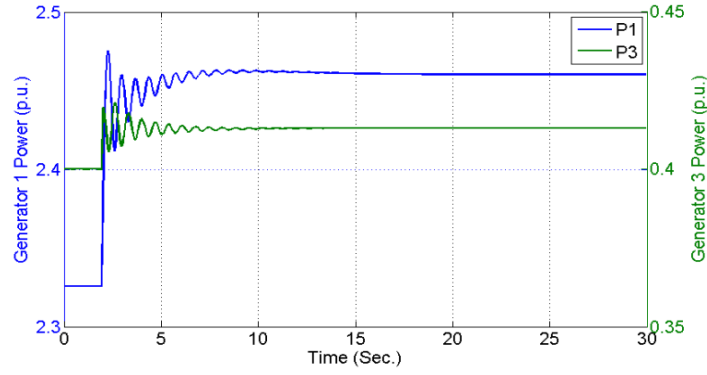
(b) Power output of 2 generators
Figure 4.7. Frequency and power output response with 5% power unbalance.

Then, we apply a sudden load increase $\Delta P = 2\%$, 5%, 8%, and 10% of the system total loading level, respectively. The frequency responses of bus 12 are shown in Figure 4.8. The result confirms that t_{nadir} remains the same (3.8s in this case) for a different level of power disturbances if the system total inertial does not change. This pattern makes it easier for us to implement the frequency nadir forecast method.
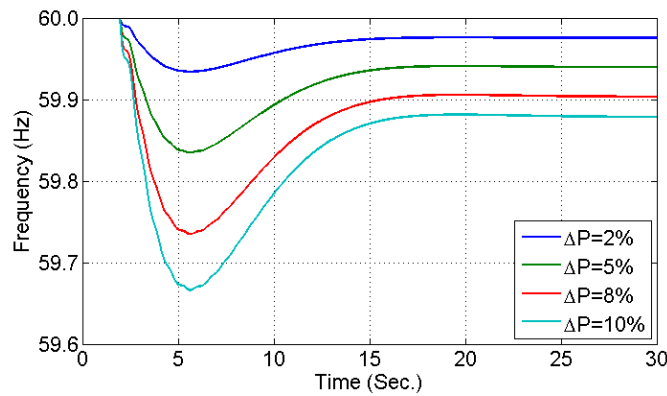
Figure 4.8. Frequency response of multiple unbalance.

4.4.2 DDC participating primary frequency regulation

Assume there is a $\Delta P = 0.271$ p.u. load step change (10% of the total system capacity) at bus 14. Responsive loads are at bus 9. k_P is set at 20 p.u./p.u. (0.33 p.u./Hz). The frequency nadir is forecasted as 59.73 Hz (actual value is 59.67 Hz), so the PRFR is activated. Disabling the SFR, the frequency response at bus 12 is shown in Figure 4.9 (a). The power output of generator 1 and power consumption of responsive loads are shown in Figure 4.9 (b) and Figure 4.9 (c), respectively. The figures indicate that the DDC obviously arrests the frequency drop and meanwhile increases the steady state frequency. However, the frequency has not been restored to within the 59.95 Hz dead-band. Therefore, another group of responsive loads still need to participate in the SCFR.

4.4.3 DDC participating secondary frequency regulation

Assume there is a $\Delta P = 0.135$ p.u. (5% of the total loading level) load increase at bus 14. Responsive loads are also at bus #9. The frequency nadir is forecasted as 59.78 Hz (actual value is 59.74 Hz) and the DDC for PRFR is not activated. After about 25 seconds, the steady-state frequency is lower than 59.95 Hz, and the SFR is activated. k_S is set at 60 p.u./p.u. (1 p.u./Hz), and the time delay for SCFR is $T_{delay2}^{i} \sim U(0, 15s)$. The frequency response at the observing bus is presented in Figure 4.10 (a). The power output of generator #1 and power consumption of responsive loads are shown in Figure 4.10 (b) and Figure 4.10 (c), respectively. We can observe that the frequency experiences an overshoot after the 15-second time delay. The overshoot is caused by mechanical inertia of the turbine governor dynamic system. During the 15-second load reduction process, the turbine governor makes the generator decrease its power output. Meanwhile, the load reduction offsets the generator power decrease. As a result, the frequency is brought closer to the 60 Hz nominal value.
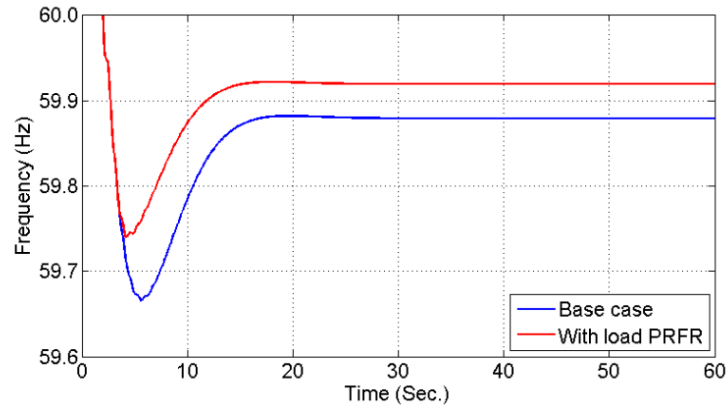
(a) Frequency at bus #12
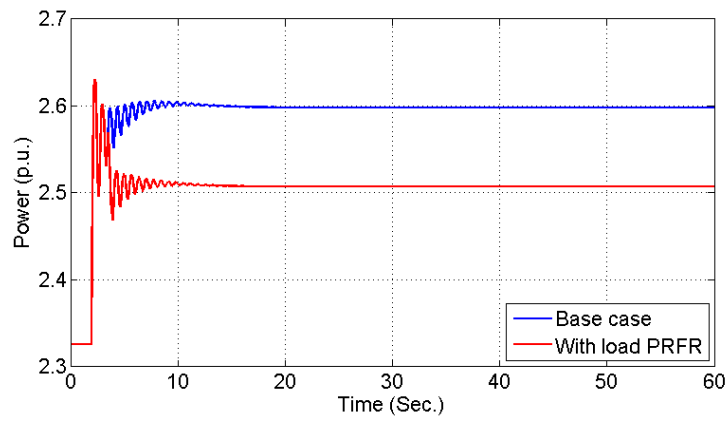
(b) Power output of generator #1
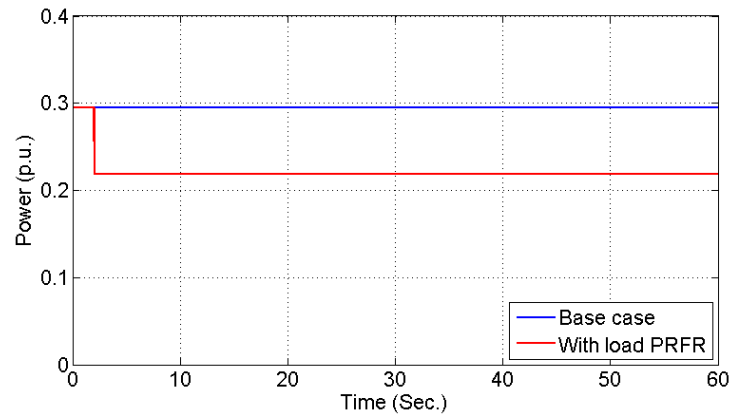
(c) Power consumption of responsive loads

Figure 4.9. Frequency and power output response with PRFR.
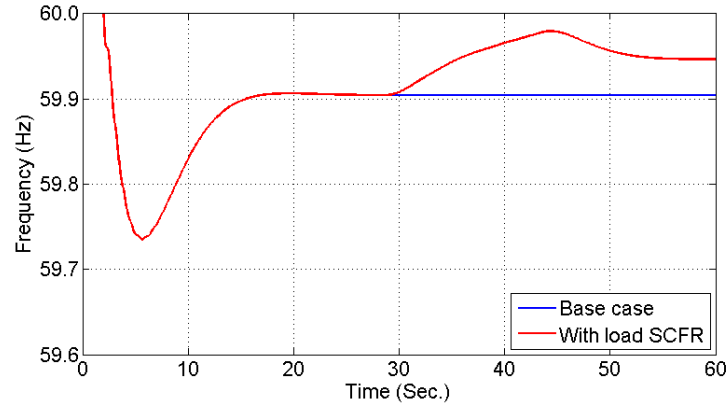
(a) Frequency at bus #12
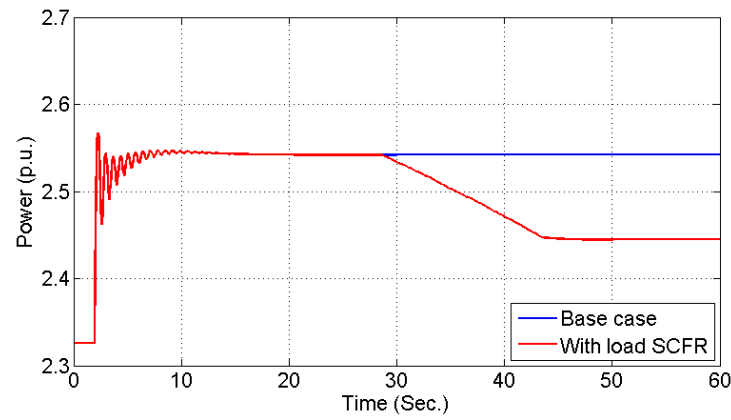
(b) Power output of generator #1
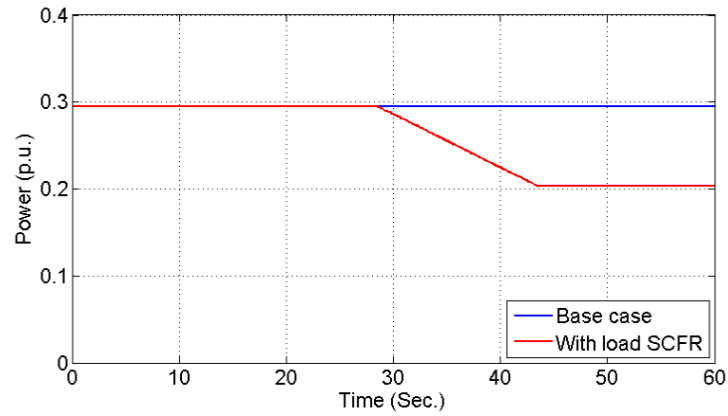
(c) Power consumption of responsive loads

Figure 4.10. Frequency and power output response with SFR.

4.4.4 Sensitivity analysis on DDC parameters

When DDC participates in SCFR, two parameters are critical for the control performance: k_S and $T_{delay2,max}$. A sensitivity study is necessary to determine the appropriate

control parameters. Figure 4.11 presents the frequency response curves with different k_S. In order to bring the frequency to within the dead-band in this particular case, a minimum of $k_S = 60$ p.u./p.u. is needed in this particular case. If k_S is larger than 60, the frequency may exceed 60 Hz for a few seconds. However, it will ultimately settle down within the dead-band because of a generator power deficit.

In particular, the base power is 100 MW in the 14-bus simulation system. The aforementioned "$k_S = 60$ p.u./p.u." means that the responsive loads can provide 0.60 p.u. (60 MW) power compensation in response to a 0.01 p.u. (0.6 Hz) frequency decrease, based on the assumption that the capacity of responsive loads is sufficient. In the transfer function model shown in Figure 3.2, however, the base power is the system total loading level. Since the total loading level is 2.71 in the 14-bus system, $k_S = 60$ p.u./p.u. also means that the responsive loads provide 0.60/2.71 = 0.221 time of the total loading level in response to 0.01 p.u. frequency decrease. Therefore, we should consider the ratio between responsive load capacity and system total loading level when tuning the k_S. The same principle is also applicable to tuning the k_P.

Figure 4.12 presents the frequency response curves with different $T_{delay2,max}$. The smaller the $T_{delay2,max}$ is, the larger the frequency overshoot will be. The reason for this is that the generation and demand power have not reached the balanced state when $T_{delay2,max}$ is expired. Therefore a $T_{delay2,max} = 15 \sim 25$s is appropriate for a smooth frequency response.
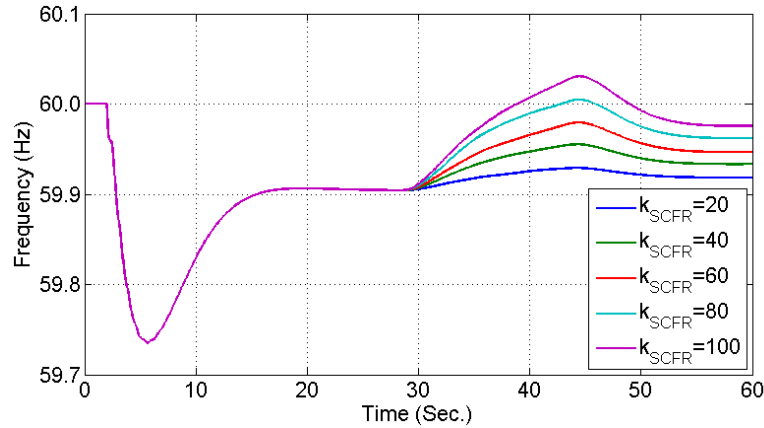
Figure 4.11. Frequency at bus 12 with different k_{SCFR}.
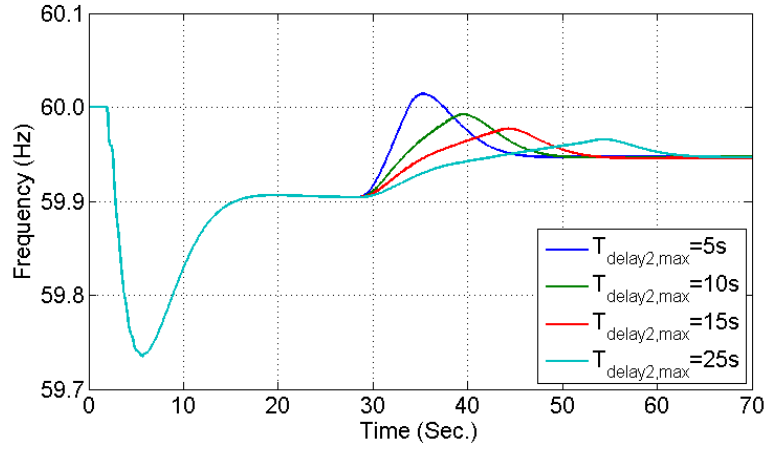
Figure 4.12. Frequency at bus 12 with different time delay.

Even if $T_{delay2,max}$ = 25s, the SCFR response time is much smaller than the AGC that lasts 5–10 minutes.

4.5 Conclusion

Decentralized control has the advantages of low cost and fast response in frequency regulation. However, its disadvantage is the difficulty in providing accurate power compensation in response to measured frequency deviation. The main contribution of this chapter is to propose a hybrid DDC strategy that combines centralized parameter-setting and decentralized control action. According to the method, each load controller first decides whether to participate in PRFR according to the forecast frequency nadir. Then at the steady-state, the load controller also participates in SCFR if the frequency is beyond the dead-band. In particular, when the amount of power compensation is calculated, the controller randomly determines whether and when to act according to the SDM. The SDM ensures that the non-communicated aggregated loads have an approximated frequency droop characteristic that is similar to generators. Additionally, the control parameters can be updated by the control center, which has a low communication requirement.

The simulation study fully emulates the real power system since the generator exciter and synchronous model are considered. Although the exciter does not directly control the power output of the prime mover, it indirectly affects the inter-machine power oscillation

during the frequency dynamic process. Therefore, to fully test the DDC performance, a detailed dynamic simulation case is recommended.

Future studies on hybrid DDC can be extended in two main aspects:

1) While this chapter only studied under-frequency control, the over-frequency control method also needs to be studied. Moreover, a smarter and more comprehensive DDC scheme should be established, which can deal with other kinds of frequency disturbances. For example, the frequency drop caused by wind power fluctuation is close to a ramp response instead of a step response [109]. These critical operating conditions should also be considered when designing the DDC strategy.

2) The proposed method assumes that all the responsive loads only have on/off operating states, as with EWHs and traditional HVACs. In recent years, variable-speed air-conditioners are being widely used. Its power consumption is adjusted according to the temperature setpoint. Therefore, variable-speed air-conditioners can be incorporated into the control strategy so that the DDC will provide more flexible frequency regulation.

Chapter 5

Thermostatic Load Control for System Frequency Regulation Considering Daily Demand Profile and Progressive Recovery

This chapter proposes a thermostatic load control strategy for the PRFR and SCFR. With the proposed control strategy, a large population of EWHs and HVACs can provide frequency service and reduce the spinning reserve requirement. Two practical issues, daily demand profile and progressive load recovery are specifically considered in the control scheme. The proposed control strategy is then verified by the dynamic simulation of IEEE RTS 24-bus system.

Nomenclature

Parameters

R_E	Thermal resistance of the water tank of EWH
C_E	Thermal capacitance of the water in EWH
Q_{EWH}	Heat energy transfer rate (heating power) of EWH
$\theta_{a,in}$	Indoor air temperature
$\theta_{w,co}$	Temperature of cold water injected into EWH
$\theta_{w,s}$	Hot water temperature setpoint of EWH
$\theta_{w,db}$	Hot water temperature deadband of EWH
R_A	Thermal resistance of the house
C_A	Thermal capacitance of the house
Q_{AC}	Heat energy transfer rate of HVAC
$\theta_{a,out}$	Outdoor ambient temperature
$\theta_{a,s}$	Air temperature setpoint of HVAC

$\theta_{a,db}$ Air temperature deadband of HVAC

η Cooling efficiency of HVAC

$T_{A,on}$, $T_{A,off}$ The ON, OFF cycle of HVAC

f_{mPRFR} The lowest frequency that the PRFR controller targets to regulate

f_{mSCFR} The lowest frequency that the SCFR controller targets to regulate

k_P, k_S The droop coefficient of TLC for PRFR and SCFR

T_{sd} The maximal value of the random time delay

T_{sd}^{a} The random time delay of a single device

T_{SCFR} Time duration of HVAC for SCFR

Variables

$\theta_w(t)$ Real-time water temperature of EWH

$S_E(t)$ The ON/OFF states of the EWH's heating element

$W_D(t)$ The rate of hot water usage

$P_{EWH}(t)$ Real-time aggregated power of EWH

$\theta_a(t)$ Real-time indoor temperature

$S_A(t)$ The ON/OFF states of the HVAC's cooling element

$P_{AC}(t)$ Real-time aggregated power of HVAC

$P_{PRFR}(t)$ The target load reduction for PRFR at t

$P_{SCFR}(t)$ The target load reduction for SCFR at t

5.1 Introduction

In recent years, the increasing penetration of renewable energy has challenged power system frequency stability in two main aspects. First, some synchronous generators have been replaced by converter-based energy sources, resulting in a decline of system total inertia [4]. Second, the intermittent features of wind and solar power can lead to a mismatch between power generation and demand. For instance, it was estimated that the maximal frequency regulation reserve needed to accommodate California's 33% renewable penetration would increase from 277 MW to 1135 MW [110]. DDC was proposed for improving the dynamic performance of a system with high renewable energy penetration. Furthermore, thermostatic loads are ideal candidate for frequency reserve due to their high power rating and thermal inertia characteristics [7]. Such loads include EWHs and HVACs.

The main purpose of DDC can be summarized as: to design a control strategy so that a large number of responsive loads can emulate the generator spinning reserve for PRFR and SCFR. Overall, the previous studies on DDC achieved satisfactory dynamic performance in some idealized cases. However, several technical concerns have not been fully addressed.

1) *The daily demand profile*: Unlike the generator spinning reserve, the responsive load capacity is not constant for frequency regulation. EWH power is affected by users' hot water consumption, while HVAC power is affected by the outdoor temperature. The demand profile should be modeled as an input for the DDC strategy. Traditional studies have assumed that responsive loads are always sufficient to be called for frequency regulation. Although the total energy usage (in MWh) of each load type is estimated in [67], the power profiles of EWH and HVAC were not studied. Ref. [111], [112] only modeled the daily demand profile of HVAC. In [113], the demand profile of EWHs was modeled based on the statistic hot-water-usage profile.

2) *Load rebound of aggregated HVACs*: Although the sudden change of a large population of HVACs' temperature setting can achieve target load reduction instantaneously [6], long-term simulation shows that the ON/OFF cycles of some HVACs tend to synchronize, which causes severe power oscillation in the following hours [63], [116]. It is also called load rebound effect in some references [117]. Ref. [55], [59], [114]-[115] are focused on optimizing the frequency response (e.g., f_{nadir}, f_{ss}, or time to reach rated frequency) but omit the specific load model and the load recovery process. The post-disturbance recovery of aggregated thermostatic loads was studied in [113]. However, the aggregated power of refrigerators oscillates for over one hour before fully damped. A random switching controller was proposed to mitigate the load rebound in [63]. However, it has a slow response and is applied to load scheduling instead of frequency regulation. Another random approach to modulating aggregated refrigerator power was proposed in [116]. The result was promising, but the devices might be switched more than once in a short time interval. The most recent literature [117] proposed an optimization method for mitigating the rebound. The method also requires the input of every room's thermal parameters, which are hard to measure. The computation effort is large if there are thousands of HVACs under control.

Additionally, we believe that it is still possible to reduce the load rebound rate in [113], [116], and [117].

To summarize, the essence of a DDC or thermostatic load control (TLC) algorithm is to "organize" a large number of loads so that they have similar function as a generator for providing frequency regulation reserve. In addition, the algorithm should consider the variation of responsive load capacity. Therefore, in this chapter, a TLC strategy for frequency regulation is proposed with the consideration of the above two practical issues. First, since the daily demand profiles of EWHs and HVACs are complementary to some degree (as will be validated in later sections), the control strategy makes full use of the two loads based on their thermal models. Second, a concise but effective controller is proposed to recover thermostatic loads smoothly after the disturbance. The load rebound is effectively mitigated.

The remaining sections of this chapter are as follows. Section 5.2 proposes the model of demand profiles. Section 5.3 proposes the TLC strategy for both PRFR and SCFR, respectively. The progressive load recovery scheme of HVACs is also studied in order to mitigate load rebound. Section 5.4 summarizes the overall control strategy and its communication path. In Section 5.5, a simulation study is done to verify the proposed strategy, especially the impact of load profile on control performance. Finally, Section 5.6 concludes the whole chapter.

5.2   Modeling of Daily Demand Profiles

In this section, the behavior models of EWHs and HVACs are proposed, respectively. With this model, the system operators are able to estimate the demand profile when they have signed DR contracts with a particular number of consumers. The demand profile is a necessary input for the dynamic TLC strategy.

5.2.1   Modeling of EWH profile

The power consumption of an EWH is determined by two factors: customers' hot water consumption and heat dissipation of the water tank. Obviously, at peak hours of hot water

consumption, more EWHs are switched on, and the total power is larger. Consequently, the EWH provides a larger amount of frequency reserve.

The heat transfer equation of an EWH is given by (5.1) [48].

$$C_E \frac{d\theta_w(t)}{dt} = S_E(t)Q_{EWH} - \frac{\theta_w(t) - \theta_{a,in}}{R_E} - \rho c_P W_D(t)\left(\theta_w(t) - \theta_{w,co}\right) \qquad (5.1)$$

Note: the room temperature $\theta_{a,in}$ is assumed constant in this model because it fluctuates within a tight range if there is an HVAC in the house. The discrete form of (5.1) is

$$\theta_w(t + \Delta t) = \theta_w(t) + \frac{\Delta t}{C_E}\left[S_E(t)Q_{EWH} - \frac{\theta_w(t) - \theta_{a,in}}{R_E} - \rho c_P W_D(t)\left(\theta_w(t) - \theta_{w,co}\right)\right] \qquad (5.2)$$

where $S_E(t)$ is the ON/OFF states of the heating element, ρ is the density of water, and c_P is the specific heat of water (Ws/kg°C). The other parameters are listed in Table 5.1. Suppose $S_E(t)$ is governed by a thermostatic switching law with the temperature deadband:

$$S_E(t) = \begin{cases} 0, & \text{if } S_E(t - \Delta t) = 1 \ \& \ \theta_w(t) \geq \theta_{w,max} \\ 1, & \text{if } S_E(t - \Delta t) = 0 \ \& \ \theta_w(t) \leq \theta_{w,min} \\ S_E(t - \Delta t), & \text{otherwise} \end{cases} \qquad (5.3)$$

where $\theta_{w,max}$ and $\theta_{w,min}$ are nominal upper and lower temperature limits.

$$\begin{aligned} \theta_{w,min} &= \theta_{w,s} - 0.5\theta_{w,db} \\ \theta_{w,max} &= \theta_{w,s} + 0.5\theta_{w,db} \end{aligned} \qquad (5.4)$$

Table 5.1. Parameters of the EWH heat transfer model.

Parameter	Value
R_E	380°C /kW
C_E	0.2kWh/°C
Q_{EWH}	3.0kW
$\theta_{a,in}$	22°C
$\theta_{w,co}$	10°C
$\theta_{w,s}$	56°C
$\theta_{w,db}$	4°C
W_D	L/min

Equations (5.1)-(5.4) indicate that the core of estimating an EWH profile is to model the profile of $W_D(t)$, which is caused by household activities that consume hot water. They are called hot water consumption activities (HWCAs) in this study. During a HWCA k, where k = {taking shower, clothes washing, dishwashing}, the hot water is gradually drawn from the tank, and the same volume of cold water is injected. Consequently, the water temperature may fall below θ_{min}, and the heating element is switched on for a while to bring the water temperature higher than θ_{min} [43]. Other small HWCAs are neglected in this model. The probabilistic model of generating $W_D(t)$ profile is proposed, which consists of four steps.

1) Generating a high-resolution HWCA profile: Based on the above discussion, we construct the EWH demand profile from a time-of-use HWCA profile. It is denoted as $PerC_k(t)$, representing the percentage of a family performing HWCA-k at time t of a day. However, the existing HWCA profile is in hourly resolution [120], which cannot accurately represent the temporal distribution of the HWCA. In the proposed model, the 2-minute-resolution profile of HWCA-k is obtained by quadratic interpolation, as shown in Figure 5.1. For example, $PerC_1(180) = 0.32\%$ means that 0.32% of the families take showers between the 180-*th* time segment (5:58:00 - 6:00:00 am). Obviously, people are more likely to take a shower in the morning than in the evening. Therefore, we have

$$\sum_{t=1}^{720} PerC_k(t) = 1 \quad (k = 1, 2, 3) \tag{5.5}$$

2) Calibrating the HWCA profile: The true probability of HWCAs should be the production of $PerC_k(t)$ and the daily frequency of this activity. The following assumptions are made to simplify the model:

- The number of HWCA-1 (taking shower) is proportional to family size. Each family has three persons.
- The daily frequency of HWCA-2 (washing clothes) and HWCA-3 (washing dishes) is not proportional to family size. The average frequency is based on the demand survey.
- The three kinds of HWCA are independent.
- The parameters θ_s and θ_{db} are homogeneous for each home. Also, θ_a and θ_w are constant.
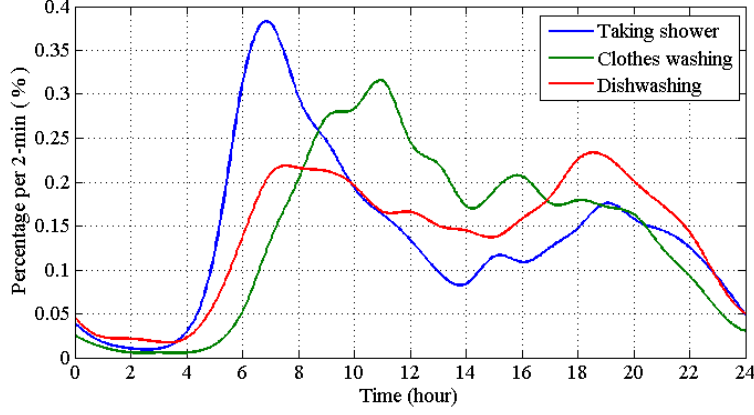
Figure 5.1. Time-of-use profile of HWCA.

- The initial water temperature of a day (0:00:00) is uniformly distributed: $\theta(0) \sim U(\theta_{min}, \theta_{max})$.

Therefore, $Pr_k(t)$, the probability of HWCA-k happening at time segment t is:

$$Pr_k(t) = PerC_k(t) \cdot m_k \cdot Freq_k \quad (t = 1, 2, ..., 720) \tag{5.6}$$

where m_k is the family size factor, and $m_k = \{3, 1, 1\}$. $Freq_k$ is the daily average frequency of activity k. According to our online demand survey [121] (will be discussed in Chapter 6), $Freq_k = \{1, 0.5, 0.5\}$ in Texas and New York.

3) Generating the random HWCA: For each time segment, if the HWCA-k does not happen, then a random number (r) uniformly distributed between 0 and 1 is generated. If r is less than the $Pr_k(t)$, then the HWCA-k happens. Thus, the state function $ON_k(t)$ is set to 1 and sustains for a random time duration of $T_{HWCA,k}$; otherwise, it remains 0. Repeating this process for three HWCAs, we can obtain the hot water usage profile of a family:

$$W_D(t) = \sum_{k=1}^{3} ON_k(t) \cdot \frac{Vol_k}{T_{HWCA,k}} \tag{5.7}$$

where the parameters Vol_k and $T_{HWCA,k}$ are shown in Table 5.2. By substituting (5.7) to (5.2) and letting $\Delta t = 2$ minute, the water temperature profile and demand profile of a typical EWH are simulated. An example is shown in Figure 5.2.

4) Summing up total demand profile: By repeating step 3) for all families, the aggregated EWH profile is obtained:

Table 5.2. Parameters used for modeling hot-water demand.

Parameter	Vol_k (L)	$T_{HWCA,k}$ (min.)
Shower	40	$U(15,25)$
Clothe washing	39	$U(30,40)$
Dish washing	16	$U(30,45)$
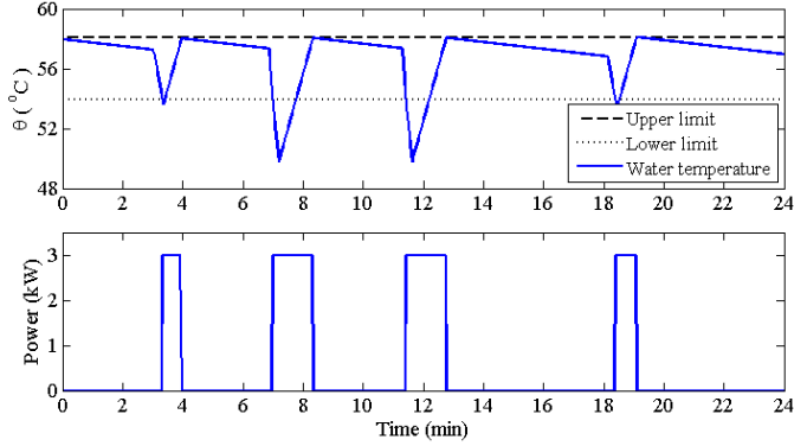
Figure 5.2. Water temperature and power consumption profile of EWH.

$$P_{EWH}(t) = \sum_{i=1}^{N_{EWH}} P_{EWH}^i(t) = \sum_{i=1}^{N_{EWH}} S_E^i(t)Q_{EWH}^i \tag{5.8}$$

where N_{EWH} is the total number of EWHs under control. In practice, the thermal parameters of the EWHs are not identical. Therefore, both homogeneous and heterogeneous parameters are simulated. A uniformly random multiplier between 0.5 and 1.5 is applied for each parameter (R_E, C_E and Q_{EWH}). The demand profile of 10,000 families with EWH is presented in Figure 5.3. Since the two curves almost overlap, we can use the average parameter to represent the random one. In other words, $P_{EWH}(t)$ can be estimated with high accuracy if only N_{EWH} and $Pr_k(t)$ are known.

Figure 5.3 indicates that that the real-time power demand of 10,000 EWHs ranges between 1.41~13.2MW. During the daytime (6:00~22:00), the EWHs provide 4.8~13.2MW frequency reserve (0.48~1.32kW for each device).

5.2.2 Modeling of HVAC profile

The HVAC can work in heating or cooling mode. The cooling mode is taken for example. In this paper, the one-order thermal transfer model of HVAC is adopted. When
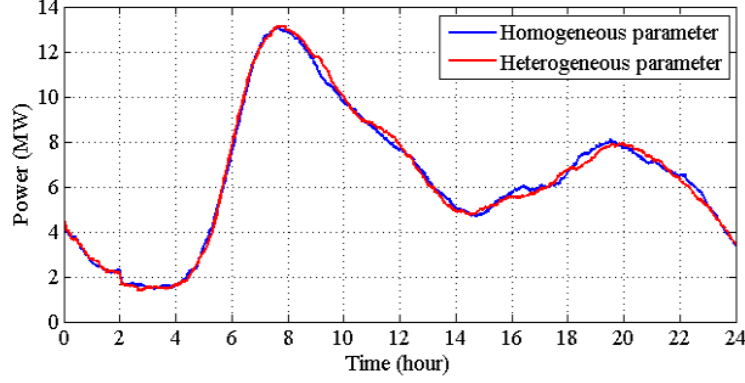
Figure 5.3. Aggregated EWH power profile for 10,000 families.

the HVAC is in operation (cooling mode), the room temperature $\theta(t)$ is determined by a differential equation [50]:

$$C_A \frac{d\theta_a(t)}{dt} = \frac{\theta_{a,out} - \theta_a(t)}{R_A} - S_A(t)Q_{AC} \tag{5.9}$$

where $S_A(t)$ is governed by a thermostatic switching law:

$$S_A(t) = \begin{cases} 0, & \text{if } S_A(t-\Delta t) = 1 \ \& \ \theta_a(t) \le \theta_{a,min} \\ 1, & \text{if } S_A(t-\Delta t) = 0 \ \& \ \theta_a(t) \ge \theta_{a,max} \\ S_A(t-\Delta t), & \text{otherwise} \end{cases} \tag{5.10}$$

The definitions of $\theta_{a,max}$ and $\theta_{a,min}$ are similar to (5.4). The discrete form of (5.9) is

$$\theta_a(t+\Delta t) = \theta_a(t) + \frac{\Delta t}{C_A}\left[\frac{\theta_{a,out} - \theta_a(t)}{R_A} - S_A(t)Q_{AC}\right] \tag{5.11}$$

The typical parameters are listed in Table 5.3 [122].

Based on the parameters, the ON and OFF cycle of an HVAC is $T_{A,on} = 43.8$ min., $T_{A,off} = 29.0$ min.. If compared with the EWH model, the "ambient temperature" in the HVAC model is the outdoor temperature that fluctuates over a wide range. To simplify the modeling, the following assumptions are made:

- The HVAC is kept in operation 24 hours of a day, and the temperature setting of each HVAC remains constant.
- The initial indoor air temperature of each day is uniformly distributed: $\theta_a(0) \sim U(\theta_{a,min}, \theta_{a,max})$.

88

Table 5.3. Parameters of the AC heat transfer model.

Parameter	Value
R_A	2.0˚C /kW
C_A	1.8kWh/˚C
Q_{AC}	7.5kW
$\theta_{a,out}$	32˚C
$\theta_{a,s}$	23˚C
$\theta_{a,db}$	2.4˚C
η	2.5

The total power consumption is estimated by

$$P_{AC}(t) = \frac{1}{\eta} \sum_{i=1}^{N_{AC}} S_A^i(t) Q_{AC}^i \qquad (5.12)$$

Based on the recorded temperature profile of a hot summer day and cool summer day in Houston, the aggregated demand profile of 10,000 HVACs with respect to the temperature difference is simulated, as shown in Figure 5.4. Similarly, a normal random multiplier between 0.5 and 1.5 is applied to each parameter (R_A, C_A and Q_{AC}). Since the thermal parameter of residential houses is much diverse than that of EWHs, there is no need to consider the homogeneous parameters. Obviously, during the daytime (9:00-20:00), the HVAC can provide a frequency reserve of $10 \sim 27.4$MW on different day types.
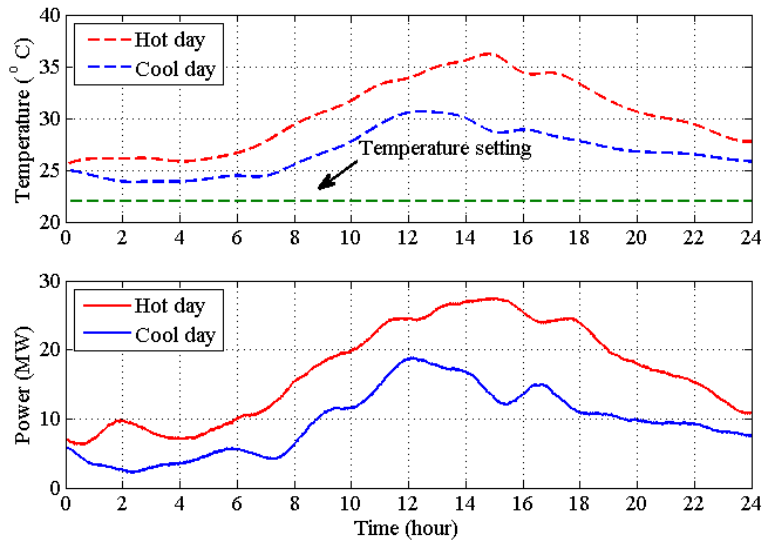
Figure 5.4. Aggregated HVAC power profile for 10,000 families.

5.2.3 Summary

Based on the proposed demand profile models, the combined demand profile of 25,000 EWHs and 25,000 HVACs is obtained, as shown in Figure 5.5. On a cool day, the frequency reserve ranges from 40 to 67MW; on a hot day, it ranges from 60 to 82MW. We can observe that the demand profiles of EWHs and HVACs are complementary during 7:00-20:00 and the loads can provide continuously sufficient frequency reserve. Therefore, 7:00-20:00 can be regarded as valid hours of TLC for frequency regulation.

5.3 Thermostatic Load Control Strategy

The purpose of TLC is to improve the frequency response of a system with renewable energy penetration. The extreme ramp rate that was recorded for a 100MW-level wind farm is 14% of capacity in a minute [123]. For large scale photovoltaic (PV) plants, cloud movement can also cause a ramp decrease in power output. Based on these considerations, TLC is designed to improve the system frequency response under both step disturbance (e.g., sudden steam generator outage, sudden large load increase) and short-term ramp disturbance (e.g., gradual wind/PV power decrease). Consequently, the loads can share the burden of turbine governor control and AGC. Due to the thermal inertia of EWH and HVAC, the load control will not affect customers' living comfort. On the other hand, the thermostatic loads are not supposed to be switched on and off repetitively within a very short period (tens of seconds). This feature should be considered when designing TLC strategy.
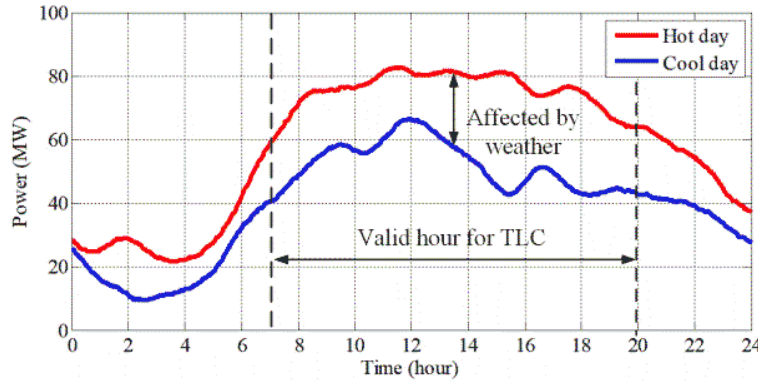
Figure 5.5. EWH and HVAC load as frequency reserve on a hot and cool day.

In this section, the system frequency response model is introduced. Then, the TLC strategy is proposed, in which EWHs participate in PRFR and HVACs participate in SCFR.

5.3.1 EWH for primary frequency regulation

A generator outage or sudden load increase causes a frequency drop ($\Delta f < 0$). In this situation, TLC is designed to emulate the frequency droop control of turbine governors. At time instant t, if the reserve for PRFR is sufficient, the target load reduction $P_{PRFR}(t)$ is computed by

$$P_{PRFR}(t) = \begin{cases} 0, & \text{if } \Delta f(t) \geq \Delta f_{db} \\ -k_P \Delta f(t), & \text{if } \Delta f(t) < \Delta f_{db} \text{ and } 0 \leq t \leq t_{nadir} \\ -k_P \Delta f(t_{nadir}), & \text{if } t > t_{nadir} \end{cases} \tag{5.13}$$

where k_P (MW/0.1Hz) is the frequency droop coefficient of the aggregate load, given by (5.14).

$$k_P = \frac{max(P_{EWH}(t))}{|\Delta f_{mPRFR}|} > 0 \tag{5.14}$$

where $max(.)$ is the maximal value of the daily demand profile (e.g., 13.2MW per 10,000 devices in Figure 5.3). Compared with under-frequency load shedding (UFLS) that deals with large frequency deviation, TLC is designed to regulate relatively small frequency deviations that happen more often. Therefore, a proper value of $\Delta f_{m,PRFR}$ can be -0.4Hz ($= 59.6 - 60$). Note: before t_{nadir}, the system frequency keeps decreasing and the load reduction gradually increases due to a droop feature; after t_{nadir}, the system frequency increases but the load reduction is still "locked" to $-k_P \Delta f(t_{nadir})$. In other words, the droop control is applied only if the frequency is falling. This control strategy can avoid repetitive action of EWHs after t_{nadir}.

In addition, the frequency reserve might be exhausted before t_{nadir} because the frequency reserve $P_{EWH}(t)$ is insufficient to regulate a large disturbance. In this situation, the feasible load reduction $P_{PRFR,feas}(t)$ is:

$$P_{PRFR,feas}(t) = min(P_{PRFR}(t), P_{EWH}(t)) \tag{5.15}$$

91

Based on the above discussion, the TLC scheme is implemented as follows:

Step 1: When $0 < t < t_{nadir}$, the aggregated EWH load acts as a frequency-dependent load with a large damping coefficient k_P. At each time step, the control center calculates the current load reduction amount $\Delta P_{PRFR}(t)$, which is the difference between the target load reductions of two consecutive steps:

$$\Delta P_{PRFR,feas}(t) = P_{PRFR,feas}(t) - P_{PRFR,feas}(t - \Delta t) \tag{5.16}$$

The time interval Δt is set to 0.5s in this chapter, considering the time interval of frequency measurement devices. Once the load aggregator calculates $\Delta P_{PRFR,feas}(t)$, it sends the OFF"signal to $N_{off}(t)$ EWHs that are now in an ON state. When the EWH load controller receives the signal, it will turn off the device. $N_{off}(t)$ is calculated by

$$N_{off}(t) = \frac{\Delta P_{PRFR,feas}(t)}{\bar{Q}_{EWH}} \tag{5.17}$$

where $\bar{Q}_{EWH}$ is the average power of the registered EWHs. PRFR is terminated at t if all ON devices are turned off ($P_{EWH}(t) < P_{PRFR}(t)$).

Step 2: When $t > t_{nadir}$, the aggregated EWH acts as a constant power load, and the control center stops performing the EWH load reduction. Also, t_{nadir} is identified by $f'(t)=0$. With the participation of TLC, the system equivalent damping coefficient (D') is raised during the period $0 \sim t_{nadir}$.

$$D' = D + \alpha k_P > D \tag{5.18}$$

where $\alpha = P_{EWH}(t)/P_{sys}$, and P_{sys} is the system total loading level. According to the sensitivity study in [102], the frequency nadir will be higher for the same condition [102]. The steady state frequency deviation is also brought closer to 60Hz, according to (5.19).

$$\Delta f'_{ss} = 60 \cdot \frac{R(\Delta P - \alpha k_P \Delta f_{nadir})}{D'R + 1} > \Delta f_{ss} \tag{5.19}$$

It should also be noted that turning off EWHs for a short period (around 10 minutes) does not cause cycle synchronization because the water temperature change of an EWH is negligible [113].

5.3.2　HVAC for secondary frequency regulation

1) Modulation of aggregated HVAC power: Section 5.2 indicates that HVACs can provide a larger amount of frequency reserve than the same number of EWHs on hot summer days. Previous studies has demonstrated that HVACs can provide both long-term regulation (load following) and short-term regulation (frequency regulation). Both regulations are subjected to a specified constraint of room temperature increase ($\Delta\theta_s$). In this subsection, a random-switching and cycle-recovery (RS-CR) method is proposed to avoid cycle synchronization. The method is based on two essential characteristics of the aggregated HVACs:

- The simulation indicates that the $\theta_a(t)$ (determined by (5.9)) can be approximated as a linear function within such a narrow deadband. Based on the three assumptions given in Section 5.2.2, we can derive that at any time t, $\theta_a(t)$ of a population of houses also obeys uniform distribution (the detailed analysis is in Appendix B).

$$\theta_a(t) \sim U(\theta_{a,min}, \theta_{a,max})\tag{5.20}$$

- Load reduction is designed to sustain for a duration of T_{SCFR} ($5 \leq T_{SCFR} \leq 15$min.). The lower bound is set to 5 minutes because the time-delay relay of HVAC ensures the minimal time for changing the ON/OFF status [111].

Therefore, an RS-CR method is designed as follows:

Step 1: When the SCFR is activated, each ON device is switched off with a specified probability p_{off}, which is sent from the aggregator. The device that is selected for being switched off is called an "activated device." Also, no control action is done with the remaining devices. Consequently, the expected load reduction is:

$$P_{SCFR} \approx p_{off}P_{AC}(t)\tag{5.21}$$

To implement this, each ON device makes a switching-off decision according to the random number r [69].

$$\begin{cases} if \ r \leq p_{off}, \ \text{switch off} \\ if \ r > p_{off}, \ \text{remain on} \end{cases}\tag{5.22}$$

where r is uniformly distributed between 0 and 1. Since the activated devices are randomly selected from the ON devices, their temperatures still obey uniform distribution.

Step 2: After T_{SCFR} ($T_{SCFR} \leq 15$ minutes), the activated devices are switched back on. As illustrated by Figure 5.6, their temperature settings are raised by $\Delta\theta_{a,s}$ for a duration of ($T_{A,off} - T_{SCFR}$). Since $\theta_a(t)$ can be measured by the thermometer in the HVAC, $\Delta\theta_{a,s}$ is given by (5.23).

$$\Delta\theta_{a,s} = \theta(t_{SCFR0} + T_{SCFR}) - \theta(t_{SCFR0}) \tag{5.23}$$

Within a narrow deadband, $\theta_a(t)$ changes linearly with t [116], $T_{A,off}$ is estimated by (5.24).

$$T_{A,off} = \frac{\theta_{db}}{\Delta\theta_s} \cdot T_{SCFR} \tag{5.24}$$

In Figure 5.6, the dashed black line represents the hypothetical $\theta_a(t)$ if there is no load control, while the solid line represents the practical $\theta_a(t)$ resulting from load control. In the SCFR period (purple shade in Figure 5.6), the indoor temperatures of activated devices rise together. After the SCFR period (T_{SFR}), the activated devices are switched back on. If $\theta_a(t)$ reaches the lower limit $\theta_{a,min} + \Delta\theta_{a,s}$, the activated devices are turned off by the thermostat. After this point, $\theta_a(t)$ automatically return to the hypothetical track. Consequently, the
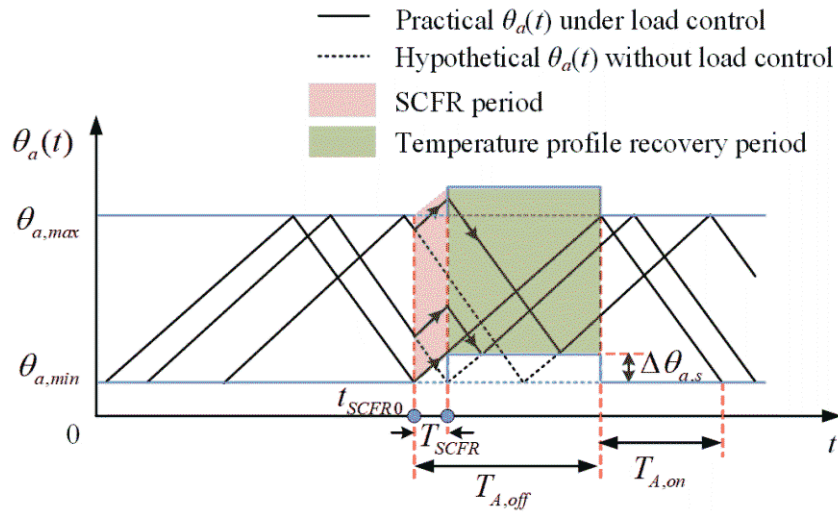
Figure 5.6. Illustration of the RS-CR method with activated devices.

temperature profile of activated devices is gradually recovered (the green shade in Figure 5.6), as if no SCFR has happened. The temperature profile is still uniformly distributed.

As discussed in previous sections, the thermal parameters (R_A, C_A and Q_{AC}) of houses are quite diverse. Thus, a uniformly random multiplier between 0.5 and 1.5 is also applied to R_A, C_A and Q_{AC}. The aggregated power response of 10,000 devices (at $\theta_a = 32°C$) is simulated based on the thermal transfer model (given by (5.11)) with $\Delta t = 2s$. At $t = 30$ minutes, SCFR is activated by the control center with $p_{off} = 0.5$ and $T_{SCFR} = 10$ minutes, which means the total load should be reduced by 50%. Figure 5.7 (a) is the temperature profile of 200 representative activated devices. Note: since $T_{A,on}$, $T_{A,off}$ and $\Delta\theta_s$ are heterogeneous for each HVAC, the $\theta_{a,max}$ and $\theta_{a,min}$ of each device are different during the cycle recovery period. This figure only shows one example of $\theta_{a,max}$ and $\theta_{a,min}$ (the black dashed line). Figure 5.7 (b) indicates that the total power almost keep constant after the SCFR period. The practical load reduction at t_{SCFR0} is 9.42MW (50.2% of the original load). After SCFR period, $\Delta\theta_{a,s}$ is 0.3-0.5°C and sustained for a cycle recovery period of 40-50 minutes, which has little impact on customers comfort. After $t = 100$ minutes, the power is recovered to the previous value and the room temperature is also recovered to the previous deadband (22.8°C, 24.2°C).

In order to evaluate the effect of the control strategy, we define the load rebound rate as

$$Rb_{AC} = 100 \cdot \frac{P^{max}_{AC\_rec}(t) - P^{min}_{AC\_rec}(t)}{\overline{P}_{AC\_rec}(t)} \tag{5.25}$$

where $P^{max}_{AC\_rec}(t)$, $P^{min}_{AC\_rec}(t)$ and $\overline{P}_{AC\_rec}(t)$ are the maximal, minimal and average value of the aggregated HVAC power during the cycle recovery period, respectively. The Rb_{AC} value is calculated as 3% in Figure 5.7 (b). However, Rb_{AC} is between 15-20% in [116]-[117]. The other concern is the response speed. According to the sequential-dispatch approach in [117], it takes 5 minutes to complete load reduction. Thus, this method is more applicable to load scheduling than frequency regulation. In all, the proposed RS-CR method shows a significant advantage over the previous method in mitigating load rebound.
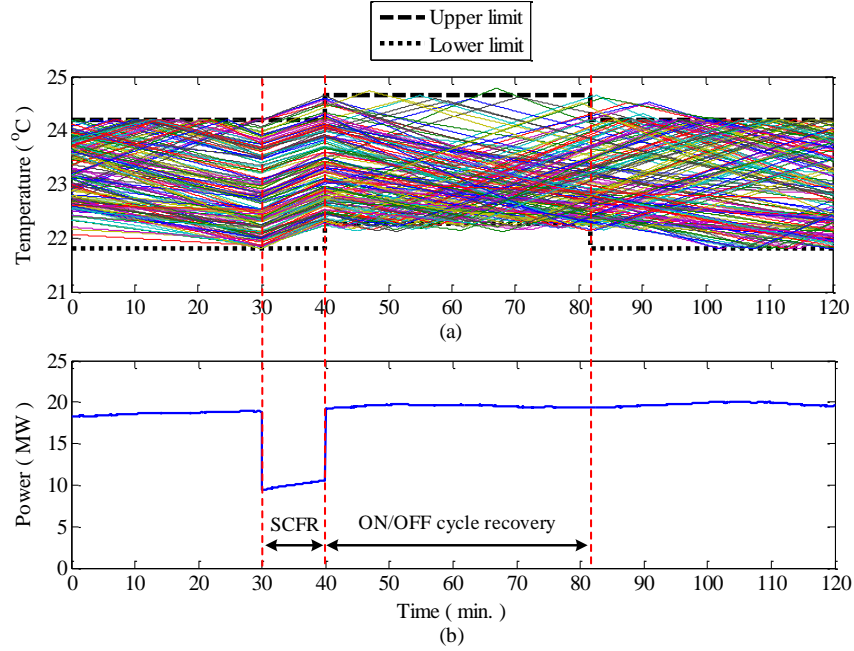
Figure 5.7. Aggregated HVAC response with RS-CR method: (a) temperature profile of 200 "activated devices"; (b) total power profile of 10,000 devices.

In practice, the outdoor temperature does not keep constant during the cycle recovery period, which lasts for tens of minutes. In the sensitivity study, we change constant $\theta_{a,out}$ into a time-varying value and let $p_{off} = 0.7$ and $T_{SCFR} = 12$ minutes. Figure 5.8 shows the aggregated HVAC power response in the hot day case in Section 5.2.2. Therefore, the proposed RS-CR method is robust under parameter changes.

2) HVAC control for frequency regulation: It has been demonstrated that the aggregated HVACs can implement short-term load reduction without cycle synchronization. The RS-CR method is also easy to implement in hardware. For the purpose of SCFR, the load aggregator generates the control signal p_{off} according to the frequency deviation.

$$p_{off} = \min\left(\frac{P_{SCFR}}{P_{AC}(t)}, 1\right) = \min\left(-\frac{k_S \Delta f(t)}{P_{AC}(t)}, 1\right) \tag{5.26}$$

where k_S (MW/Hz) is the SCFR droop coefficient. The method for calculating k_S is similar to k_P. The demand profile $P_{AC}(t)$, estimated by the load aggregator, is a required input for the RS-CR method. Here is a numerical example. A load aggregator controls 1000 HVACs and $k_S = 20$MW/Hz. $P_{AC}(t)$ is time-varying due to outdoor temperature variation. In

(a) Hot day morning   (2) Hot day afternoon
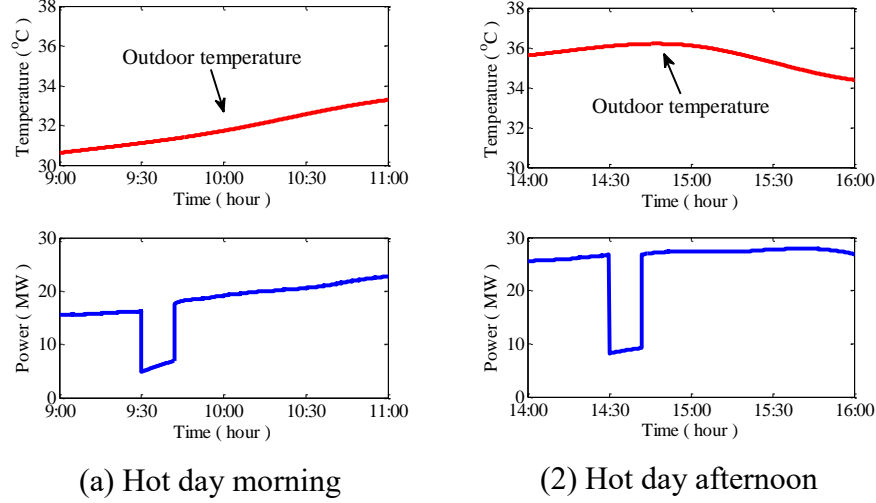
Figure 5.8. Aggregated HVAC response with RS-CR method under time-varying outdoor temperature.

scenario 1, $P_{AC}(t) = 3.0$MW and the frequency reaches a steady state of $\Delta f_{ss} = -0.08$Hz, then p_{off} is calculated as $-20*(-0.08)/3 = 0.533$. In scenario 2, $P_{AC}(t) = 2.4$MW and the same Δf_{ss} happens, then p_{off} is 0.667. This method ensures that the aggregate HVACs provide the same load reduction for the same frequency deviation, no matter how the demand profile changes. This is different from previous work in that only "one snapshot" of the demand profile is considered [116], [117].

However, if a large number of devices are switched off instantaneously, the step load change will cause a frequency overshot. To avoid this, each device is switched off with a random time delay T_{sd}^a:

$$T_{sd}^a \sim U(0, T_{sd}) \tag{5.27}$$

where T_{sd} is the maximal value of the time delay. The delay has two functions. First, it ensures a relatively smooth frequency response, which can be verified by the SFR model in Section 4.4.4. Second, before the time delay expires, if the frequency is detected to be higher than the rated frequency (e.g., 60 Hz), a "stop" signal will be sent from the load aggregator. Then, the activated devices keep their ON state if the random delay hasn't expired. Therefore, the random delay can prevent the TLC over-compensation, in case the SFR reserve is higher than needed.

5.4 A Summary of TLC Scheme

The daily demand profile model and dynamic TLC strategy have been proposed in Section 5.2 and 5.3, respectively. This section summarizes the overall dynamic TLC scheme, coordinating PRFR and SCFR. In a bulk power system, multiple load aggregators work independently. Each one may control the responsive loads of a community. As shown in Figure 5.9, the communication path is designed as follows:

- *Frequency measurement*: The load aggregator measures the local bus frequency. The measurement error of the existing FDR is less than 0.0001Hz, which is sufficient for frequency regulation application [124].

- *PRFR module*: The load aggregator monitors the ON/OFF state of each EWH with a sampling time of 2 minutes. A list of operating states is updated in the control center. According to the simulation in Section 5.2.1, an EWH changes its state up to 10 times a day. Therefore, it is not necessary to update the state second by second. Instead, a sampling rate of 2 minutes is sufficient, because the probability of an EWH keeping its on/off state within 2 minutes is:
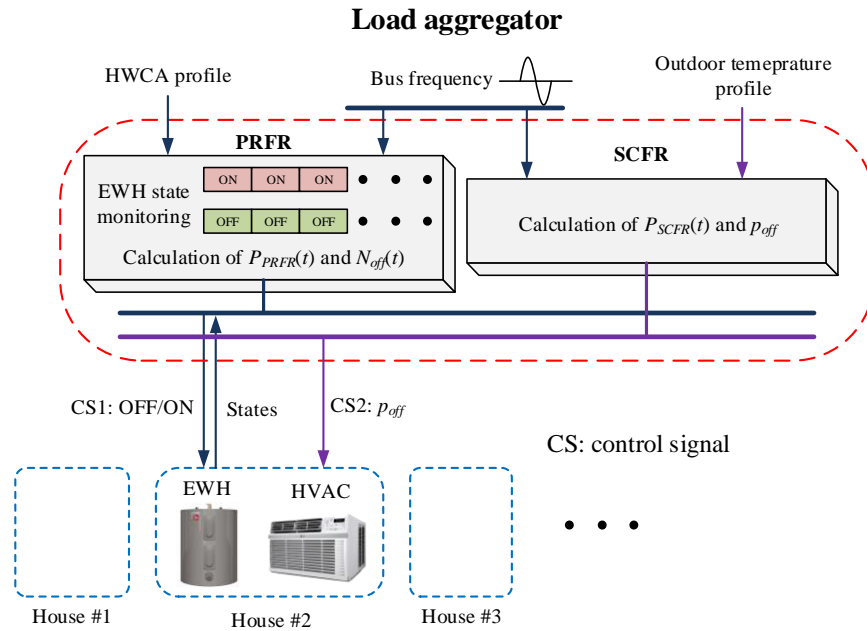
Figure 5.9. Communication path of a TLC system.

$$Prob = 1 - \frac{10}{720} = 98.61\%$$

In PRFR, the load aggregator sends the control signal to a number of load controllers with a time step of 0.5s. A Wifi-based smart plug can be used as a load controller. Since the EWH is a purely resistive load, it is connected to the power outlet through a smart plug, which can disconnect the EWH instantaneously.

- *SCFR module*: In SCFR, the center calculates p_{off} according to (5.26) and sends it to each load controller. It also sends the "stop signal" to the load controller if the frequency reaches 60Hz. The controller, which is embedded in the thermostat of the HVAC, is able to turn off the compressor and changes the temperature setting when needed.

The control flowchart is shown in Figure 5.10. Suppose a disturbance causes a frequency drop. If the measured frequency falls below the threshold, 59.96Hz, then the control center will activate the PRFR. The load reduction is conducted every 0.5s until the frequency nadir is reached. When the frequency reaches a new steady state that is lower than 59.96Hz, then the center will activate the SCFR. It computes the p_{off} and sends the signal to each HVAC controller. Then, the system frequency can be brought higher than 59.96Hz on condition that the frequency reserve is sufficient. Note: The "steady-state" is identified by the formula $|f_{mav}(t) - f_{mav}(t - \Delta t)| < 0.005$Hz, where f_{mav} is the moving average of the latest 5 frequency samples and Δt=0.5s.

5.5   Power System Simulation

This subsection verifies the proposed TLC strategy through a simulation study using the Matlab PSAT toolbox (V. 2.1.10) [101]. The IEEE RTS 24-bus, 11-machine dynamic testing system is employed, shown in Figure 5.11. The system base power is S_{base} = 100MVA. The system loading level (P_{sys}) varies from 1563.8MW to 2650.5MW through the day [125]. The testing system includes the turbine governor model, the exciter model and the synchronous generator model. The parameters of generator turbine governors are shown in Table 5.4. We assume that 25,000 EWHs and 25,000 HVACs are registered for TLC. Such loads are distributed at five load buses: Bus #4, #9, #15, #19 and #20. At each
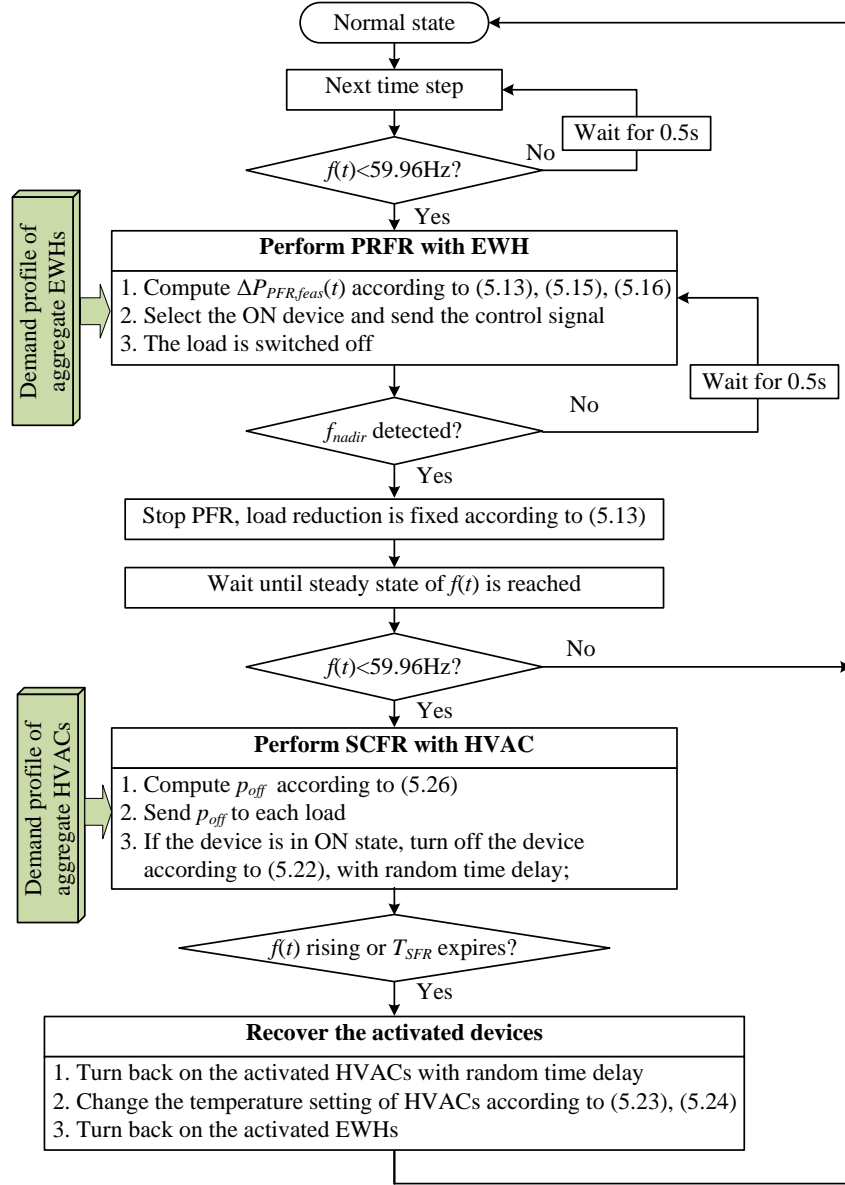
Figure 5.10 Flowchart of TLC scheme.

bus, a load aggregator organizes the corresponding EWHs and HVACs for frequency regulation.
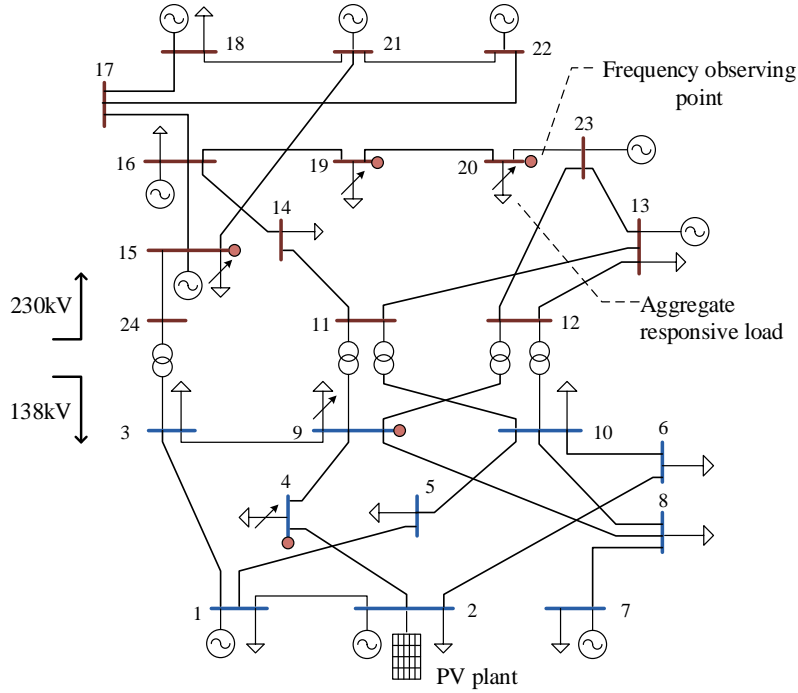
Figure 5.11. IEEE RTS 24 bus system.

Table 5.4. Parameters of turbine governors [1]

Generator bus	Rated power (MVA)	T_G (s)	T_C (s)	T_R (s)	F_H	R
1	270	0.33	0.3	10	0.24	0.04
2	80	0.13	0.25	9	0.28	0.05
7	300	0.22	0.26	14	0.35	0.08
13	300	0.24	0.37	12	0.23	0.06
15	240	0.2	0.25	8	0.26	0.05
16	200	0.18	0.33	11	0.22	0.04
18	450	0.13	0.25	13	0.19	0.05
21	450	0.22	0.26	14	0.35	0.08
22	350	0.24	0.37	35	0.14	0.06
23	660	0.18	0.25	13.5	0.28	0.05

[1] Generator at Bus #22 is hydro generator whose time constant is larger. Others are steam generators.

Based on the daily demand profile, $max(P_{EWH}(t)) = 13.2$MW, $max(P_{AC}(t)) = 27.4$MW. The maximal frequency deviations we target to regulate are: $\Delta f_{mPRFR} = -0.33$Hz and $\Delta f_{mSCFR} = -0.12$Hz. Then, the frequency droops are:

$$k_P = \frac{max\left(P_{EWH}(t)\right)}{\left|\Delta f_{mPRFR}\right|} = \frac{2.5 \times 13.2}{0.33} = 10.0MW / 0.1Hz$$

$$k_P = \frac{max\left(P_{AC}(t)\right)}{\left|\Delta f_{mSCFR}\right|} = \frac{2.5 \times 27.4}{0.12} = 57.1MW / 0.1Hz$$

5.5.1 Response to step disturbance

A generation outage of 80MW happens at Bus #2 on both hot day and cool day in summer. However, due to the difference in system loading level and responsive load capacity, the frequency responses are not necessarily the same.

At the peak hour (18:10 of the hot day), P_{sys} = 2650.5MW. According to the load profile model in Section 5.2, the responsive load capacity (before the disturbance happens) is scaled by times of aggregated power of 10,000 devices:

$$P_{EWH}(t_0) = 2.5 \times 6.88 = 17.20MW$$

$$P_{AC}(t_0) = 2.5 \times 23.29 = 58.97MW$$

The maximal time delay T_{sd} is 22s, which is a compromise between a fast response and mitigating the frequency overshoot. The simulated bus frequency is shown in Figure 5.12 (a). With the participation of TLC, the steady-state frequency is promoted from 59.922Hz to 59.973Hz, which is within the 60±0.04Hz deadband. Besides, Figure 5.12 (b) indicates that the responsive loads are sufficient to implement the TLC strategy. The response speed is much faster than AGC, which takes several minutes.

At the off-peak hour (15:30 of the cool day), however, P_{sys} = 2465MW. The power consumptions of two loads are:

$$P_{EWH}(t_0) = 2.5 \times 5.27 = 13.17MW$$

$$P_{AC}(t_0) = 2.5 \times 12.17 = 30.42MW$$

As shown in Figure 5.13 (a), $f(t)$ is slightly lower than peak-hour case because the 80MW outage takes a larger portion of the system loading level ($0.0325P_{sys}$) than the peak hour case ($0.0302P_{sys}$). With the participation of TLC, the steady-state frequency is promoted from 59.917Hz to 59.960Hz. The reason for being less effective is that the responsive loads are insufficient to implement the TLC. Specifically, the EWH is exhausted at t =
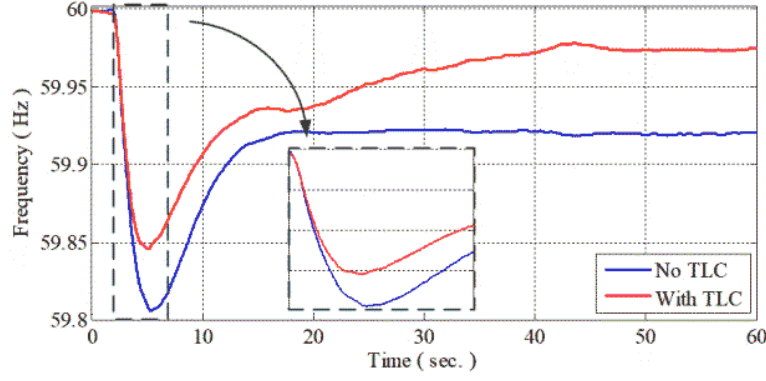
(a) Bus #19 frequency
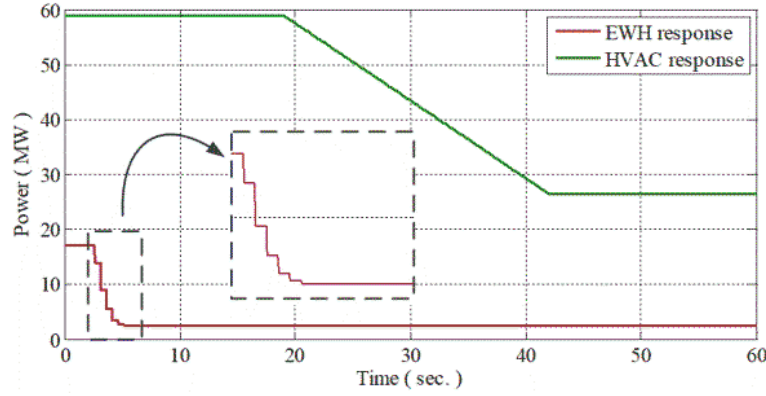
(b) Aggregated responsive load variation

Figure 5.12. Disturbance response of TLC during peak hours.

4.15s, before f_{nadir} is reached. In this case, AGC needs to call a larger amount of spinning reserve to bring the frequency back to 60Hz.

5.5.2   *Response to ramp disturbance*

A PV plant with a rated power of 300MW is connected to Bus #2 to replace part of the steam generators. The cloud movement can cause a rough ramp decrease in PV power output when it is approaching above the PV plant and a ramp increase when it is leaving. At the peak hour (13:00 of the hot day), $P_{sys} = 2518.0$MW. The demands of 25,000 EWHs and 25,000 HVACs are: $P_{EWH}(t_0) = 15.24$MW and $P_{AC}(t_0) = 64.65$MW. The cloud approaches at $t=10$s and leaves completely at $t = 550$s. At $t = 503$s, when the frequency increase is detected, those HVACs that were previously switched off are switched back on with a random time delay. The PV power output and the frequency response are shown in Figure 5.14. It is observed that the TLC can maintain a higher steady-state frequency when
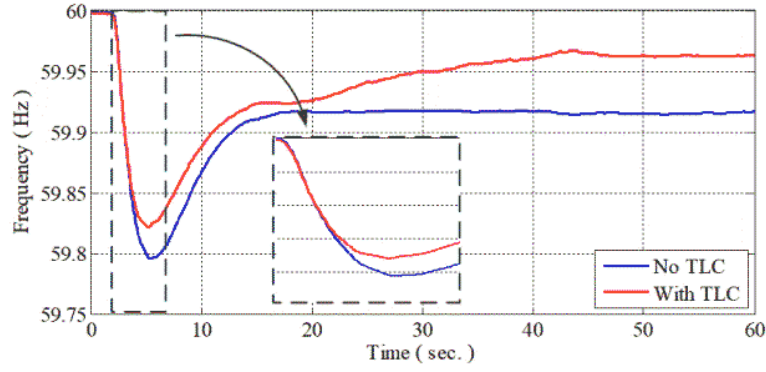
(a) Bus #19 frequency
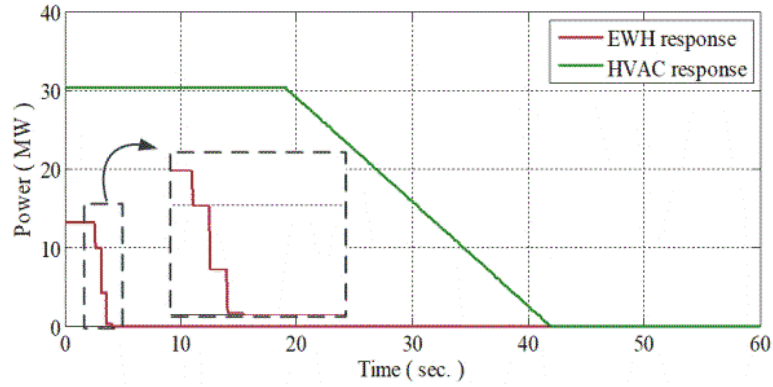
(b) Aggregated responsive load variation

Figure 5.13. Disturbance response of TLC during off-peak hours.

a short-term PV power shortage happens. Therefore, the requirement of generator spinning reserve is reduced.

5.5.3   *Discussion*

The simulation study illustrates that if the same disturbance happens at different time slots of a day, the frequency response can be different due to the variation of responsive load profile and system loading level. The performance of TLC in three scenarios is compared in Table 5.5. In conclusion, during "valid TLC hours", the 25,000 EWHs and HVACs can recover the system frequency to the 59.96Hz deadband through the proposed TLC strategy.
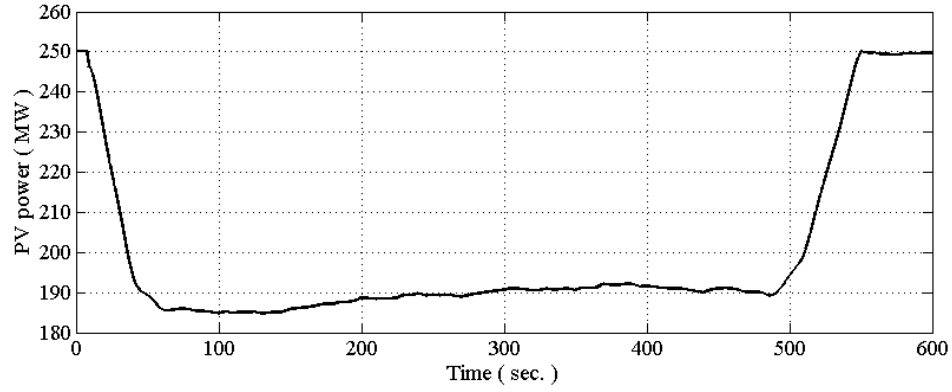
(a) PV power output
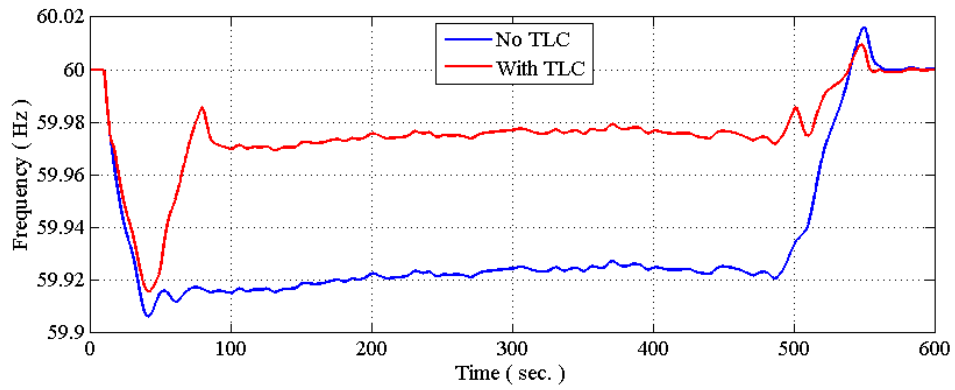
(b) Bus #19 frequency

Figure 5.14. Response of TLC under PV penetration.

Table 5.5. Parameters used for modeling hot-water demand [1]

Scenario	f_{nadir} (Hz)		f_{ss} (Hz) [2]	
	Without TLC	With TLC	Without TLC	With TLC
1	59.808	59.849	59.922	59.973
2	59.797	59.824	59.917	59.960
3	59.906	59.916	59.923	57.975

[1] Scenario 1 is step disturbance, peak hour; Scenario 2 is step disturbance, off-peak hour; and Scenario 3 is ramp disturbance, peak hour.
[2] Since there is noise in frequency, f_{ss} means the average frequency after SFR.

The control parameters, k_P and k_S, are determined by the load aggregator based on the maximal value of the demand profile. For instance, if EWHs only takes a small portion of the system total loading level (N_{EWH} is small), it is meaningless to set a large k_P. k_P can also be set to a larger value if more residential EWHs are registered for TLC in the future. The load aggregator is also a flexible resource in frequency regulation. The comparison

between homogeneous and heterogeneous cases shows that it works effectively even if the thermal parameters of EWHs and HVACs are random.

5.6 Conclusion

In this chapter, a dynamic TLC strategy is proposed. Two common thermostatic loads, EWHs and HVACs, are utilized for PRFR and SCFR, respectively. Given a particular number of loads (without knowing the rated power of individual devices), we can estimate the 24-hour demand profile, which provides essential input for conducting TLC. The simulation result reveals that the daily demand profiles of the same number of EWHs and HVACs are complementary. This is the first contribution of the chapter. The second contribution is the proposed TLC strategy for PFR and SFR, with the consideration of progressive cycle recovery after a disturbance. In particular, the RS-CR method can regulate the aggregated HVAC power without causing power rebound. This method is easy to implement in existing HVAC thermostats. The advantage is the indoor temperate does not have to be monitored by the load aggregator. Meanwhile, the impact on customers comfort is negligible.

Overall, TLC is an ancillary approach to frequency regulation of bulk power systems. It acts as compensation for turbine governor control and AGC. The performance of TLC not only depends on the robustness of the control algorithm but also on whether the demand capacity is sufficient. In comparison with the previous study, this paper conducts a study on more practical issues of TLC. The proposed method and verification study have addressed the two issues claimed in Section 5.1. Therefore, TLC can improve the dynamic performance of a system with high penetration of renewable energy.

Chapter 6

Estimating the Profile of Incentive-Based Demand Response (IBDR) by Integrating Technical Models and Social-Behavioral Factors

DR is widely recognized as an important approach to balancing the power grid and reducing peak load of power systems. In order to better estimate the capability and the expense of peak load reduction through DR, we need to obtain a residential load profile and customers' attitudes toward DR programs. Based on a large-scale online survey collected among over 1,500 customers from New York and Texas in the U.S., this study investigates the relationships among household appliance activities, load profiles, and incentive-based DR (IBDR) participation for peak load curtailment through reward payment. The daily load profiles of major home appliances are developed. Additionally, this chapter estimates the expense of reducing the yearly peak of the local grid load. Finally, the study addresses the importance of investigating the multifaceted factors affecting IBDR participation and provides useful suggestions to utility companies when implementing DR programs.

6.1 Introduction

According to the U.S. Energy Information Administration, nearly 4×10^6 GWh of electricity was consumed by the commercial, residential, and industrial sectors in 2015, with the residential sector having the largest share of total electricity consumption (38%) [126]. Since the residential load is affected by customers' habits and weather condition, extra generation reserve should always be available for serving the system's yearly peak load, which only lasts for a few hours [127]. This is considered uneconomical [9]. Additionally, generators with high marginal costs might be called on for supplying the

peak load [128]. As energy demand increases, especially during peak demand hours when the load is close to the power system's supply capacity, there is an increased risk of system failure and economically inefficient investment [129]. Therefore, balancing real-time power demand and power supply has recently motivated greater utilization of DR programs.

The current potential for using residential loads as DR is significant. To provide an example, in the Southern part of the United States, EWHs and HVACs comprise 18.5% and 16.0% of yearly energy consumption of residential loads, respectively. In Florida, these two indices are 18.1% and 25.3%, respectively [130]. Due to thermal inertia characteristics, turning EWHs off or changing HVACs' thermostat settings for a short period of time causes a negligible impact on customer comfort [131]. Therefore, these two loads have great potential for peak load reduction via DR programs. Implementing DR programs is an effective approach to decrease or shift energy demand by altering customers' electricity usage in response to electricity price signals or financial incentives [126], [132]. With the participation of DR, the expense for generation reserve can also be reduced.

In the literature, DR programs are generally classified into two categories: price-based demand response (PBDR) and incentive-based demand response (IBDR). Note, IBDR is also known as coupon-based demand response (CBDR). In PBDR programs, customers pay for the electricity at different prices throughout a day. In IBDR programs, customers receive certain amount of financial reward for reducing appliance usage in peak hours, such as through direct load control, interruptible load, and emergency demand reduction [132]-[134]. Studies suggest that IBDR programs are more effective than PBDR programs because people are more motivated to accept an incentive program in which they see "bonus" terms [135]-[136]. When designing an IBDR program, it is essential to quantify how much demand changes in response to the incentive reward change, which is called elasticity in economic terms [40]. Consequently, the expense of peak load reduction can be estimated.

Previous studies in [126], [132], [137], [138], [11] investigated the demand elasticity of residential loads, that is, demand reduction potential with respect to different prices. However, there are several important factors that have not been thoroughly addressed:

- The majority of the previous studies on demand elasticity were based on PBDR, such as the potential demand reduction with a dynamic pricing scheme [126]. However, little work has been done targeting the elasticity of IBDR, namely the relationship between total peak demand reduction and financial incentives.

- Studies such as [132], [137]-[138] discussed demand elasticity estimation based on the overall demand change in response to electricity price or financial incentives. However, there is little consideration of specific demand categories or activities, such as EWHs or HVACs. Differentiating the DR capacity from EWHs, HVACs, or other loads will provide more useful and specific information for utility companies to control load accurately.

- The previous studies considered technical impacts regarding DR [11]. However, there was limited number of studies attempting to connect DR potentials with many non-technical factors such as habits of home appliance usage, willingness of DR participation, or other social- behavioral factors (e.g., environmental concern).

Based on the motivations listed above, a DR survey is designed considering social-behavioral factors. Then, the modeling of load profiles for major home appliances is proposed, such as HVACs and EWHs. Based on the survey result and the load profile models, we evaluate the DR potential and the cost of reducing a particular amount of peak load through IBDR programs. The methods and contributions of this work are summarized as follows:

- First, the study considers multiple dimensions affecting DR participation, including household activities, load profiles, and requested financial reward.

- Second, the survey is based on 1575 customers, considered sufficient to be statistically representative for a 95% confidence level based on representative demographics in gender, income and ethnicity from two different climate zones (Texas and New York) [139].

- Third, a systematic method is established to develop daily profiles for different loads, especially HVACs and EWHs, by integrating the social-behavioral survey result and the technical models.

- Finally, the expenses of IBDR for peak load reduction are further estimated from the survey results and the load models. The expense estimation provides utility companies with essential references for implementing future IBDR programs with fine-tuned DR profiles.

The remaining sections are organized as follows. Section 6.2 briefly discusses survey design and data collection procedures. Part of the survey result is presented in Section 6.3. Section 6.4 introduces the thermal transfer model of HVACs and EWHs. Then, the modeling of daily load profiles is proposed. Section 6.5 estimates the expense of peak load reduction through IBDR in two representative states in the U.S., Texas (TX) and New York (NY). Section 6.6 concludes the chapter.

6.2 Formulation of the Problem

6.2.1 Survey Overview

In order to better estimate the DR participation in peak load reduction, we designed a large-scale online survey to investigate residential customers' frequency of engaging in certain household activities (e.g., heating and cooling), energy consuming habits, and their willingness to participate in IBDR programs. Other social-psychological factors were considered based on social psychology discipline (see Table 6.1 for an overview of survey design). Recent studies have widely addressed the importance of integrating residential load modeling and social-psychological factors [126], [140]-[142]. Based on interdisciplinary research between social psychology and power system, this survey is designed to collect information from 1575 residents in the states of TX and NY. The two states are chosen because they represent different climate zones and are sufficiently diverse in terms of ethnicity and income.

Among the 1575 valid responses collected, 785 are from TX and 790 are from NY. The number of survey responses is sufficient to make the survey results representative and

Table 6.1. Overview of demand response participation survey.

Category	Variables/content
Demographics	Age, gender, income, household square footage, occupation, education, political orientation, ethnic background, and living city
Household appliances activities	- Frequency and time of using washer, dryer and dishwasher, and showering in a typical week - Time when someone is at home during peak hours in a typical week - Method of cooling home - Electricity payment structure
Energy-using habits	- Typical temperature settings when someone is at home and no one is at home - Energy efficiency behaviors – turning off appliances when they are not used, setting lower temperatures in winter and higher temperatures in summer to save electricity, only washing clothes with full loads.
Demand response (DR) program	- Basic introduction of DR - Previous experience with DR programs - Willingness to participate in DR programs (considering specific household activities, thermal comfort, time of commitment, and incentive amount, etc.) - Reasons for participating or not participating in DR [1] - Perceived benefits of DR
Social-psychological factors	- Social norms, sense of community, environmental and cost concerns - Trust in utility companies, thermal comfort, frequency of discussing energy efficiency, intention to save energy - The top three appliances that are considered critical by customers

[1] The customers are not required to fill up this survey item.

statistically valid [139]. Among these participants, 21% come from a single-person household, 34% from 2-person household, 20% from 3-person household, and 25% from 4-person or 5-or-more-person household. The average family size is calculated as 2.7 persons. In TX, approximately 72.2% of customers have fixed pricing, while others have dynamic pricing or peak-and-off-peak pricing. In NY, approximately 58.2% of customers have fixed pricing, while others have dynamic pricing or peak-and-off-peak pricing. The high percentage of fixed-pricing schemes indicates that IBDR is the only financial incentive for customers to reduce their peak load.

6.2.2 Measures

1) Household appliance activities: Two main home appliance activities in this study include the temperature setting of HVAC and the hot water usage.

According to the thermal transfer principle, the power profile of the HVAC is related to the difference between the outdoor temperature and thermostat temperature setting [143]. Therefore, we measure typical household temperature settings when someone is at home and when no one is at home during summer weekdays. Considering that a household's temperature setting might be slightly different on different days, we set the options of 3 ˚F range in measuring HVAC activities so that it is easier for customers to make the choice (Note: American people are more familiar with Fahrenheit than Celsius). For example, customers can choose the answer of "64 - 66 ˚F" or "67 - 69 ˚F".

The load profile of EWHs is affected by people's HWCA. The three main HWCAs include 1) taking a shower, 2) doing laundry, and 3) washing dishes [43]. They are denoted as HWCA-k, where k = 1, 2, 3. Specifically, this study measures 1) the frequency (e.g., how many times) of using washing machine, dryer and dishwasher per week, and 2) the starting time (in hour) that customers typically engage in HWCAs during the weekday.

2) Willingness to participate in IBDR: To encourage customers' participation in IBDR programs, many utility companies across the U.S. have provided financial incentives anywhere between $ 25 and $ 100 per year, between $ 5 and $ 20 per month, or between 3 cents to $ 1 per kWh saved [132]. The fixed-dollar reward is more likely to be accepted by customers because it is quite straightforward for them [144]. Based on the current IBDR

programs in U.S., the measure of IBDR participation in this study consists of two kinds of load reduction: through automatic control and through manual curtailment behavior. Automatic control (IBDR Program-1) refers to raising the HVAC temperature settings on hot summer weekdays via installation of a free remote controller. Manual curtailment (IBDR Program-2) refers to avoiding using certain household appliances for certain periods of time. Instead of directly asking for the level of IBDR participation (e.g., from "level 1" to "level 5"), the participants were asked to indicate the minimum monthly requested reward (offered from June to August) to participate in two IBDR programs. The reward payment option is integer dollars ranging from $ 5 to $ 20.

Specially, the proposed IBDR Program-1 asked: "Suppose your utility company offers you a DR program with a free automatic controller which is installed in your HVAC system and it will

- Raise your thermostat setting by 2-3 ˚F for up to 45 minutes on summer weekdays when the total demand is high;

- During very hot days (when outdoor temperature is over 95 ˚F and power is in high demand), raise your thermostat by up to 5 ˚F (but not higher than 79 ˚F) for up to 45 minutes.

Would you participate in this program?"

Similarly, the IBDR Program-2 asked, "suppose your electric company offers you another IBDR program: You will receive text messages requiring you to do the following things during hot summer weekdays when the outside temperature is higher than 90 ˚F:

- Avoid using dishwasher;

- Avoid using washing machine and dryer.

Would you participate in this program?"

Note: We assume the consumers will follow the contract with their utility or aggregator; otherwise, a penalty may apply. Also, the activity of delaying taking a hot shower during peak hours was not asked because it might cause excessive discomfort to customers.

6.3 Survey Result

This section presents a statistical analysis on HVAC thermostat settings, frequency of HVAC usage and hot water usage activities, and willingness to participate in an IBDR.

6.3.1 HVAC Thermostat Settings

The average temperature settings during summer weekdays are 72.0 ˚F and 69.5 ˚F when someone is at home in TX and NY, respectively. When no one is at home, the temperature settings are 74.7 ˚F and 71.5 ˚F in TX and NY, respectively. Besides, 0.51% of residents of TX did not use a cooling system.

6.3.2 Hot Water Consumption Activity

The frequency of HWCAs and daily time distribution of HWCA for both TX and NY is obtained. Table 6.2 presents the daily average usage of three appliances with respect to HWCAs. On average, we observed that each family used the washing machine, dryer and dishwasher roughly 0.5 times per day.

Generally, the HWCA profiles obtained in hourly resolution were not accurate enough for modelling the residential load profile. Therefore, we conducted quadratic interpolation with the original data to obtain the HWCA profile of a 5 minute resolution, as shown in Figure 6.1. The HWCA profile is denoted as $PerC_k(t)$, representing the percentage between 5-minute hot water usage and the daily total usage. For example, in Figure 6.1 (a), $PerC_1(97) = 0.85\%$ means that 0.85% of the families take hot showers in the 97-*th* time segment (8:00:00 - 8:05:00). Thus, the cumulative percentage of all time steps equals to 1.

$$\sum_{t=1}^{288} PerC_k(t) = 1 \ \ (k = 1, 2, 3) \tag{6.1}$$

Table 6.2. Daily average usage frequency of home appliances.

State	Washing machine	Dryer	Dishwasher
TX	0.537	0.539	0.502
NY	0.449	0.425	0.474
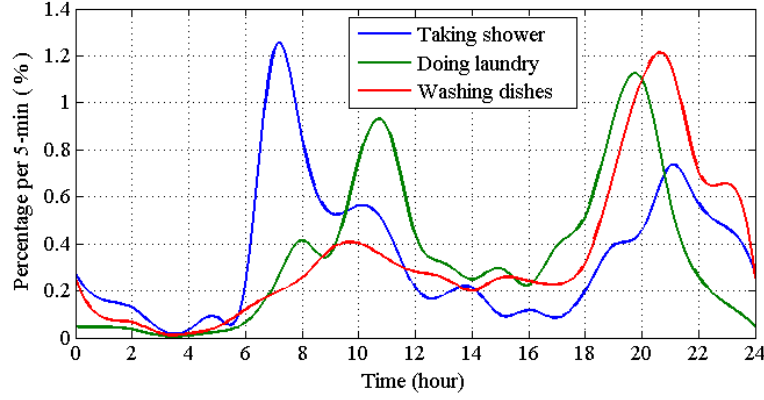
(a) Texas
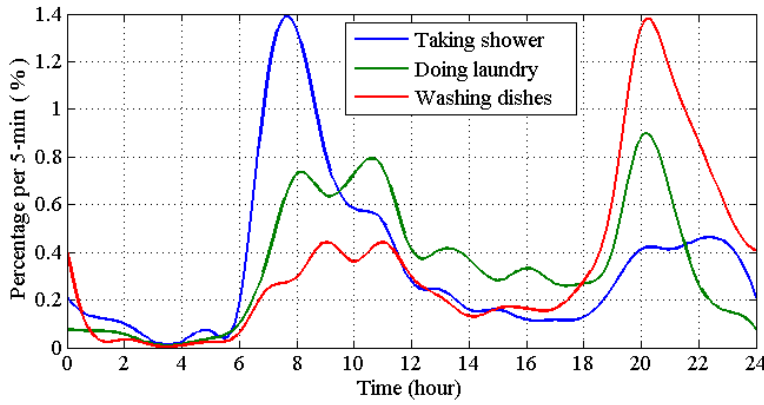
(b) New York

Figure 6.1. Statistical daily HWCA profile.

The figure indicates that the majority of residents take shower in the morning (6:00 - 9:00), the off-peak hours; while they choose to wash clothes and dishes in the evening.

6.3.3   Elasticity and Willingness to Participate in IBDR

In the two IBDR programs we proposed, customers identified the minimum monthly financial reward for reducing power consumption during peak hours in the three-month period. Based on traditional economics assumptions, if the reward payment is higher, the number of customers participating in IBDR programs will increase. We assume that if a customer accepts the program at a minimal monthly reward of πmin dollars, he/she will definitely accept the program at a reward of π dollars ($\pi > \pi_{min}$). Figure 6.2 presents the cumulative participation rate concerning different monthly reward. Note that we have excluded 15 participants from the denominator when calculating the participation rate: 4

115
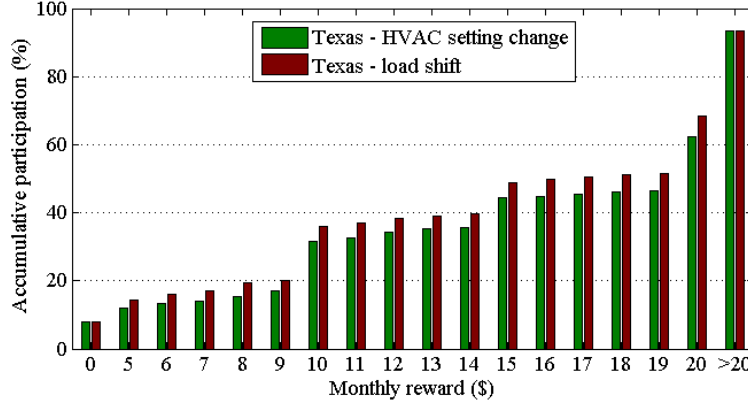
(a) Texas
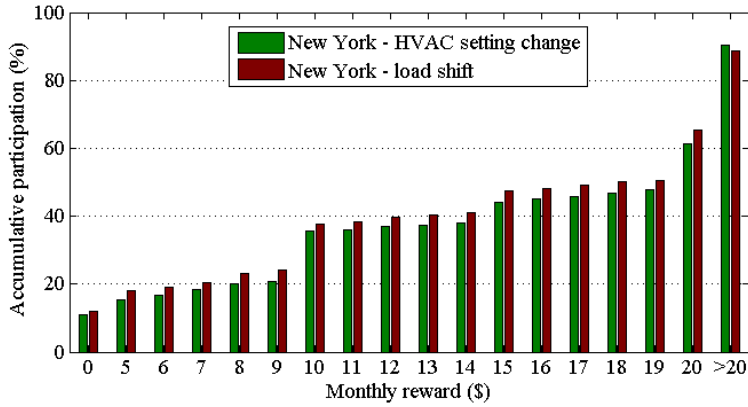
(b) New York

Figure 6.2. Accumulative participation rate of two DR programs.

out of 790 NY residents choose not to accept IBDR Program-1 because they don't have an HVAC; while 11 residents in NY choose not to accept IBDR Program-2 because they don't have a washer, dryer or dishwasher. Based on the survey result, $ 5 or $ 10 monthly payments are acceptable values for load aggregator companies [132]. Therefore, they are adopted for further analysis. The following important conclusions can also be made:

- The participation rates of IBDR Program-1 and IBDR Program-2 display a similar trend. In fact, when a customer chooses π_{min} for participating in Program-1, he/she tends to choose the same payment value for Program-2.

- The participation rates for both TX and NY do not increase linearly with the increased reward amount. In particular, the rate experiences a sudden increase when the reward reaches the integer times of $5.

116

- The participation rates at $5, 10, 15, and 20 are roughly linear.

This chapter also investigates the reasons for not accepting the two DR programs. For Program-1, some participants indicate an unwillingness to be controlled, which is consistent with the conclusion in [132], other reasons include 1) being a renter without the permission to install a thermostat controller, and 2) having seniors or babies at home who are sensitive to temperature change. For Program-2, some participants indicate an unwillingness to be controlled or a wish to do laundry whenever needed.

6.4 Modeling of Daily Load Profile

The IBDR program entails the aggregator "buying" permission to control customers' home appliance in order to reduce the system peak load. Since daily activities on home appliances are important for DR program design, utilities need to know specifically how much load can be reduced in each hour [145]. The modeling of HVAC and EWH load profiles were proposed in [43], [50], respectively.

The scheme of load modeling is shown in Figure 6.3: The light-blue block represents model input; the green block represents household activities; and the orange block represents model output. Household activities may cause one or two loads being switched on. For example, space cooling involves the HVAC, while washing clothes involves the EWH, washing machine and dryer. In this model, we assume that each family has one HVAC, EWH, washing machine, dryer and dishwasher. The number of each type of appliance therefore equals the number of families (N_F) who participate in the IBDR program.

The daily power profiles of all the appliances in Figure 6.3 will be modeled based on the survey result in Section 6.3. In Subsection 6.4.1, the direct calculation method of HVAC load profile (related to Program-1) is proposed and compared with the simulation-based method. In Subsections 6.4.2 and 6.4.3, the load profile models of appliances related to Program-2 are proposed. The load profiles clearly indicate the potential capacity for DR programs.
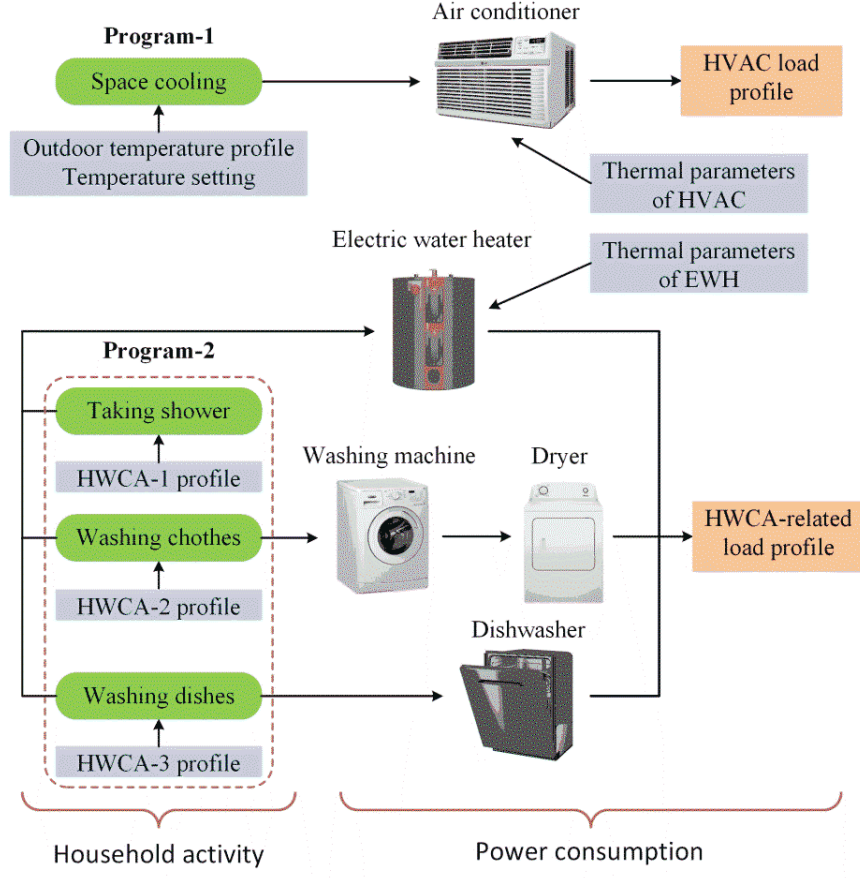
Figure 6.3. Load profile modeling scheme of one family.

6.4.1 Modeling of HVAC Profile

HVACs maintain the room temperature through a thermostat. There are two-order and one-order thermal transfer models that describe the thermal dynamic process of HVACs [50], [146]. In this paper, the one-order model is adopted for simplicity. When the HVAC is working in cooling mode, the heat transfer function is a single differential equation [50]:

$$C_A \frac{d\theta_a(t)}{dt} = \frac{1}{R_A}\left[\theta_{a,out}(t) - \theta_a(t)\right] - S_A(t)Q_A \tag{6.2}$$

The discrete form of (6.2) is

$$\theta_a(t + \Delta t) = \theta_a(t) + \frac{\Delta t}{C_A}\left[\frac{\theta_{a,out}(t) - \theta_a(t)}{R_A} - S_A(t)Q_A\right] \tag{6.3}$$

The main parameters of the heat transfer model are listed in Table 6.3 [117], [122]. In addition, the ON/OFF function $S_A(t)$ is governed by a thermostatic switching law with the temperature deadband:

$$S_A(t) = \begin{cases} 0, & \text{if } S_A(t-\Delta t) = 1 \ \& \ \theta_a(t) \le \theta_{a,min} \\ 1, & \text{if } S_A(t-\Delta t) = 0 \ \& \ \theta_a(t) \ge \theta_{a,max} \\ S_A(t-\Delta t), & \text{otherwise} \end{cases} \quad (6.4)$$

$\theta_{a,max}$ and $\theta_{a,min}$ are upper and lower temperature limits of the deadband. Let $\theta_{a,s}$ be the temperature setting, then

$$\begin{aligned} \theta_{a,min} &= \theta_{a,s} - 0.5\theta_{a,db} \\ \theta_{a,max} &= \theta_{a,s} + 0.5\theta_{a,db} \end{aligned} \quad (6.5)$$

In order to simplify the modeling of aggregated HVAC, it is reasonable to make the following assumptions [143]:

- An HVAC is kept in operation through the day. The temperature setting remains constant.

- R_A is inverse proportional to Ar and C_A is proportional to Ar, as listed in Table 6.3.

- A uniformly random multiplier between 0.5 and 1.5 is applied to the Ar and Q_A values of each house. Then, R_A and C_A are randomized accordingly.

- The initial indoor temperature of a day is uniformly distributed: $\theta(0) \sim U(\theta_{a,min}, \theta_{a,max})$.

Table 6.3. Parameters of the heat transfer model of HVACs.

Parameter	Typical value
House area Ar	150 m^2 (in average)
Thermal resistance of the target house R_A	100/Ar ˚C/kW
Thermal capacitance of the target house C_A	0.015Ar kWh/˚C
Heat transfer rate Q_A	0.14Ar kW
Temperature setting of HVAC $\theta_{a,s}$	22 ˚C
Thermostat deadband of HVAC $\theta_{a,db}$	2.4 ˚C
Cooling efficiency η	2.5

Based on (6.3)-(6.4) and the randomized $\theta(0)$, the $S_A(t)$ of a house can be simulated. Repeating the procedure for all houses, we can estimate the aggregated load profile of HVACs [143]:

$$P_A(t) = \frac{1}{\eta} \sum_{i=1}^{N_F} S_A^i(t) Q_A^i \qquad (6.6)$$

Based on the parameters in Table 6.3 and outdoor temperature data, the aggregated load profile of 10,000 HVACs is simulated, as shown in Figure 6.4. The outdoor temperature includes a typical hot summer day and a cool summer day in Houston in 2017 [147]. In this scenario, during the daytime (9:00 - 20:00), every 10,000 HVACs consume 30 - 80 MW power depending on the outdoor temper- ature. The power demand of HVACs in particular is quite high during 12:00 - 17:00 of a hot day and there is great potential for peak load reduction.

Although very accurate, the above simulation-based method does not provide an intuitive, explicit impact of temperature setting change on the load profile. Thus, a direct calculation method is developed based on the characteristics of aggregated HVACs. In this
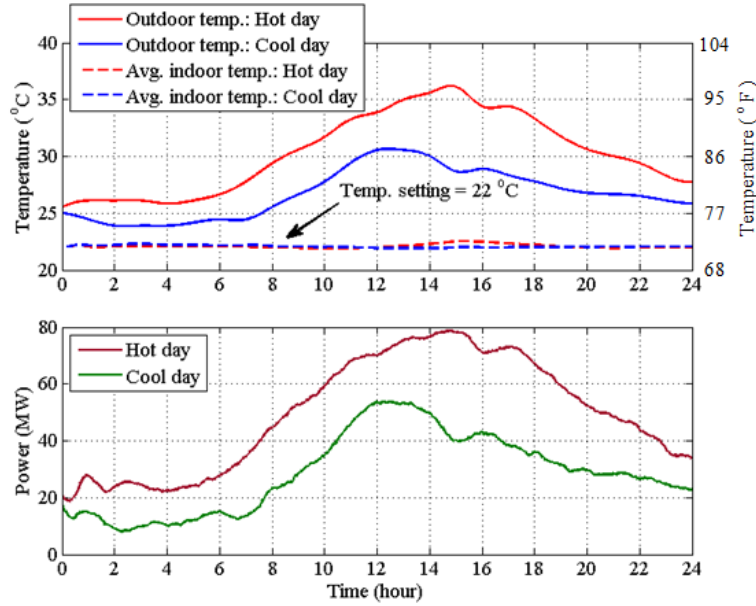
Figure 6.4. Temperature and load profile of 10,000 HVACs.

method, we use the average Ar and Q_A to represent the random parameters (to fix the random multiplier as 1). Averaging the heat transfer equation of all HVACs gives (6.7) [116], [148],

$$\frac{1}{N_F}\sum_{i=1}^{N_F}C_A\frac{d\theta_a^i(t)}{dt}=\frac{1}{N_F}\sum_{i=1}^{N_F}\left\{\frac{1}{R_A}\left[\theta_{a,out}(t)-\theta_a^i(t)\right]-S_A^i(t)Q_A\right\} \tag{6.7}$$

where $\theta_a^i(t)$ is the room temperature of the i-th HVAC. According to the linearity characteristic of the derivative, (6.7) is transformed into

$$C_A\frac{d}{dt}\left[\frac{1}{N_F}\sum_{i=1}^{N_F}\theta_a^i(t)\right]=\frac{1}{R_A}\left[\theta_{a,out}(t)-\frac{1}{N_F}\sum_{i=1}^{N_F}\theta_a^i(t)\right]-\frac{1}{N_F}\sum_{i=1}^{N_F}S_A^i(t)Q_A \tag{6.8}$$

According to the simulation result in Figure 6.4, the average indoor temperature $\bar{\theta}_a(t)$ slightly fluctuates around $\theta_{a,s}$ and can be approximated as constant. Then,

$$\bar{\theta}_a(t)=\frac{1}{N_F}\sum_{i=1}^{N_F}\theta_a^i(t)\approx\theta_{a,s} \tag{6.9}$$

Substituting (6.9) into (6.8) gives

$$C_A\frac{d}{dt}\left(\bar{\theta}_{a,s}\right)=\frac{1}{R_A}\left[\bar{\theta}_{a,out}(t)-\theta_{a,s}\right]-\Pi Q_A=0 \tag{6.10}$$

where $\Pi=\frac{1}{N_F}\sum_{i=1}^{N_F}S_A^i(t)$ is the ratio of devices that are in the ON state [116]. Thus, the total power consumption is

$$P_A(t)=\Pi\left(N_F\frac{Q_A}{\eta}\right)=\frac{N_F}{\eta}\left(\Pi Q_A\right)=\frac{N_F\left(\theta_{a,out}(t)-\theta_{a,s}\right)}{\eta R_A} \tag{6.11}$$

An important conclusion is drawn from (6.11): the power consumption of aggregated HVACs is proportional to the difference between the outdoor/indoor temperature. It is not necessary to know the heating transfer rate of each HVAC when estimating $P_A(t)$. Eq. (6.11) can also be explained in an intuitive manner: Each HVAC is switched on and off periodically to compensate the heat injection from outside to inside the house; during the steady state in which $\bar{\theta}_a(t)$ keep constant, the power consumption of aggregated HVACs

should be proportional to the product of the temperature difference and the house thermal conductance G_A ($G_A = 1/R_A$).

With the same outdoor temperature profile (shown in Figure 6.4) and the thermal parameters, we can calculate load profiles by using Eq. (6.11). The load profiles obtained by simulation and direct calculation are compared in Figure 6.5. The figure indicates that even if the thermal parameters are heterogeneous in the simulated profile, the calculated load profile matches well with the simulated one. Furthermore, the load reduction achieved by IBDR Program-1 can be directly estimated if the change of $\theta_{a,s}$ is known without many other parameters.

6.4.2 Modeling of EWH Profile

The power consumption of EWHs is determined by two independent factors: water tank heat dissipation and customers' hot water usage. If more customers use hot water, more EWHs will be switched on due to a decrease in the water temperature. An analytical behavior model of EWHs is proposed, combining the above two factors.

1) Effect of Heat Dissipation: This paper considers the one-order thermal transfer model of EWHs. The heat transfer equation is given by (6.12) [48].

$$C_E \frac{d\theta_w(t)}{dt} = S_E(t)Q_E - \frac{1}{R_E}\left[\theta_w(t) - \theta_{a,in}\right] - \rho c_P W(t)\left(\theta_w(t) - \theta_{w,co}\right) \tag{6.12}$$
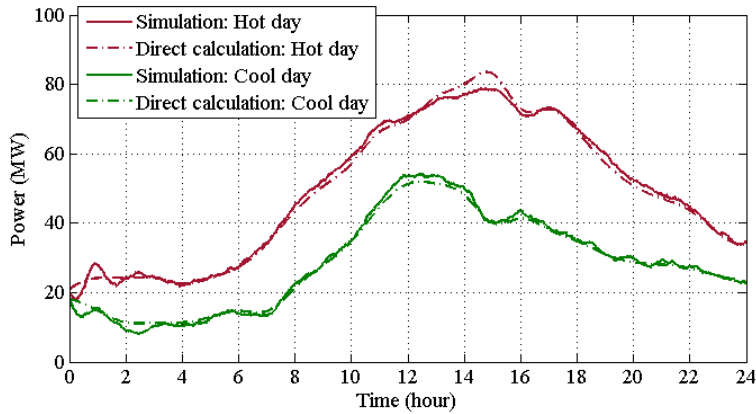
Figure 6.5. Load profiles obtained by simulation and direct calculation.

where $\theta_w(t)$ is the real-time water temperature in the EWH water tank, c_P is the specific heat of water (J/kg˚C) and $W(t)$ is the rate of water usage (l/s). The main parameters are listed in Table 6.4 [48]. $S_E(t)$ is given by (5.3).

If there are no HWCAs, we have $W(t) = 0$. Similar to (6.11), the aggregated power of N_F devices is given by (6.13). The only difference is that the heating efficiency of an EWH is 100% because of its purely resistive feature.

$$P_{E,HD}(t) \approx \frac{N_F \left(\theta_{w,s} - \theta_{a,in} \right)}{R_E} \tag{6.13}$$

where $P_{E,HD}(t)$ is the total power of EWHs caused by heat dissipation.

2) Effect of HWCA: In each HWCA, hot water is assumed to be drawn gradually from the tank, and the same volume of cold water is injected simultaneously. As a consequence, the water temperature will fall below $\theta_{w,min}$, and the heating element will switch on for a time duration of $T_{E,k}$ to bring the water temperature above $\theta_{w,min}$ [43]. An HWCA usually lasts for 10 - 60 minutes, which is much shorter than the operation cycle (around 10 hours) [48]. Therefore, we can neglect the water heat dissipation during $T_{E,k}$. Since $\theta_{w,s} - \theta_{w,co} \gg \theta_{w,db}$, $T_{E,k}$ is given by,

$$T_{E,k} = \frac{C_w \rho Vol_k \left(\theta_w(t) - \theta_{w,co} \right)}{Q_E} \approx \frac{C_w \rho Vol_k \left(\theta_{w,s} - \theta_{w,co} \right)}{Q_E} \tag{6.14}$$

where ρ is the density of water, and Vol_k is the hot water demand of the HWCA-k. The typical HWCA parameters and the corresponding $T_{E,k}$ are shown in Table 6.5, representing

Table 6.4. Parameters of the heat transfer model of EWHs.

Parameter	Value
Thermal resistance of the water tank R_E	380 ˚C/kW
Thermal capacitance of the water C_E	0.2 kWh/˚C
Heat energy transfer rate Q_E	2.5 kW
Indoor air temperature $\theta_{a,in}$	22 ˚C
Cold water temperature $\theta_{w,co}$	10 ˚C
Water temperature setting $\theta_{w,s}$	56 ˚C
Thermostat deadband $\theta_{w,db}$	4 ˚C

Table 6.5. Parameters for modeling hot water demand.

Parameter	Vol_k (Liter)	$T_{E,k}$ (min.)
Shower	40	50
Clothes washing	39	49
Dishwashing	16	20

the general household practice of American residents [118]-[119]. Furthermore, if uniformly random multipliers are applied to Vol_k and Q_E, Eq. (6.14) can still be used to calculate the operation duration of the aggregated EWH. The detailed deduction is in Appendix-C. Based on (6.12), the 24-hour water temperature and power consumption of a typical EWH is simulated, as shown in Figure 6.6. According to the figure, the HWCA with the smallest water demand can even cause the heating element to be switched on to recover the water temperature.

The aggregated power profile of EWHs is based on the HWCA profile obtained from our survey (shown in Figure 6.1). We make the following assumptions in order to simplify the modeling:

- $\theta_{w,s}$ and $\theta_{w,db}$ are homogeneous for each home. Also, $\theta_{a,in}$ and $\theta_{w,co}$ are constant.

- The number of HWCA-1 (taking shower) per day is proportional to the family size (m). Based on the survey, each family has 2.7 persons in average. The daily average numbers of HWCA-2 (doing laundry) and HWCA-3 (washing dishes) are used in the model.
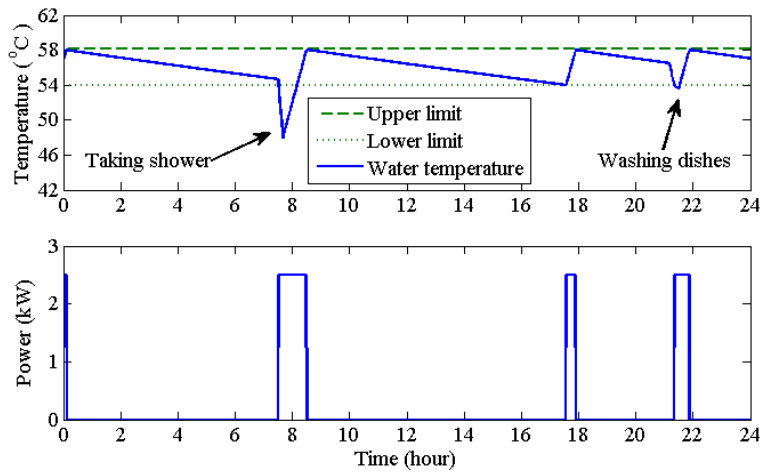
Figure 6.6. Water temperature and power consumption profile of EWHs.

- Since N_F is a large number in practice, the total number of HWCAs at t is proportional to the statistical percentage at this time step (shown in Figure 6.1).

According to the Law of Large Numbers [149], the total number of the HWCA-k at time t is:

$$N_{E,k}(t) \approx E[N_{E,k}(t)] = [N_F \cdot PerC_k(t) \cdot m_k \cdot Freq_k] \quad (t = 1, 2, \cdots, 288) \tag{6.15}$$

where $N_{E,k}(t)$ is the total number of EWHs being switched on at t, m_k is the family size factor, and $m = \{2.7, 1, 1\}$, $Freq_k$ is the times of doing the event k. According to the survey result in Table 6.1, $Freq = \{1, 0.54, 0.50\}$ in TX case. [.] is the rounding sign. Therefore, at time step t, there are $N_{E,k}(t)$ EWHs being switched on and kept in operation for a time duration of $T_{E,k}$.

For the HWCA-k, we first initialize the vector $\boldsymbol{P}_{HWCA,k} = [0, 0, L, 0]_{288 \times 1}$, where $\boldsymbol{P}_{HWCA,k}$ is the EWH power consumption caused by HWCA-k. Then, after the time step t, $\boldsymbol{P}_{HWCA,k}$ is updated by Eq. (6.16).

$$P_{HWCA,k}^{new}(i) = P_{HWCA,k}^{old}(i) + N_{E,k}(t) \cdot Q_E \quad (i = t+1, t+2, \ldots, t + [T_{E,k}]) \tag{6.16}$$

where $P_{HWCA,k}^{old}(i) / P_{HWCA,k}^{new}(i)$ is the total power before/after updating at t, respectively. In the example of HWCA-3, we have $T_{E,k} = 20$ minutes (4 time steps). As illustrated by Figure 6.7, the value $P_{HWCA,3}(t+4)$ is the cumulative power caused by the HWCA at t, $t + 1$, $t + 2$ and $t + 3$. Following the same procedure for the other two HWCAs, we can estimate the EWH power consumption caused by HWCAs, denoted as $P_{HWCA}(t)$. The total power consumption of EWHs is the combination effect of heat dissipation and three HWCAs, given by (6.17).

$$P_E(t) = P_{E,HD}(t) + P_{HWCA}(t) = P_{E,HD}(t) + \sum_{k=1}^{3} P_{HWCA,k}(t) \tag{6.17}$$

Finally, Figure 6.8 presents the aggregated EWH power profile $P_E(t)$ of 10,000 EWHs. Although the registered capacity of EWHs is 25 MW, the real-time power demand ranges between 1.09 - 11.52 MW. Specially, there are two peak load points in the daily load profile. One is 11.52MW at around 8:00 and the other is 10.82MW at around 21:00.
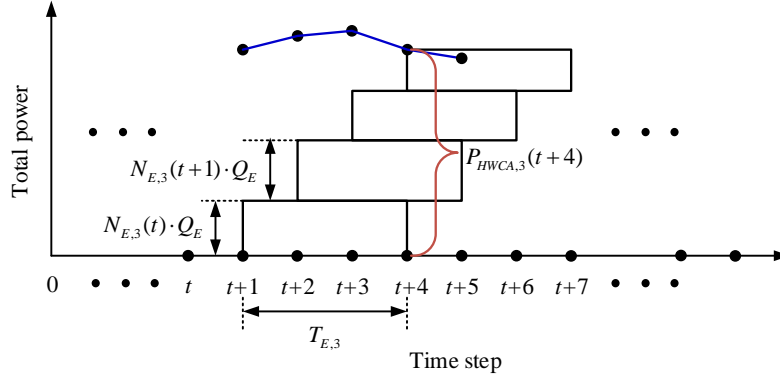
Figure 6.7. Formulation of probabilistic load profile of EWHs.
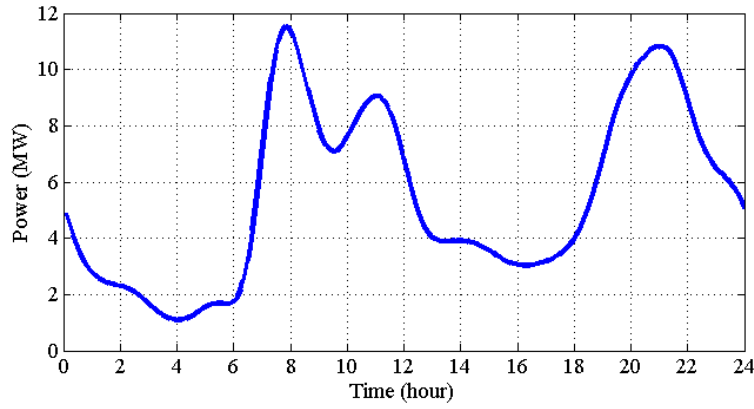
Figure 6.8. Aggregated EWH power profile for 10,000 families.

6.4.3   Modeling of Laundry Profile and Dishwashing Profile

The washing machine, dryer, and dishwasher can be approximated as the constant power loads. The basic parameters of three appliances are listed in Table 6.6 [150]-[152]. According to the definition in Subsection 6.4.2, the aggregated load profiles of the three appliances are modeled based on the profiles of HWCA-2, HWCA-2 and HWCA-3, respectively.

1) Washing Machine: Similar to (6.15)-(6.16), the total number of washing machines being switched on at time t is:

$$N_{WM}(t) \approx \left[N_F \cdot PerC_2(t) \cdot m_2 \cdot Freq_2 \right] \quad (t = 1, 2, \cdots, 288) \qquad (6.18)$$

Then, $N_{WM}(t)$ washing machines keep in operation for a duration of T_{WM}. The vector $\boldsymbol{P}_{WM}$ is updated by Eq. (6.19).

Table 6.6. Basic information of home appliances.

Appliance (abbreviation)	Rated power (kW)	Average operation duration (minutes)
Washing machine (WM)	$P_{WM} = 0.85$	$T_{WM} = 40$
Dryer (DY)	$P_{DY} = 3.60$	$T_{DY} = 40$
Dishwasher (DW)	$P_{DW} = 1.20$	$T_{DW} = 35$

$$P_{WM}^{new}(i) = P_{WM}^{old}(i) + N_{WM}(t) \cdot P_{WM} \quad (i = t+1, t+2, ..., t+T_{WM}) \tag{6.19}$$

2) Dryer: According to Table 6.2, the average daily frequencies of using washing machines and using dryers can be approximated as equal values. Therefore, after $N_{WM}(t)$ washing machines finish working (at the time $t + T_{WM}$), the same number of dryers ($N_{DY}(t) = N_{WM}(t)$) are switched on for a duration of T_{DY}.

$$P_{DY}^{new}(i) = P_{DY}^{old}(i) + N_{WM}(t) \cdot P_{DY} \quad (i = t+T_{WM}+1, t+T_{WM}+2, ..., t+T_{WM}+T_{DY}) \tag{6.20}$$

3) Dishwasher: The total number of dishwashers being switched on at time t is

$$N_{DW}(t) \approx [N_F \cdot PerC_3(t) \cdot m_3 \cdot Freq_3] \quad (t = 1, 2, \cdots, 288) \tag{6.21}$$

Then, $N_{DW}(t)$ dishwashers are kept in operation for a duration of T_{DW}.

$$P_{DW}^{new}(i) = P_{DW}^{old}(i) + N_{DW}(t) \cdot P_{DW} \quad (i = t+1, t+2, ..., t+T_{DW}) \tag{6.22}$$

4) Combining Three Appliances: Finally, the load profiles of three appliances are calculated and added up: $P_{WM}(t)$, $P_{DY}(t)$ and $P_{DW}(t)$. Figure 6.9 presents the combined load profiles in TX case. The three appliances are marked with different colors. Apparently, the power consumption of three appliances is much smaller than that of EWHs because: 1) they operate less frequently than EWHs; 2) the power ratings of washing machines and dishwashers are smaller than those of EWHs.

6.5 Expense of Load Reduction by IBDR Programs: A Case Study

Based on the survey result in Section 6.3 and load profile model in Section 6.4, we are able to estimate the potential capacity of major home appliances for IBDR programs and to assess the relevant expense of implementing them.
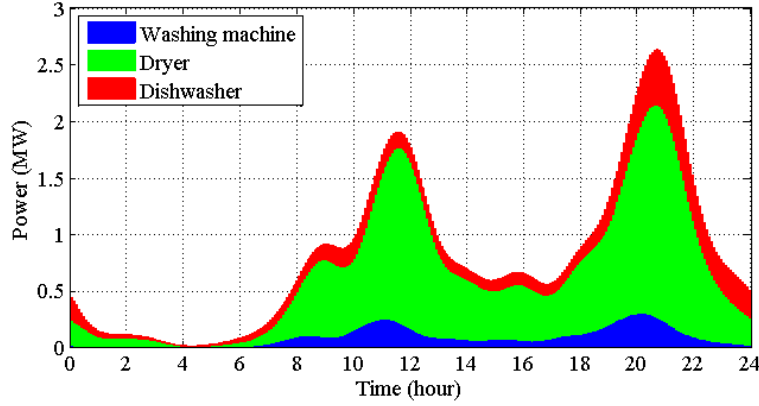
Figure 6.9. Aggregated power profile of three appliances for 10,000 families.

6.5.1 *Indices of Yearly Peak Load*

In this study, the duration of x% yearly peak load ($T_{x\%,yrpk}$) is defined, meaning the cumulative number of hours when the system loading level exceeds x% ($0 < x < 100$) of the yearly peak load (P_{yrpk}) of the local grid. We conduct a case study with two representative cities selected from TX and NY: Houston and New York City (NYC). According to the load profile from ERCOT [127] and NYISO [153], the $T_{x\%,yrpk}$ indices of Houston and NYC are shown in Table 6.7. Additionally, the 95% (or above 95%) yearly peak load only happen in June, July and August. For the two cities, Figure 6.10 presents the load profiles and air temperature profiles (from [147]) in the week when P_{yrpk} happens. We can observe that the load usually exceeds $0.95P_{yrpk}$ during 13:00 - 18:00 in Houston and during 13:00 - 19:00 in NYC, when the outdoor temperature is relatively high. Therefore, there is a strong correlation between daytime loading level and outdoor temperature.

Table 6.7. P_{yrpk} and $T_{95\%peak}$ of different cities in 2017.

Target city	Houston[1], TX	NYC & Long Island[2], NY
P_{yrpk}	20.10 GW	15.83 GW
Date of yearly peak load	Friday, August 18th	Thursday, July 20th
$T_{95\%peak}$	51 hour	55 hour
$T_{98\%peak}$	13 hour	16 hour

[1] Houston represents the metro area of the city.
[2] NYC and Long Island are adjacent and of similar weather.

128
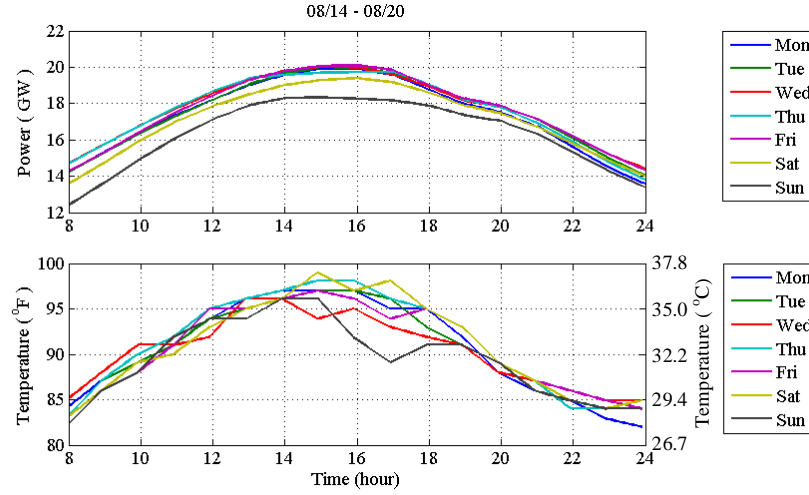
(a) Houston, TX
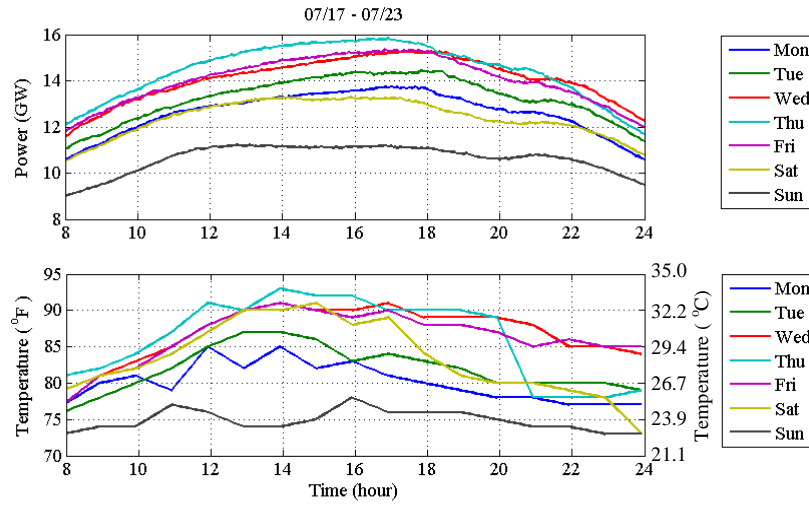
(b) NYC and Long Island, NY.

Figure 6.10. Daily load & outdoor temperature profile in 2017.

Daily $x\%$ peak energy ($E_{x\%,yrpk}$) is defined as cumulative energy consumption when the loading level exceeds $x\% \cdot P_{yrpk,}$, as illustrated in Figure 6.11. Obviously, $E_{x\%,yrpk}$ is zero if the peak load of this day is lower than $x\% \cdot P_{yrpk}$. The $E_{x\%,yrpk}$ curves of several heavy-load days are shown in Figure 6.12, which illustrates that we need to cut off the largest amount of peak energy on August 18th (in Houston) or on July 20th (in NYC & Long Island) if desiring to reduce P_{yrpk} to the same value.
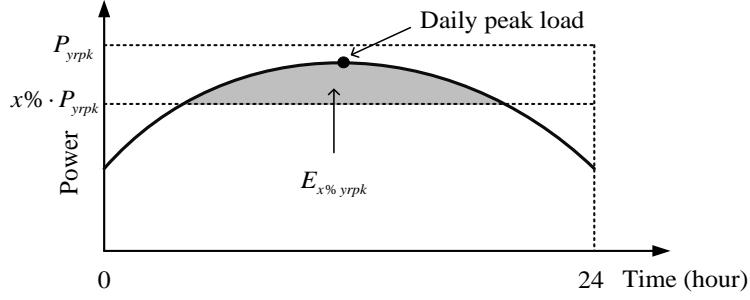
Figure 6.11. Definition of peak energy.

(a)   (b)
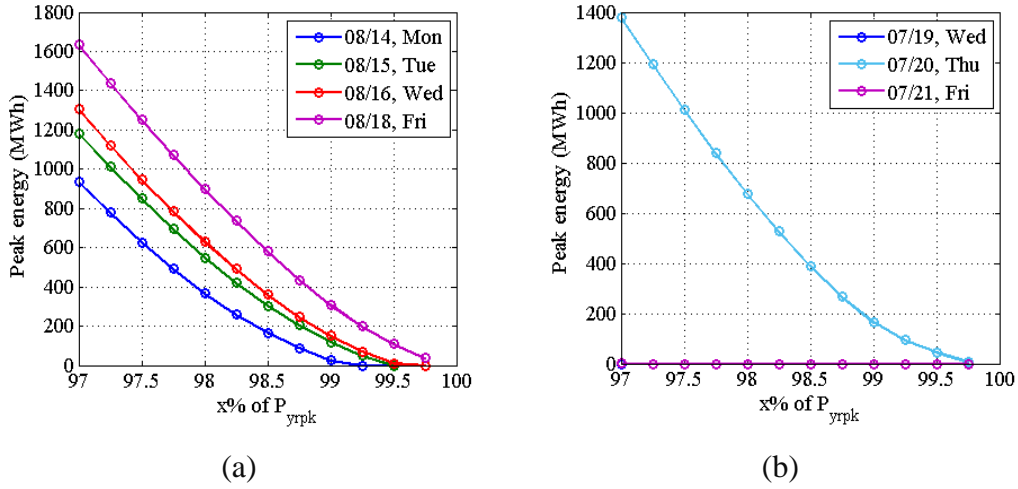
Figure 6.12. Daily peak energy in 2017: (a) Houston; (b) NYC and Long Island.

6.5.2 Peak Load Reduction by the IBDR Program-1

According to (6.11), the load reduction amount caused by temperature setting change ($\Delta\theta_{a,s}$) is:

$$\Delta P_A(t) = \frac{N_F\left(\theta_{a,out}(t) - \theta_{a,s}\right)}{\eta R_A} - \frac{N_F\left(\theta_{a,out}(t) - \left(\theta_{a,s} + \Delta\theta_{a,s}\right)\right)}{\eta R_A} = \frac{N_F\Delta\theta_{a,s}}{\eta R_A} \tag{6.23}$$

Eq. (6.23) calculates the potential load reduction that is caused by the HVAC control. The 2017 temperature profile in Houston indicates that the outdoor temperature exceeded 95 ˚F for at least 10 days in July or August. Based on the DR survey questionnaire, the DR aggregator is allowed to raise the HVAC temperature setting by 5 ˚F (= 2.78 ˚C). In NYC and Long Island, however, the temperature hardly exceeds 95 ˚F in the summer [147].

130

Consequently, the DR aggregator is allowed to raise the temperature setting by only 3 ˚F (= 1.67 ˚C).

In recent years, many optimal control strategies have been proposed to achieve this target load reduction while preventing a power rebound after load recovery [116], [117], [154]. In particular, the optimal sequential dispatch strategy proposed in [117] can realize the flexible control of HVACs for 15 - 60 minutes. According to our DR survey, each HVAC can be controlled for a maximal duration of $T_{DR1,max}$ = 45 minutes. Therefore, the maximal load reduction capability of IBDR program-1 ($\Delta E_{DR1,max}$) is estimated by (6.24).

$$\Delta E_{DR1,max} = \Delta P_A(t) \cdot T_{DR1,max} = \frac{N_F \Delta \theta_{a,s} T_{DR1,max}}{\eta R_A} \tag{6.24}$$

Based on the virtual IBDR contract (presented in Subsection 6.2.2) and housing market data, the input parameters of (6.24) and the calculation results are shown in Table 6.8.

Taking Houston as an example, if the monthly reward is \$5, the daily peak load on August 18th (= P_{yrpk}) is reduced by 243.8 MW and 1.21% according to the peak energy curve in Figure 6.12 (a). Similarly, if the monthly reward is \$10, P_{yrpk} is reduced by 459.0 MW and 2.28%, respectively. On the remaining hot days (e.g., August 14th, 15th, and 16th), the system loading level can also be reduced below 19.64 GW (= 20.10 − 0.459) with a smaller load reduction amount. Therefore, the required power generation capacity for Houston can be reduced by 459 MW, which means the utilities may delay the construction of the additional generation unit for yearly peak load.

The expenses of IBDR reward payment and constructing generation units are listed in Table 6.9. Generally, the IBDR program-1 is conducted in three summer months per year. Therefore, the cost of increasing per 100MW generation unit (with natural gas) equals the reward payment for 36.2 years (Option 1) or 13.0 years (Option 2) in TX. In addition, when a generation unit is started for peak load, it also involves fuel costs and start-up costs according to the unit commitment [159]. However, the details are beyond the scope of this study.

Table 6.8. Calculation of load reduction capability and cost.

Parameters and result		Houston, TN	NYC & Long Island, NY
Basic parameters	Ar	160 m^2	200 m^2
	R_A	0.625 ˚C/kW	0.500 ˚C/kW
	$\Delta\theta_{a,s}$	2.78 ˚C	1.67 ˚C
	$T_{DR1,max}$	0.75 hour	0.75 hour
	Total number of houses N_{hs} [155]-[157]	2.605×10^6	3.386×10^6
	P_{yrpk}	20.10 GW (on Aug. 18th)	15.83 GW (on Jul. 20th)
Option 1: $ 5 monthly reward	k_{DR1} [1]	12.0%	15.3%
	$N_F = k_{DR1} \times N_{hs}$	3.126×10^5	5.181×10^5
	$\Delta E_{DR1,max}$	417.1 MWh	519.4 MWh
	ΔP_{yrpk} (Percentage of P_{yrpk})	243.8 MW (1.21%)	274.7 MW (1.74%)
	Total reward payment per month	$1.563×10^6	$2.590×10^6
Option 2: $ 10 monthly reward	k_{DR1}	31.5%	35.8%
	$N_F = k_{DR1} \times N_{hs}$	8.206×10^5	1.212×10^6
	$\Delta E_{DR1,max}$	1095 MWh	1215 MWh
	ΔP_{yrpk} (Percentage of P_{yrpk})	459.0 MW (2.28%)	442.1 MW (2.79%)
	Total reward payment per month	$8.206×10^6	$1.212×10^7

[1] k_{DR1} is the participation rate of the DR program-1.

Table 6.9. Average cost for serving peak load in U.S.

State	IBDR cost (million $/100MW)	Construction cost of generation unit (million $/100MW) [158]
TX	Option 1: 0.641/month Option 2: 1.788/month	Natural gas: 69.6 Petroleum liquid: 102.1
NY	Option 1: 0.943/month Option 2: 2.735/month	Biomass: 153.1 Wind plant: 166.1

Furthermore, the IBDR can also be used for frequency regulation service. Due to its short time scale (several minutes), it has little impact on customers comfort [83]. Therefore, the benefit of an IBDR program is not limited to peak load reduction.

6.5.3 Peak Load Reduction by the IBDR Program-2

The HWCA-related load profile is shown in Figure 6.13, which was obtained by adding up the load profile of EWHs, washing machine, dryer and dishwashers. Comparing Figure 6.10 and Figure 6.13, we can conclude that the peak of the HWCA-related load profile (7:30 - 8:30 and 19:30 - 21:30) does not synchronize with the system peak load (14:00 - 18:00). Therefore, the HWCA-related loads do not have sufficient potentials for peak load reduction in TX and NY and are not recommended for future IBDR programs. However, EWHs are good candidates for under-frequency load shedding when the system meets with a contingency [83].

6.6 Conclusion

IBDR has considerable potential for power system peak load reduction from a utility's perspective. This chapter presents a systematic approach to evaluate IBDR potential by combining a technical model and a social-behavioral survey. The result validates the proposed approach and serves as a guide for utilities' IBDR programs. The contribution is
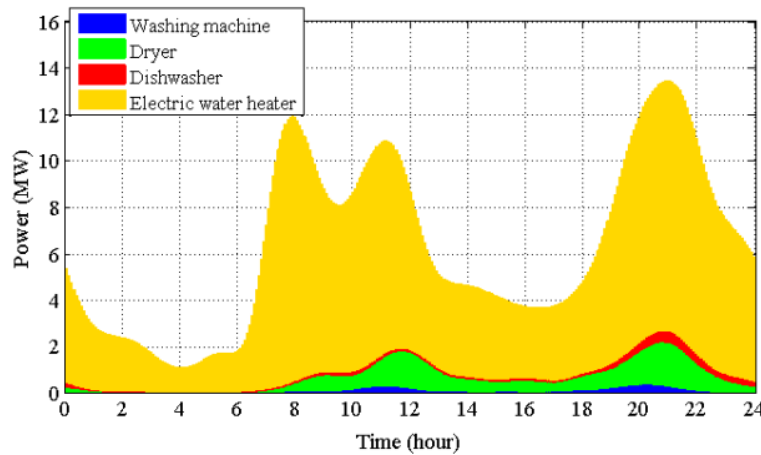
Figure 6.13. Aggregated power profile of loads related to IBDR Program-2.

summarized as follows.

- The approach of combining the technical model and the survey of consumers' behavior patterns is a new method for utility companies to evaluate an IBDR profile in their service territories. The survey described in this chapter was conducted among consumers in the states of TX and NY, so the study results can be directly used as guidelines for IBDR potentials in areas similar to TX or NY. Meanwhile, the survey methodology can be generalized for other areas even if they have consumers with different behavior patterns.

- Customers' habits of appliance usage and motivation for participating in IBDR programs were investigated based on the large-scale survey of over 1,500 customers. The survey result is reliable because social-behavioral factors are considered in the design of the questionnaire. In particular, the result suggests that it is most beneficial for utility companies to provide the monthly reward payment of $5 or $10. Reasons for not participating in IBDR program were also addressed. The result analysis provides critical guidance to power utilities on designing effective IBDR programs.

- Furthermore, the modeling of a daily load profile is proposed for evaluating the cost performance of IBDR. The survey result is an input of the load model. Based on the result analysis and the proposed load model, the expense of reducing the yearly peak load for a particular amount is estimated. In particular, the IBDR program is more economic in TX due to higher outdoor temperature. The cost of building extra generation units (with natural gas) equals the reward payment for 36.2 years (with the option of a $5 monthly reward) or 13.0 years (with the option of a $10 monthly reward). The conclusion helps utilities to compare the expense of peak load reduction and the expense of building the new generation units.

This research work has useful implications for future works with a more comprehensive economic evaluation of IBDR, including the fuel costs and start-up costs under unit commitment consideration. With large-scale participation in DR, the benefits to the industry include the savings for: 1) the expense of building extra generation units for supplying the yearly peak load; and 2) the expense of generation spinning reserve for daily peak load.

Chapter 7

Conclusions and Future Works

7.1 Conclusions and Contributions

Demand side control for frequency regulation is a promising research topic owing to the increasing penetration of renewable energy and new requirements of smart grid development. Many pioneering works have been done on this topic in recent years which have approached the topic from diverse angles and with a variety of assumptions. In this dissertation, DDC is designed for both PRFR and SCFR. The participation of DDC can improve the dynamic performance of a system and reduce the requirements of generator spinning reserve.

Chapter 3 proposes an analytical method for obtaining ASFR model parameters. The method is proven by mathematical deduction and verified by time domain simulation. First, the analytical ASFR model is shown to replace the bus frequency of the MM-SFR model with very high accuracy (<1% error). Second, the ASFR model represents the small-scale system with acceptable accuracy (<5% error). Third, in a large-scale system, the ASFR model is less accurate for representing the bus frequency but can still represent the COI frequency accurately. Therefore, as a fast calculation tool, the ASFR model supports studies related to power system dynamics, such as demand control for frequency regulation, maximal wind power penetration with frequency criteria, and dynamic model reduction. In this dissertation, the ASFR model provides the later DDC studies with a solid theoretical foundation.

Chapter 4 proposes a hybrid DDC strategy combineing centralized parameter-setting and decentralized control action. According to this method, each load controller first decides whether to participate in PRFR according to the forecast frequency nadir. Then at the steady-state, the load controller also participates in SCFR if the frequency is beyond the dead-band. The SDM ensures that the non-communicated aggregated loads have an

approximated frequency droop characteristic similar to generators. Additionally, the control parameters can be updated by the control center, which has a low communication requirement.

Chapter 5 is an extension of the study in Chapter 4. Two typical thermostatic loads, EWHs and HVACs, are considered in the DDC strategy. Thus, we use a more specific term, TLC to replace DDC. In the TLC strategy, the 24-hour demand profile is estimated. Furthermore, the RS-CR method can regulate the aggregated HVAC power to achieve the specified load reduction amount for the specified period in a decentralized manner. The control strategy is easy to implement in existing HVAC thermostats but effectively mitigates the load rebound during the recovery period.

Chapter 6 presents a systematic approach to evaluate IBDR potential by combining the technical model and a social-behavioral survey. This is a new method for utility companies to evaluate the IBDR profile in their service territories. The survey result is reliable because social-behavioral factors are considered in the design of the questionnaire. Furthermore, the modeling of daily load profile is proposed for evaluating the potential of IBDR. Based on the result analysis and the proposed load model, the expense of reducing the yearly peak load for a particular amount is estimated and compared with the expense of building an extra generation unit. Meanwhile, since short-term load control does not affect customers comfort, it is convenient to include frequency regulation service in IBDR programs.

7.2 Suggestions for Future Works

This dissertation can be improved and extended in the following aspects:

- The analytical method to aggregate the MM-SFR model can be extended to other multi-branch s-domain transfer function models. One example is the aggregation of multiple exciters, which is a major step in power system dynamic model reduction. In addition to the power system application, the aggregation method provides the control theory with a generic idea for reducing the multi-branch transfer function that consists of the inertia element.

136

- IBDR can be utilized to provide both long-term and short-term ancillary services. The long term service aims at enhancing system security and reducing customers' electricity bills, including load following, peak shaving and valley filling. The short-term service aims at improving the system dynamic response, including PRFR and SCFR. Although sufficient achievement has been made on these two topics, a framework for coordinating the long-term control and short-term control for the same group of responsive loads is still lacking.

- In addition to the technical phase of DDC, some economic issues are also interesting to explore. First, it is necessary to design a future ancillary service market including DDC. Second, the economic advantages of DDC need to be quantitatively verified. Both the technical and economic issues can be important future research directions.

- HVAC is the largest commercial and residential load in many cities. This dissertation is focused on traditional constant-speed air conditioners, in which the compressor is turned on and off periodically to keep the room temperature within the deadband. However, in recent years, more variable-speed air conditioners have been utilized, especially in commercial buildings. Therefore, the TLC strategy for variable-speed air conditioners should be studied in the future.

References

[1] B. Hassan, *Robust Power System Frequency Control*, New York: *Springer*, 2009, p. 3.

[2] P. Sorensen, N. A. Cutululis, *et al.*, "Power fluctuations from large wind farms," *IEEE Trans. Power Syst.*, vol. 22, no. 3, pp. 958-965, Aug. 2007.

[3] X. Kou and F. Li, "Interval optimization for available transfer capability (ATC) evaluation considering wind power uncertainty," *IEEE Trans. Sustain. Energy*, in press.

[4] ERCOT concept paper: future ancillary services in ERCOT, *Electric Reliability Council of Texas*, 2013. [Online] http://www.ferc.gov/CalendarFiles/20140421084800-ERCOT-ConceptPaper.pdf. \

[5] Q. Zhang, K. Dehghanpour and Z. Wang, "Distributed CVR in unbalanced distribution systems with PV penetration," *IEEE Trans. Smart Grid*, in press.

[6] H. Hu, Q. Shi, Z. He, J. He, and S. Gao, "Potential harmonic resonance impacts of PV inverter filters on distribution systems," *IEEE Trans. Sustain. Energy*, vol. 6, no. 1, pp. 151-161, Jan. 2015.

[7] Z. Xu, J. Østergaard, and M. Togeby, "Demand as frequency controlled reserve," *IEEE Trans. Power Syst.*, vol. 26, no. 3, pp. 1062–1071, Aug. 2011.

[8] M. H. Albadi and E. F. El-Saadany, "A summary of demand response in electricity markets," *Electr. Power Syst. Res.*, vol. 78, no. 11, pp. 1989-1996, Nov. 2008.

[9] US Department of Energy, "Benefits of demand response in electricity markets and recommendations for achieving them," report to the United States congress, Feb. 2006. [Online] http://eetd.lbl.gov.

[10] H. Zhong, L. Xie, and Q. Xia, "Coupon incentive-based demand response: theory and case study," *IEEE Trans. Power Syst.*, vol. 28, no. 2, pp. 1266-1276, May 2013.

[11] Q. Hu, F. Li, X. Fang, and L. Bai, "A framework of residential demand aggregation with financial incentives," *IEEE Trans. Smart Grid*, vol. 9, no. 1, pp. 497-505, Jan. 2018.

[12] X. Fang, Q. Hu, F. Li, B. Wang, and Y. Li, "Coupon-based demand response considering wind power uncertainty: a strategic bidding model for load serving entities," *IEEE Trans. Power Syst.*, vol. 31, no. 2, pp. 1025-1037, Mar. 2016.

[13] D. T. Nguyen, M. Negnevitsky, and M. de Groot, "Pool-based demand response exchange — concept and modeling," *IEEE Trans. Power Syst.*, vol. 26, no. 3, pp. 1677–1685, Aug. 2011.

[14] A. Ketabi and M. Hajiakbari Fini, "An underfrequency load shedding scheme for islanded microgrids," *Int. J. of Elect. Power & Energy Syst.*, vol. 62, pp. 599-607, Nov. 2014.

[15] W. Ju, K. Sun, and J. Qi, "Multi-layer interaction graph for analysis and mitigation of cascading outages," *IEEE J. Emerging Selected Topics Circ. and Syst.*, vol. 7, no. 2, pp. 239-249, Jun. 2017.

[16] J. A. Short, D. G. Infield, and L. L. Ferris, "Stabilization of grid frequency through dynamic demand control," *IEEE Trans. Power Syst.*, vol. 23, no. 3, pp. 1284–1293, Aug. 2007.

[17] M. R. Vedady Moghadam, R. T. B. Ma, and R. Zhang, "Distributed frequency control in smart grids via randomized demand response," *IEEE Trans. Smart Grid*, vol. 5, no. 6, pp. 2798-2809, Nov. 2014.

[18] A. Molina-Garciá, F. Bouffard, and D. S. Kirschen, "Decentralized demand-side contribution to primary frequency control," *IEEE Trans. Power Syst.*, vol.26, no.1, pp.411-419, Feb. 2011.

[19] A. Molina-Garcia, I. Munoz-Benavente, A. D. Hansen, and E. Gomez-Lazaro, "Demand-side

contribution to primary frequency control with wind farm auxiliary control", *IEEE Trans. Smart Grid*, vol. 29, no. 5, pp. 2391-2399, Sep. 2014.

[20] Q. Shi, Y. Xu, Y. Sun, W. Feng, F. Li and K. Sun, "Analytical approach to estimating the probability of transient stability under stochastic disturbances," in *2018 IEEE PES General Meeting*, Portland, OR, pp. 1-5.

[21] W. Feng, J. Wu, *et al.*, "A graph computation based sequential power flow for large-scale AC/DC systems," in *2019 IEEE PES General Meeting*, Atlanta, GA, pp. 1-5.

[22] M. Aunedi, P. A. Kountouriotis, J. E. O. Calderon, D. Angeli, and G. Strbac, "Economic and environmental benefits of dynamic demand in providing frequency regulation," *IEEE Trans. Smart Grid*, vol. 4, no. 4, pp. 2036-2048, Dec. 2013.

[23] J. H. Eto, "Demand response spinning reserve demonstration," *Ernest Orlando Lawrence Berkeley National Laboratory*, May 2007.

[24] P. Kundur, *Power System Stability and Control*, New York: *McGraw-Hill*, 1994, p. 602-609 & p. 132-135.

[25] P. M. Anderson and M. A. Mirheydar, "A low-order system frequency response model," *IEEE Trans. Power Syst.*, vol. 5, pp. 720–729, Aug. 1990.

[26] M. Parashar, J. S. Thorp, and C. E. Seyler, "Continuum modeling of electromechanical dynamics in large-scale power systems," *IEEE Trans. Circuits Syst. I*, vol. 51, no. 9, pp. 1848-1858, Sept. 2004.

[27] H. Liu, L. Zhu, *et al.*, "ARMAX-based transfer function model identification using wide-area measurement for adaptive and coordinated damping control," *IEEE Trans. on Smart Grid*, vol. 8, no. 3, pp. 1105-1115, May 2017.

[28] J. Guo, Y. Zhang, *et al.*, "Design and implementation of a real-time off-grid operation detection tool from a wide-area measurements perspective," *IEEE Trans. on Smart Grid*, vol. 6, no. 4, pp. 2080-2087, Jul. 2015.

[29] S. Tsai, L. Zhang, *et al.*, "Frequency sensitivity and electromechanical propagation simulation study in large power systems," *IEEE Trans. Circuits Syst. I*, vol. 54, no. 8, pp. 1819-1828, Aug. 2007.

[30] EPRI power system dynamics tutorial, *EPRI*, Product ID: 1016042, 2009. [Online] http://www.epri.com/abstracts/Pages/ProductAbstract.aspx?ProductId=000000000001016042.

[31] Y. G. Rebours, D. S. Kirschen, M. Trotignon and S. Rossignol, "A survey of frequency and voltage control ancillary services—Part I: technical features," *IEEE Trans. Power Syst.*, vol. 22, no. 1, pp. 350-357, Feb. 2007.

[32] H. Bevrani, A. Ghosh and G. Ledwich, "Renewable energy sources and frequency regulation: survey and new perspectives," *IET Renew. Power Gener.*, vol. 4, no. 5, pp. 438-457, Sept. 2010.

[33] Y. Zhang, M. E. Raoufat, K. Tomsovic and S. M. Djouadi, "Set theory-based safety supervisory control for wind turbines to ensure adequate frequency response," *IEEE Trans. Power Syst.*, vol. 34, no. 1, pp. 680-692, Jan. 2019.

[34] S. Wang and K. Tomsovic, "A novel active power control framework for wind turbine generators to improve frequency response," *IEEE Trans. Power Syst.*, vol. 33, no. 6, pp. 6579-6589, Nov. 2018.

[35] S. Wang and K. Tomsovic, "Fast frequency support from wind turbine generators with auxiliary dynamic demand control," *IEEE Trans. Power Syst.*, in press.

[36] H. Liu, Z. Hu, Y. Song, and J. Lin, "Decentralized vehicle-to-grid control for primary frequency regulation considering charging demands," *IEEE Trans. Power Syst.*, vol. 28, no. 3, pp. 3480-3489, Aug. 2013.

[37] D. Zhu and G. Hug-Glanzmann, "Coordination of storage and generation in power system frequency control using an Hα approach," *IET Gener. Transm. Distrib.*, vol. 7, no. 11, pp. 1263-1271, Nov. 2013.

[38] Y. Zhu, C. Liu, K. Sun, D. Shi and Z. Wang, "Optimization of battery energy storage to improve power system oscillation damping," *IEEE Trans. Sustain. Energy.*, vol. 10, no. 3, pp. 1015-1024, Jul. 2019.

[39] Y. Zhu, C. Liu, B. Wang, and K. Sun, "Damping control for a target oscillation mode using battery energy storage," *J. Mod. Power Syst. Clean Energy*, vol. 6, no. 4, pp. 833-845, Feb. 2018.

[40] D. Kirschen and G. Strbac, *Fundamentals of Power System Economics*, Wiley & Sons, Ltd, Chichester, West Sussex, U.K., 2004, p. 111 & p. 16.

[41] H. Jiang, J. Lin, Y. Song, and D. J. Hill, "MPC-based frequency control with demand-side participation: a case study in an isolated wind-aluminum power system," *IEEE Trans. Power Syst.*, vol. 30, no. 6, pp. 3327-3337, Nov. 2015.

[42] P. J. Douglass, R. Garcia-Valle, P. Nyeng, J. Ostergaard, and M. Togeby, "Smart demand for frequency regulation: experimental results," *IEEE Trans. Smart Grid*, vol. 4, no. 3, pp. 1713-1720, Sept. 2013.

[43] J. Kondoh, N. Lu, and D. J. Hammerstrom, "An evaluation of the water heater load potential for providing regulation service," *IEEE Trans. Power Syst.*, vol.26, no.3, pp.1309-1316, Aug. 2011.

[44] K. Dehghanpour and S. Afsharnia, "Designing a novel demand side regulation algorithm to participate in frequency control using iterated mappings," *IET Gener. Transm. Distrib.*, vol. 8, no. 10, pp. 1687-1699, Oct. 2014.

[45] Y. J. Kim, L. K. Norford and J. L. Kirtley, "Modeling and analysis of a variable speed heat pump for frequency regulation through direct load control," *IEEE Trans. Power Syst.*, vol. 30, no. 1, pp. 397-408, Jan. 2015.

[46] Y. J. Kim, E. Fuentes and L. K. Norford, "Experimental study of grid frequency regulation ancillary service of a variable speed heat pump," *IEEE Trans. Power Syst.*, vol. 31, no. 4, pp. 3090-3099, Jul. 2016.

[47] B. J. Johnson, M. R. Starke, O. A. Abdelaziz, R. K. Jackson and L. M. Tolbert, "A MATLAB based occupant driven dynamic model for predicting residential power demand," *2014 IEEE PES T&D Conference and Exposition*, Chicago, IL, USA, 2014, pp. 1-5.

[48] M. Shad, A. Momeni, R. Errouissi, *et al.*, "Identification and estimation for electric water heaters in direct load control programs," *IEEE Trans. Smart Grid*, vol. 8, no. 2, pp. 947-955, Mar. 2017.

[49] Y. Lin, P. Barooah, S. Meyn, and T. Middelkoop, "Experimental evaluation of frequency regulation from commercial building HVAC systems," *IEEE Trans. Smart Grid*, vol. 6, no. 2,

pp. 776-783, Mar. 2015.

[50] D. S. Callaway, "Tapping the energy storage potential in electric loads to deliver load following and regulation, with application to wind energy," *Energ. Convers. Manag.*, vol. 50, no. 9, pp. 1389–1400, 2009.

[51] B. J. Johnson, M. R. Starke, O. A. Abdelaziz, R. K. Jackson and L. M. Tolbert, "A dynamic simulation tool for estimating demand response potential from residential loads," *2015 IEEE PES Innovative Smart Grid Technologies Conference (ISGT)*, Washington, DC, 2015, pp. 1-5.

[52] S. A. Pourmousavi and M. H. Nehrir, "Introducing dynamic demand response in the LFC model," *IEEE Trans. Power Syst.*, vol. 29, no. 4, pp. 1562-1572, Jul. 2014.

[53] S. A. Pourmousavi and M. H. Nehrir, "Demand response for smart microgrid: initial results," *Proc. 2nd IEEE PES Innov. Smart Grid Technol. (ISGT)*, pp. 1–6, 2011.

[54] S. A. Pourmousavi, M. H. Nehrir and C. Sastry, "Providing ancillary services through demand response with minimum load manipulation," *2011 North American Power Symposium*, Boston, MA, pp. 1-6, 2011.

[55] S. A. Pourmousavi and M. H. Nehrir, "Real-time central demand response for primary frequency regulation in microgrids," *IEEE Trans. Smart Grid*, vol. 3, no. 4, pp. 1988-1996, Dec. 2012.

[56] Y. Du and F. Li, "A hierarchical real-time balancing market considering multi-microgrids with distributed sustainable resources," *IEEE Trans. Sustain. Energy*, in press.

[57] Y. Q. Bao, Y. Li, B. Wang, M. Hu, and P. Chen, "Demand response for frequency control of multi-area power system," *J. Mod. Power Syst. Clean Energy*, vol. 5, no. 1, pp. 20-29, 2017.

[58] L. Chang-Chien, L. An, T. Lin, and W. Lee, "Incorporating demand response with spinning reserve to realize an adaptive frequency restoration plan for system contingencies," *IEEE Trans. Smart Grid*, vol. 3, no. 3, pp.1145-1153, Sep. 2012.

[59] P. Babahajiani, Q. Shafiee, H. Bevrani, "Intelligent demand response contribution in frequency control of multi-area power systems," *IEEE Trans. Smart Grid*, vol. 9, no. 2, pp. 1282-1291, Mar. 2018.

[60] E. Mallada, C. Zhao, and S. Low, "Optimal load-side control for frequency regulation in smart grids," *2014 52nd Annual Allerton Conference on Communication, Control, and Computing (Allerton)*, Monticello, IL, 2014, pp. 731-738.

[61] C. Zhao, U. Topcu, N. Li, and S. Low, "Design and stability of load-side primary frequency control in power systems," *IEEE Trans. Autom. Control*, vol. 59, no. 5, pp. 1177–1189, May 2014.

[62] R. Weckx, D. Hulst, and J. Driesen, "Primary and secondary frequency support by a multi-agent demand control system," *IEEE Trans. Power Syst.*, vol. 30, no. 3, pp. 1394-1404, May 2015.

[63] D. Angeli and P. A. Kountouriotis, "A stochastic approach to dynamic-demand refrigerator control," *IEEE Trans. on Control Syst. Technol.*, vol. 20, no. 3, pp. 581-592, May 2012.

[64] S. H. Tindemans, V. Trovato and G. Strbac, "Decentralized control of thermostatic loads for flexible demand response," *IEEE Trans. Control Syst. Technol.*, vol. 23, no. 5, pp. 1685-1700, Sep. 2015.

[65] V. Trovato, I. Martinez Sanz, B. Chaudhuri; G. Strbac, "Advanced control of thermostatic

loads for rapid frequency response in Great Britain," *IEEE Trans. Power Syst.*, vol. 32, no. 3, pp. 2106-2117, May 2017.

[66] G. Benysek, J. Bojarski, R. Smolenski, M. Jarnut, and S. Werminski, "Application of stochastic decentralized active demand response (DADR) system for load frequency control," *IEEE Trans. Smart Grid, in press.*

[67] D. Chakravorty, B. Chaudhuri, and S. Y. R. Hui, "Rapid frequency response from smart loads in Great Britain power system," *IEEE Trans. Smart Grid*, vol. 8, no. 5, pp. 2160-2169, Sep. 2017.

[68] Y. Q. Bao, Y. Li, *et. al*, "Design of a hybrid hierarchical demand response control scheme for the frequency control," *IET Gener., Transm. & Distrib.*, vol. 9, no. 15, pp. 2303-2310, Nov. 2015.

[69] Q. Shi, H. Cui, F. Li, Y. Liu, W. Ju, and Y. Sun, "A hybrid dynamic demand control strategy for power system frequency regulation," *CSEE J. Power Energy Syst.*, vol. 3, no. 2, pp. 17-26, Jun. 2017.

[70] Y. Li, T. Yong, J. Cao, *et al.*, "A consensus control strategy for dynamic power system look-ahead scheduling," *Neuro Computing*, vol. 168, pp. 1085-1093, Nov. 2015.

[71] J. Hu, J. Cao, J. M. Guerrero, T. Yong, and J. Yu, "Improving frequency stability based on distributed control of multiple load aggregators," *IEEE Trans. Smart Grid*, vol. 8, no. 4, pp. 1553-1567, Jul. 2017.

[72] O. Ma, N. Alkadi, P. Cappers, *et al.*, "Demand response for ancillary services," *IEEE Trans. Smart Grid*, vol. 4, no. 4, pp. 1988-1995, Dec. 2013.

[73] B. Kirby and E. Hirst, "Load as a resource in providing ancillary services," Oak Ridge National Laboratory and Consultants in Electric-Industry Restructuring, Oak Ridge, Tennessee.

[74] A. Majzoobi, A. Khodaei, "Application of microgrids in providing ancillary services to the utility grid," *Energy*, vol. 123, pp. 555-563, Mar. 2017.

[75] M. D. Ilić, N. Popli, J. Y. Joo and Y. Hou, "A possible engineering and economic framework for implementing demand side participation in frequency regulation at value," *IEEE PES General Meeting*, San Diego, CA, 2011, pp. 1-7.

[76] E. Ela, V. Gevorgian, A. Tuohy, *et al.*, "Market designs for the primary frequency response ancillary service—Part I: motivation and design," *IEEE Trans. Power Syst.*, vol. 29, no. 1, pp. 421-431, Jan. 2014.

[77] J. Chow, *Power system coherency and model reduction*, Springer, 2013, pp. 33-35.

[78] S. H. Jakobsen and K. Uhlen, "Vector fitting for estimation of turbine governing system parameters," *2017 IEEE Manchester PowerTech*, Manchester, 2017, pp. 1-6.

[79] D. L. H. Aik, "A general-order system frequency response model incorporating load shedding: analytic modeling and applications," *IEEE Trans. Power Syst.*, vol. 21, no. 2, pp. 709-717, May 2006.

[80] W. Ju, J. Qi, and K. Sun, "Simulation and analysis of cascading failures on an NPCC power system test bed," in 2015 *IEEE PES Society General Meeting*, Denver CO, 26–30 Jul. 2015, pp. 1-5.

[81] L. Sigrist, I. Egido and L. Rouco, "A method for the design of UFLS schemes of small isolated power systems," *IEEE Trans. Power Syst.*, vol. 27, no. 2, pp. 951-958, May 2012.

[82] L. Cai, Z. He and H. Hu, "A new load frequency control method of multi-area power system via the viewpoints of Port-Hamiltonian system and cascade system," *IEEE Trans. Power Syst.*, vol. 32, no. 3, pp. 1689-1700, May 2017.

[83] Q. Shi, F. Li, Q. Hu, and Z. Wang, "Dynamic demand control for system frequency regulation: concept review, algorithm comparison, and future vision," *Electr. Power Syst. Res.*, vol. 154, pp. 75-87, Jan. 2018.

[84] S. Liao, J. Xu, *et al.*, "Load-damping characteristic control method in an isolated power system with industrial voltage-sensitive load," *IEEE Trans. Power Syst.*, vol. 31, no. 2, pp. 1118-1128, Mar. 2016.

[85] N. Nguyen and J. Mitra, "An analysis of the effects and dependency of wind power penetration on system frequency regulation," *IEEE Trans. Sustain. Energy*, vol. 7, no. 1, pp. 354-363, Jan. 2016.

[86] H. Pulgar-Painemal, Y. Wang, *et al.*, "On inertia distribution, inter-area oscillations and location of electronically-interfaced resources," *IEEE Trans. Power Syst.*, vol. 33, no. 1, pp. 995-1003, Jan. 2018.

[87] Y. Wang, H. D. Silva-Saravia and H. A. Pulgar-Painemal, "Actuator placement for enhanced grid dynamic performance: a machine learning approach," *IEEE Trans. Power Syst.*, vol. 34, no. 4, pp. 3119-3128, Jul. 2019.

[88] H. Yu, R. Bansal, and Z. Dong, "Fast computation of the maximum wind penetration based on frequency response in small isolated power systems," *Applied Energy*, vol. 113, pp. 648-659, Jan. 2014.

[89] N. W. Miller, M. Shao, and S. Venkataraman, "California iso (CAISO) frequency response study," General Elect. Int., Schenectady, NY, USA, Tech. Rep., 2011.

[90] H. Golpîra, H. Seifi, *et al.*, "Maximum penetration level of micro-grids in large scale power systems: frequency stability viewpoint," *IEEE Trans. Power Syst.*, vol. 31, pp. 5163-5171, 2016.

[91] P. M. Anderson and A. A. Fouad, *Power System Control and Stability*. Ames, IA: Iowa State Univ. Press, 1977, pp. 70-73.

[92] U. Rudez and R. Mihalic, "Analysis of underfrequency load shedding using a frequency gradient," *IEEE Trans. Power Del.*, vol. 26, no. 2, pp. 565-575, Apr. 2011.

[93] H. Ahmadi and H. Ghasemi, "Security-constrained unit commitment with linearized system frequency limit constraints," *IEEE Trans. Power Syst.*, vol. 29, no. 4, pp. 1536-1545, Jul. 2014.

[94] Y. Wang, H. Silva-Saravia and H. Pulgar-Painemal, "Estimating inertia distribution to enhance power system dynamics," in *2017 North American Power Symposium (NAPS)*, Morgantown, WV, 2017, pp. 1-6.

[95] U. Rudez and R. Mihalic, "Monitoring the first frequency derivative to improve adaptive underfrequency load-shedding schemes," *IEEE Trans. Power Syst.*, vol. 26, no. 2, pp. 839-846, May 2011.

[96] F. Milano and A. Ortega, "Frequency divider," *IEEE Trans. Power Syst.*, vol. 32, no. 2, pp. 1493–1501, Mar. 2017.

[97] B. Wang and K. Sun, "Formulation and characterization of power system electromechanical oscillations," *IEEE Trans. on Power Syst.*, vol. 31, no. 6, pp. 5082-5093, Nov. 2016.

[98] H. Saadat, *Power system analysis*, McGraw-Hill, Boston, 1999, pp. 535.

[99] "Balancing and frequency control," NERC Resources Subcommittee, Princeton, NJ, USA, Tech. Rep. Jan. 2011, pp. 38.

[100] J. F. Restrepo and F. D. Galiana, "Unit commitment with primary frequency regulation constraints," *IEEE Trans. Power Syst.*, vol. 20, no. 4, pp. 1836-1842, Nov. 2005.

[101] F. Milano. (Mar. 2006). Power system analysis toolbox documentation for PSAT version 2.0.0_1. [Online]. Available: http://faraday1.ucd.ie/ psat.html.

[102] H. Huang and F. Li, "Sensitivity analysis of load-damping characteristic in power system frequency regulation," *IEEE Trans. Power Syst.*, vol. 28, no. 2, pp. 1324-1335, May 2013.

[103] H. Golpira and A. R. Messina, "A center-of-gravity-based approach to estimate slow power and frequency variations," *IEEE Trans. Power Syst.*, vol. 33, no. 1, pp. 1026-1035, Jan. 2018.

[104] Y. Zhang, K. Tomsovic, S. M. Djouadi, and H. Pulgar-Painemal, "Hybrid controller for wind turbine generators to ensure adequate frequency response in power networks," *IEEE J. Emerging Select. Topics Circ. and Syst.*, vol. 7, no. 3, pp. 359-370, Sep. 2017.

[105] Y. Li, Z. Xu, and K. P. Wong, "Advanced control strategies of PMSG-based wind turbines for system inertia support," *IEEE Trans. Power Syst.*, vol. 32, no. 4, pp. 3027-3037, Jul. 2017.

[106] B. Qin, H. Sun, *et al.*, "Robust H_∞ control of doubly fed wind generator via state-dependent Riccati equation technique," *IEEE Trans. Power Syst.*, vol. 34, no. 3, pp. 2390-2400, May 2019.

[107] Y. Zhang, P. Markham, *et al.*, "Wide-area frequency monitoring network (FNET) architecture and applications," *IEEE Trans. Smart Grid*, vol. 1, no. 2, pp. 159–167, Sept. 2010.

[108] F. Bai, X. Wang, and *et al.*, "Measurement-based frequency dynamic response estimation using geometric template matching and recurrent artificial neural network," *CSEE J. Power Energy Syst.*, vol. 2, no. 3, pp. 10–18, Sep. 2016.

[109] C. Huang, F. Li, T. Ding, Z. Jin, and X. Ma, "Second-order cone programming-based optimal control strategy for wind energy conversion systems over complete operating regions," *IEEE Trans. Sustain. Energy*, vol. 6, no. 1, pp. 263–271, Jan. 2015.

[110] U. Helman, "Resource and transmission planning to achieve a 33% RPS in California-ISO modeling tools and planning framework," in *Proc. FERC Technical Conf. Planning Models and Software*, 2010.

[111] X. Wu, J. He, Y. Xu, J. Lu, N. Lu and X. Wang, "Hierarchical control of residential HVAC units for primary frequency regulation," *IEEE Trans. Smart Grid*, vol. 9, no. 4, pp. 3844-3856, Jul. 2018.

[112] M. M. Olama, T. Kuruganti, J. Nutaro, and J. Dong, "Coordination and control of building HVAC systems to provide frequency regulation to the electric grid," *Energies*, vol. 11, no. 7, pp. 1-15, Jul. 2018.

[113] F. Conte, S. Massucco, and *et al.*, "Stochastic modelling of aggregated thermal loads for impact analysis of demand side frequency regulation in the case of Sardinia in 2020", *Int. J. Electr. Power Energy Syst.*, vol. 93, pp. 291-307, Dec. 2017.

[114] A. Kasis, E. Devane, I. Lestas, "Primary frequency regulation in power networks with ancillary service from load-side participation," *IFAC-PapersOnLine*, vol. 50, no. 1, pp. 4394-4399, Jul. 2017.

[115] A. Delavari and I. Kamwa, "Improved optimal decentralized load modulation for power system primary frequency regulation," *IEEE Trans. Power Syst.*, vol. 33, no. 1, pp. 1013-1025, Jan. 2018.

[116] S. H. Tindemans, V. Trovato and G. Strbac, "Decentralized control of thermostatic loads for flexible demand response," *IEEE Trans. Control Syst. Technol.*, vol. 23, no. 5, pp. 1685-1700, Sept. 2015.

[117] W. Cui, Y. Ding and *et al.*, "Evaluation and sequential-dispatch of operating reserve provided by air conditioners considering lead-lag rebound effect," *IEEE Trans. Power Syst.*, vol. 33, no. 6, pp. 6935-6950, Nov. 2018.

[118] J. Widén, M. Lundh, and *et al.*, "Constructing load profiles for household electricity and hot water from time-use data—Modelling approach and validation," *Energy Build.*, vol. 41, no. 7, pp. 753-768, Jul. 2009.

[119] R. Torquato, Q. Shi, W. Xu, and W. Freitas, "A Monte Carlo simulation platform for studying low voltage residential networks," *IEEE Trans. Smart Grid*, vol. 5, no. 6, pp. 2766-2776, Nov. 2014.

[120] "Embedded energy in water studies study 3: end-use water demand profiles," CALMAC Study, ID CPU0052, vol. 1 of 1, Apr., 2011.

[121] Q. Shi, C. Chen, A. Mammoli, and F. Li, "Estimating the profile of incentive-based demand response (IBDR) considering technical models and social-psychological factors", *IEEE Trans. Smart Grid*, in press.

[122] J. L. Mathieu, M. Dyson, and D. S. Callaway, "Using residential electric loads for fast demand response: the potential resource and revenues, the costs, and policy recommendations," *Proc. ACEEE Summer Study Build.*, 2012, pp. 189–203.

[123] T. Ackermann, *Wind power in power systems*, Springer, 2005, pp. 154.

[124] Y. Liu, L. Zhan, and *et al.*, "Wide-area-measurement system Development at the distribution level: an FNET/GridEye example," *IEEE Trans. Power Del.*, vol. 31, no. 2, pp. 721-731, Apr. 2016.

[125] A. J. Conejo, M. Carri´on and J. M. Morales, *Decision making under uncertainty in electricity markets*. New York: Springer, 2010, pp. 479.

[126] A. Asadinejad, A. Rahimpour, *et al.*, "Evaluation of residential customer elasticity for incentive based demand response programs," *Electr. Power Syst. Res.*, vol. 158, pp. 26-36, May 2018.

[127] ECORT load profile. [Online]. Available: http://www.ercot.com/mktinfo/loadprofile/alp.

[128] A. Khodaei, M. Shahidehpour, and S. Bahramirad, "SCUC with hourly demand response considering intertemporal load characteristics," *IEEE Trans. Smart Grid*, vol. 2, no. 3, pp. 564-571, Sep. 2011.

[129] H. T. Haider, O. H. See, and W. Elmenreich, "A review of residential demand response of smart grid," *Renew. Sustain. Energy Rev.*, vol. 59, pp. 166–178, Jun. 2016.

[130] 2015 residential energy consumption survey. [Online]. Available: www.eia.gov/consumption/residential/.

[131] A. Mammoli, P. Vorobieff, and *et al.*, "Energetic, economic and environmental performance of a solar-thermal-assisted HVAC system," *Energy Build.*, vol. 42, no. 9, pp. 1524-1535, Sep. 2010.

[132] X. Xu, C. Chen, X. Zhu, and Q. Hu, "Promoting acceptance of direct load control programs in the United States: financial incentive versus control option," *Energy*, vol. 147, pp. 1278-1287, May 2018.

[133] N. Lu, "An evaluation of the HVAC load potential for providing load balancing service," *IEEE Trans. Smart Grid*, vol. 3, no. 3, pp. 1263–1270, 793 Sep. 2012.

[134] R. Tyagi and J. W. Black, "Emergency demand response for distribution system contingencies," *2010 IEEE PES T&D*, New Orleans, LA, 2010, pp. 1-4.

[135] G. Baker, M. C. Jensen, *et al.*, "Compensation and incentives: practice versus theory," *J. Finance*, vol. 43, no. 3, pp. 593–616, 1988.

[136] J. Luft, "Bonus and penalty incentives contract choice by employees," *J. Account. Econ.*, vol. 18, no. 2, pp. 181–206, 1994.

[137] T. N. Taylor, P. M. Schwarz, and J. E. Cochell, "24/7 hourly response to electricity real-time pricing with up to eight summers of experience," *J. Regul. Econ.*, vol. 27, no. 2, pp. 235-2005.

[138] Q. Hu, X. Fang, and *et al.*, "An approach to assess the responsive residential demand to financial incentives," in *2015 IEEE PES General Meeting*, Denver, CO, 2015, pp. 1-5.

[139] A. Asadinejad and K. Tomsovic, "Optimal use of incentive and price based demand response to reduce costs and price volatility," *Electr. Power Syst. Res*, vol. 144, pp. 215-223, Mar. 2017.

[140] Dillman, *et al.*, "*Internet, phone, mail and mixed-mode surveys: the tailored design method*," 3th edition, John Wiley, Hoboken, NJ, 2014.

[141] C. Chen, X. Xu, and Arpan, L. "Between the technology acceptance model and sustainable energy technology acceptance model: investigating smart meter acceptance in the United States," *Energy Res. Social Science*, vol. 25, pp. 93-104, 2017.

[142] S. D' Oca, C. Chen, T. Hong, Z. Belafi, "Synthesizing building physics with social psychology: An interdisciplinary framework for context and occupant behavior in office buildings," *Energy Res. Social Science*, vol. 34, pp. 240-251, Dec. 2017.

[143] Q. Shi, F. Li, *et al.*, "Thermostatic load control for system frequency regulation considering daily demand profile and progressive recovery," *IEEE Trans. Smart Grid*, in press, DOI: 10.1109/TSG.2019.2900724.

[144] X. Xu, C. Chen, A. Washizu, H. Ishii and H. Yashiro, "Willingness to pay for home energy management system: A cross-country comparison," in *2018 IEEE PES General Meeting*, Portland, OR, 2018, pp. 1-5.

[145] M. Cai, M. Pipattanasomporn, and S. Rahman, "Day-ahead building-level load forecasts using deep learning vs. traditional time-series techniques," *Appl. Energy*, vol. 236, pp. 1078-1088, Feb. 2019.

[146] W. Wei, *et al.*, "Hierarchical and distributed demand response control strategy for thermostatically controlled appliances in smart grid," *J. Mod. Power Syst. Clean Energy*, vol. 5, no. 1, pp. 30-42, Jan. 2017.

[147] Historical weather data. [Online]. Available: https://www.wunderground.com/

[148] V. Trovato, S. H. Tindemans and G. Strbac, "Leaky storage model for optimal multi-service allocation of thermostatic loads," *IET Gener., Transm. Distrib.*, vol. 10, no. 3, pp. 585-593, Mar. 2016.

[149] C. M. Grinstead and J. L. Snell, "*Introduction of probability*," Providence, RI, USA, American Mathematical Society, 1997. pp. 307-308.

[150] C. Jiang, "A probabilistic bottom-up technique for modeling and simulation of residential distributed harmonic sources," M.Sc. dissertation, University of Alberta, spring 2012, pp. 56.

[151] W. Feng, C. Yuan, R. Dai, G. Liu and F. Li, "Graph computation based power flow for large-scale AC/DC system," in *2018 International Conference on Power System Technology (POWERCON)*, Guangzhou, 2018, pp. 468-473.

[152] M. Dong, P. C. M. Meira, W. Xu and W. Freitas, "An event window based load monitoring technique for smart meters," *IEEE Trans. Smart Grid*, vol. 3, no. 2, pp. 787-796, Jun. 2012.

[153] NYISO load profile. [Online]. Available: http://mis.nyiso.com/public/P-58Blist.htm.

[154] Y. Li, Y. Shen, L. Zhou, and F. Li, "Progressive time-differentiated peak pricing (PTPP) for aggregated air-conditioning load in demand response programs," *Int. Trans. Elect. Energy Syst.*, vol. 29, no. 1, pp. 1–16, Jan. 2019.

[155] Comprehensive housing market analysis in Texas, Houston. [Online]. Available: https://www.huduser.gov/portal/publications/pdf/HoustonTX -comp-17.pdf.

[156] Comprehensive housing market analysis in New York. [Online]. Available: https://www.huduser.gov/portal/publications/pdf/NYC-comp 16.pdf.

[157] W. Feng, X. Kou, Q. Zhang and F. Li, "Impact of neutral current on concentric cable overloading," in *2018 IEEE/PES Transmission and Distribution Conference and Exposition (T&D)*, Denver, CO, 2018, pp. 1-5.

[158] U. S. Energy Information Administration (EIA). [Online]. Available: https://www.eia.gov/todayinenergy/detail.php?id=31912.

[159] X. Wang, Z. Hu, M. Zhang and M. Hu, "Two-stage stochastic optimization for unit commitment considering wind power based on scenario analysis," *2016 China International Conference on Electricity Distribution (CICED)*, Xi'an, 2016, pp. 1-5.

Appendices

Appendix A Deduction of Error Function Parameters

The Formulation of ASFR Model

According to the definition of the ASFR model (shown in Figure 3.4), we have

$$\sum_{i=1}^{N}\left(K_{mi} \cdot \frac{1}{R_i} \cdot Gen_i(s) \right) = \frac{1}{R} \cdot Gen(s) \tag{A1}$$

where

$$Gen(s) = \frac{1 + F_H T_R s}{(1 + T_G s)(1 + T_C s)(1 + T_R s)}$$

Substituting (3.17) to the right-hand side of (A1) gives

$$\sum_{i=1}^{N}\left(\frac{K_{mi}}{R_i} \cdot Gen_i(s) \right) = \left(\sum_{i=1}^{N} \frac{K_{mi}}{R_i} \right) \cdot Gen(s) \tag{A2}$$

Substituting (3.17) and (3.18) to (A2) gives

$$\sum_{i=1}^{N}\left(\kappa_i \cdot Gen_i(s) \right) = \left(\sum_{i=1}^{N} \kappa_i \right) \cdot Gen(s)$$

$$\sum_{i=1}^{N}\left(\left(\kappa_i \Big/ \sum_{i=1}^{N} \kappa_i \right) \cdot Gen_i(s) \right) = Gen(s) \tag{A3}$$

$$\sum_{i=1}^{N}\left(\lambda_i \cdot Gen_i(s) \right) = Gen(s)$$

Linear Approximation of Turbine Governor Function

The right side of (3.22) can be expressed as a polynomial function:

$$\frac{A_R(1 + F_{Hi}T_{Ri}s)}{1 + T_{Ri}s} + \frac{A_G}{(1 + T_{Gi}s)(1 + T_{Ci}s)} = \frac{p_3 s^3 + p_2 s^2 + p_1 s + p_0}{q_3 s^3 + q_2 s^2 + q_1 s + q_0} \tag{A4}$$

The coefficients of the right side of (A4) are shown in Table A1.

Table A1. Coefficients of the transfer function.

i	p_i	q_i
3	$A_R F_{Hi} T_{Ri} T_{Gi} T_{Ci}$	$T_{Ri} T_{Gi} T_{Ci}$
2	$A_G (F_{Hi} T_{Ri} T_{Gi} + F_{Hi} T_{Ri} T_{Ci} + T_{Gi} T_{Ci})$	$T_{Ri} T_{Gi} + T_{Ri} T_{Ci} + T_{Ci} T_{Gi}$
1	$A_R (F_{Hi} T_{Ri} + T_{Gi} + T_{Ci}) + A_G T_{Ri}$	$T_{Ri} + T_{Gi} + T_{Ci}$
0	$A_R + A_G$	1

Assume there exists a pair of A_R and A_G values that make the left and right side of (A5) have an equal frequency characteristic:

$$\frac{p_3 s^3 + p_2 s^2 + p_1 s + p_0}{q_3 s^3 + q_2 s^2 + q_1 s + q_0} = \frac{F_{Hi} T_{Ri} s + 1}{(1 + T_{Gi} s)(1 + T_{Ci} s)(1 + T_{Ri} s)} \tag{A5}$$

Let $p_1 = F_{Hi} T_{Ri}$ and $p_0 = 1$, and solve for

$$\begin{cases} A_R = \dfrac{(1 - F_{Hi}) T_{Ri}}{(1 - F_{Hi}) T_{Ri} + T_{Gi} + T_{Ci}} \approx 0.9 \\ A_G = 1 - A_R \approx 0.1 \end{cases} \tag{A6}$$

Substituting (A6) to the expression of other coefficients, we can conclude $p_3/q_3 = A_R F_{Hi} <$ 0.36 and $p_2/q_2 \approx A_G F_{Hi} < 0.1$. Therefore, at the low-frequency band, the coefficients p_3 and p_2 can be neglected. Then, the approximated equation (3.22) is proved.

The Coefficients of the Error Function

The coefficients of $P_R(s)$ are deducted as follows:

$$a_0 = \lambda_1 + \lambda_2 - 1 = 0 \tag{A7}$$

$$a_3 = (\lambda_1 F_{H1} + \lambda_2 F_{H2} - F_H) T_{R1} T_{R2} T_R = 0 \tag{A8}$$

The expression of a_1 is simplified by substituting $\lambda_1 + \lambda_2 = 1$ and $X = \lambda_1 X_1 + \lambda_2 X_2$, respectively:

$$\begin{aligned} a_1 &= \lambda_1 (F_{H1} T_{R1} + T_{R2} + T_R) + \lambda_2 (F_{H2} T_{R2} + T_{R1} + T_R) - (F_H T_R + T_{R1} + T_{R2}) \\ &= \lambda_1 (1 - \lambda_1) F_{H1} T_{R1} - \lambda_1 \lambda_2 (F_{H1} T_{R2} + F_{H2} T_{R1}) + \lambda_2 (1 - \lambda_2) F_{H2} T_{R2} \\ &= \lambda_1 \lambda_2 (F_{H1} T_{R1} - F_{H1} T_{R2} - F_{H2} T_{R1} + F_{H2} T_{R2}) \\ &= \lambda_1 \lambda_2 (F_{H1} - F_{H2})(T_{R1} - T_{R2}) \end{aligned} \tag{A9}$$

Similarly, the expression of a_2 is simplified. a_2 is amplified twice as follows:

$$
\begin{aligned}
a_2 &= \lambda_1(F_{H1}T_{R1}T_{R2} + F_{H1}T_{R1}T_R + T_{R2}T_R) + \lambda_2(F_{H2}T_{R1}T_{R2} + F_{H2}T_{R2}T_R + T_{R1}T_R) \\
&\quad - (F_H T_{R1}T_R + F_H T_{R2}T_R + T_{R1}T_{R2}) \\
&= \left[(\lambda_1 T_{R2} + \lambda_2 T_{R1})(\lambda_1 T_{R1} + \lambda_2 T_{R2}) - T_{R1}T_{R2}\right] + \lambda_1\lambda_2(F_{H1}T_{R2} - F_{H2}T_{R1})(T_{R1} - T_{R2}) \\
&\leq \left[\left(\frac{\lambda_1 T_{R2} + \lambda_2 T_{R1} + \lambda_1 T_{R1} + \lambda_2 T_{R2}}{2}\right)^2 - T_{R1}T_{R2}\right] + \lambda_1\lambda_2(F_{H1}T_{R2} - F_{H2}T_{R1})(T_{R1} - T_{R2}) \quad \text{(A10)} \\
&= \left[0.25\left((\lambda_1 + \lambda_2)(T_{R1} + T_{R2})\right)^2 - T_{R1}T_{R2}\right] + \lambda_1\lambda_2(F_{H1}T_{R2} - F_{H2}T_{R1})(T_{R1} - T_{R2}) \\
&\leq 0.25\left[(T_{R1} - T_{R2})^2 + (F_{H1}T_{R2} - F_{H2}T_{R1})(T_{R1} - T_{R2})\right]
\end{aligned}
$$

We can observe that the second term of a_2 reaches the maximum when $T_{R1} = 14$s, $T_{R2} = 6$s, $F_{H1} = 0.15$s and $F_{H2} = 0.4$s:

$$
\begin{aligned}
&\left|(F_{H1}T_{R2} - F_{H2}T_{R1})(T_{R1} - T_{R2})\right| \\
&< \left|\frac{1}{F_{H2}T_{R2}^2}(\frac{F_{H1}}{F_{H2}} - \frac{T_{R1}}{T_{R2}})(\frac{T_{R1}}{T_{R2}} - 1)\right| \\
&< \left|\frac{1}{0.4 \times 6^2} \times \left(\frac{0.15}{0.4} - \frac{14}{6}\right) \times \left(\frac{14}{6} - 1\right)\right| \\
&<< (T_{R1} - T_{R2})^2
\end{aligned}
$$

Therefore, the upper bound of a_2 can be approximated as $0.25(T_{R1} - T_{R2})^2$.

Appendix B Characteristics of Thermostatic Loads

Let T be the cycle of a thermostatic-controlled load, where $T = T_{on} + T_{off}$. $\Phi \sim U(0, T)$ is the uniformly-distributed phasor, as shown in Figure B1. $q(t)$ is a periodic function:

$$q(t) = \begin{cases} Q, & \text{if } 0 \le t < T_{on} \\ 0, & \text{if } T_{on} \le t < T \end{cases} \tag{B1}$$

$X(t) = q(t + \Phi)$ is called random-phasor periodic function. At any given time t, the mean value of the function is

$$E[X(t)] = E[q(t + \Phi)] = \int_0^T q(t + \varphi) \frac{1}{T} d\varphi = \frac{1}{T} \int_t^{t+T} q(\tau) d\tau \tag{B2}$$

Since $q(t)$ is a periodic function:

$$E[X(t)] = \frac{1}{T} \int_0^T q(\tau) d\tau = \frac{1}{T} \cdot Q \cdot T_{on} = \frac{T_{on}}{T_{on} + T_{off}} Q = \pi_{on} Q \tag{B3}$$

Within a narrow temperature deadband, the temperature of a single device can be approximated as linear function of time.

$$\theta(t) = \begin{cases} \theta_{\min} + \beta_{off}(t - \Phi), 0 \le t - \Phi < T_{off} \\ \theta_{\max} + \beta_{on}(t - \Phi - T_{off}), T_{off} \le t - \Phi < T \end{cases} \tag{B4}$$

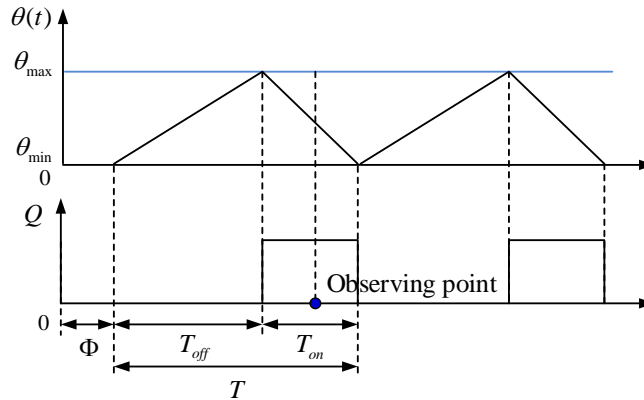As shown in Figure B1, the slopes β_{off} and β_{on} are given by

Figure B1. Illustration of HVAC operation cycle.

$$\beta_{off} = \frac{\theta_{db}}{T_{off}}$$

$$\beta_{on} = -\frac{\theta_{db}}{T_{on}} \tag{B5}$$

For a large number of devices, we have $t - \Phi \sim U(0, T)$ at any observing point t. For all the loads that are in the ON state, since $\beta_{on} < 0$,

$$\beta_{on}T < \beta_{on}(t - \Phi) \le \beta_{on}T_{off} \tag{B6}$$

The distribution of room temperature is given by

$$\begin{aligned}
\theta(t) &= \theta_{max} - \beta_{on}T_{off} + \beta_{on}(t - \Phi) \\
&\sim U\left(\theta_{max} - \beta_{on}T_{off} + \beta_{on}T, \ \theta_{max} - \beta_{on}T_{off} + \beta_{on}T_{off}\right) \\
&\sim U\left(\theta_{max} + \beta_{on}(T - T_{off}), \ \theta_{max}\right) \\
&\sim U\left(\theta_{max} - \frac{\theta_{db}}{T_{on}}T_{on}, \ \theta_{max}\right) \\
&\sim U\left(\theta_{min}, \ \theta_{max}\right)
\end{aligned} \tag{B7}$$

Similarly, all the loads that are in the OFF state have the same distribution.

Appendix C Average Approximation of EWH Modeling

To model the uncertainty of EWH model parameters, we apply a uniformly random multiplier between 0.5 and 1.5 to Q_E and Vol_k:

$$Q_E^i = U\left(0.5\bar{Q}_E, 1.5\bar{Q}_E\right)$$
$$Vol_k^i = U\left(0.5\overline{Vol}_k, 1.5\overline{Vol}_k\right)$$

(C1)

where Q_E^i is the heating rate of the i-th EWH, and Vol_k^i is the hot water demand of the i-th device, HWCA-k. $\bar{Q}_E$ and $\overline{Vol}_k$ are the corresponding average values. According to the characteristics of uniform distribution, we have

$$\sum_{i=1}^{N} Q_E^i = N \cdot \bar{Q}_E$$
$$\sum_{i=1}^{N} Vol_k^i = N \cdot \overline{Vol}_k$$

(C2)

Thus, the total EWH power caused by HWCA-k happening at t is:

$$P_{total,k}(t) = \sum_{i=1}^{N_E(t)} Q_E^i = N_E(t)\bar{Q}_E$$

(C3)

The total energy consumption of HWCA-k ($E_{total,k}$) is:

$$
\begin{aligned}
E_{total,k} &= \sum_{i=1}^{N_E(t)} Q_E^i \cdot T_{E,k} \\
&= \sum_{i=1}^{N_E(t)} Q_E^i \cdot \frac{C_w \rho Vol_k^i \left(\theta_{w,s} - \theta_{w,co}\right)}{Q_E^i} \\
&= C_w \rho \left(\theta_{w,s} - \theta_{w,co}\right) \cdot \sum_{i=1}^{N_E(t)} Vol_k^i \\
&= C_w \rho \left(\theta_{w,s} - \theta_{w,co}\right) \cdot N_E(t)\overline{Vol}_k
\end{aligned}
$$

(C4)

Finally, the expected duration of EWH operation is calculated:

$$\bar{T}_{E,k} \approx \frac{E_{total,k}}{P_{total,k}} = \frac{C_w \rho \overline{Vol}_k \left(\theta_{w,s} - \theta_{w,co}\right)}{\bar{Q}_E}$$

(C5)

Therefore, we can use the average value of Q_E and Vol_k to approximate their uniformly distributed values.

Appendix D Publications

Journal papers:

[J1] **Q. Shi**, H. Cui, F. Li, Y. Liu, W. Ju, and Y. Sun, "A hybrid dynamic demand control strategy for power system frequency regulation," *CSEE Journal of Power and Energy Systems*, vol. 3, no. 2, pp. 176-185, Jun. 2017.

[J2] **Q. Shi**, F. Li, Q. Hu, and Z. Wang, "Dynamic demand control for system frequency regulation: concept review, algorithm comparison, and future vision," *Electric Power System Research*, vol. 154, pp. 75-87, Jan. 2018.

[J3] **Q. Shi**, F. Li, and H. Cui, "Analytical method to aggregate multi-machine SFR model with applications in power system dynamics," *IEEE Transactions on Power System*, vol. 33, no. 6, pp. 6355-6367, Nov. 2018.

[J4] **Q. Shi**, F. Li, G. Liu, D. Shi, Z. Yi, and Z. Wang, "Thermostatic load control for system frequency regulation considering daily demand profile and progressive recovery," *IEEE Transactions on Smart Grid*, in press, DOI: 10.1109/ TSG.2019.2900724.

[J5] **Q. Shi**, C. Chen, Andrea Mammoli, and F. Li, "Estimating the profile of incentive-based demand response (IBDR) considering technical models and social-psychological factors", *IEEE Transactions on Smart Grid*, in press, DOI: 10.1109/TSG.2019.2919601.

[J6] **Q. Shi**, C. Yuan, W. Feng, G. Liu, R. Dai, F. Li, and Z. Wang, "Enabling model-based LTI for large-scale power system security monitoring and enhancement with graph-computing-based power flow calculation", *Electric Power System Research*, under review.

[J7] **Q. Shi**, F. Li, Mohammed Olama, Jin Dong, Cody, Rooks, and Teja Kuruganti, "Enhancing distribution system resilience via network reconfiguration and distributed energy resurces," to be submitted.

[J8] H. Han, S. Gao, **Q. Shi**, H. Cui, and F. Li, "Security-based active load response strategy considering uncertainties in power systems," *IEEE Access*, vol. 5, no. 1, pp. 16953-16962, Dec. 2017.

[J9] H. Han, H. Cui, S. Gao, **Q. Shi**, A. Fan, C. Wu, "A remedial strategic scheduling model for load serving entities considering the interaction between grid level energy storage and virtual power plants," *Energies*, vol. 11, no. 9, pp. 1-19, Sep. 2018.

[J10] X. Zhu, H. Han, S. Gao, **Q. Shi**, H. Cui, and G. Zu, "A multi-stage optimization approach for active distribution network scheduling considering coordinated electrical vehicle charging strategy," *IEEE Access*, no. 1, pp. 50117-50130, Sep. 2018.

[J11] M. Wang, Y. Mu, F. Li, H. Jia, X. Li, **Q. Shi**, and T. Jiang, "State space model of aggregated electric vehicles for frequency regulation," *IEEE Transactions on Smart Grid*, in press.

[J12] W. Feng, C. Yuan, **Q. Shi**, R. Dai, G. Liu, Z. Wang, and F. Li, "Using virtual buses and optimal multipliers to converge the sequential AC/DC power flow under high load cases," *Electric Power System Research*, in revision.

[J13] Y. Shen, Y. Li, Q. Zhang, **Q. Shi**, and F. Li, "Progressive load control of residential HVAC units for power system frequency regulation," *Electric Power System Research*, under review.

Conference papers:

[C1] C. Jiang, **Q. Shi**, Y. Tian, X. Li, S. Lin and Y. Liu, "Sensitivity study on the stray voltage of low voltage residential networks," in *2016 8th International Power Electronics and Motion Control Conf. (IMPEC – ECCE Asia)*, Hefei, China, pp. 1-6.

[C2] L. Bai, T. Jiang, F. Li, H. Jia, **Q. Shi**, H. Chen, and G. Li, "Confidence interval estimates for loading margin sensitivity for voltage stability monitoring in the presence of renewable energy," in *2016 IEEE Power & Energy Soc. Gen. Meeting*, Boston, MA, pp. 1-5.

[C3] **Q. Shi**, H. Liang, T. Hou, L. Bai, W. Xu and F. Li, "Passive filter installation for harmonic mitigation of residential distribution systems," in *2017 IEEE Power & Energy Soc. Gen. Meeting*, Chicago, IL, pp. 1-5.

[C4] **Q. Shi**, Y. Xu, Y. Sun, W. Feng, F. Li and K. Sun, "Analytical approach to estimating the probability of transient stability under stochastic disturbances," in *2018 IEEE Power & Energy Soc. Gen. Meeting*, Portland, OR, pp. 1-5.

[C5] Y. Shen, Q. Zhang, **Q. Shi**, F. Li, Y. Li, Y. Wang, and S. Wang, "Progressive demand control of thermostatically controlled appliances for power system frequency regulation," in *2019 IEEE Power & Energy Soc. Gen. Meeting*, Atlanta, GA, pp 1-5.

[C6] W. Feng, J. Wu, C. Yuan, G. Liu, **Q. Shi**, and F. Li, "A graph computation based sequential power flow for large-scale AC/DC systems," in *2019 IEEE Power & Energy Soc. Gen. Meeting*, Atlanta, GA, pp 1-5.

Vita

Qingxin Shi joined Professor Fangxing Li's group at the University of Tennessee at Knoxville in August 2015 to pursue a Ph.D. degree in Electrical Engineering. He received his B.S. degree from Zhejiang University, Hangzhou, China, in 2011, and M.Sc. degree from the University of Alberta, Edmonton, Canada, in 2014. His research interests include demand response, demand side control for frequency regulation and resilient distribution systems.